NISTIR 4589

Performance of 1/3-Scale Model Precast Concrete Beam-Column Connections Subjected to Cyclic Inelastic Loads—Report No. 2

Geraldine S. Cheok
H. S. Lew

June 1991

U.S. Department of Commerce
Robert A. Mosbacher, *Secretary*
National Institute of Standards and Technology
John W. Lyons, *Director*
Building and Fire Research Laboratory
Gaithersburg, MD 20899

ABSTRACT

Results are presented from the experimental test program on precast concrete beam-column connections subjected to inelastic cyclic loads being conducted at the National Institute of Standards and Technology. This report is the second in a series and covers the test results from Phase II of a three phase program. The objective of the test program is to develop an economical moment resistant precast beam-column joint for high seismic zones.

Test specimens are 1/3-scale models of a prototype interior concrete beam-column connection. The 1985 UBC design criteria for seismic Zones 2 and 4 were used. Six specimens were tested. The experimental variables include the location of the post-tensioning force and the type of post-tensioning tendons used. Comparisons of the performance among these specimens are made. Comparisons with the monolithic specimens (Phase I [Ref. 1]) are also presented. These comparisons are made based on the failure mode, energy absorption characteristics, strength and ductility of the connection.

KEY WORDS: beam-columns; concrete; connections; cyclic loading; ductility; energy absorption; joints; moment-resistance; post-tensioning; precast concrete.

ACKNOWLEDGEMENT

The authors would like to extend their thanks to the individuals who contributed to this project. The assistance of the laboratory staff for the Center of Building Technology especially that of Mr. Frank Rankin is gratefully acknowledged. Also, the authors would like to express their thanks to the advisory committee for providing technical guidance throughout the project. Members of the steering committee include Dr. Robert Englekirk, Dr. S. K. Ghosh, Mr. Daniel Jenny, Mr. Paul Johal, Dr. Nigel Priestley. The assistance of Ms. Suzanne Nakaki in providing the design of the test specimens is also much appreciated.

TABLE OF CONTENTS

List of Tables

List of Figures

1.0 INTRODUCTION

1.1 General

A study of the behavior of 1/3-scale model precast concrete beam-column connections subject to cyclic inelastic loading was initiated at the National Institute of Standards and Technology (NIST) in 1987. The objective of the experimental program was to develop recommended guidelines for the design of a precast concrete beam-column connection for regions of high seismicity. A project steering committee consisting of individuals from the Prestressed/Precast Concrete Institute (PCI), Portland Cement Association (PCA), academia and private sector is working with NIST throughout the test program.

The test program consisted of three phases. Phase I was an exploratory phase where four monolithic beam-column connections and two precast concrete specimens were tested. The results of the monolithic specimens served as a reference for the precast concrete tests. Phase II of the program involved the testing of six (6) precast specimens. Several methods of improving the energy dissipation characteristics of the precast concrete connection were explored. In Phase III, means of improving the hysteretic behavior of the precast concrete connection both analytically and experimentally will be examined.

Phase I results were reported in Reference 1, and this report presents the results of Phase II of the test program. Included in Reference 1 is a more detailed introduction of the test program and a literature review of related studies. A summary of the test results from Phase I is presented in the following section.

1.2 Summary of Phase I Results

In Phase I of the precast concrete concrete beam-column connection study at NIST, six (6) specimens were tested. Two of the specimens were monolithic concrete connections designed to UBC (1985) seismic Zone 2 criteria (A-M-Z2 and B-M-Z2). The other four specimens were designed to UBC (1985) seismic Zone 4 criteria. Two of the Zone 4 specimens were monolithic specimens (A-M-Z4 and B-M-Z4) while the remaining two were precast concrete with post-tensioned beam-column connections (A-P-Z4 and B-P-Z4). The nomenclature for the specimens is as follows:

1. First character: Specimen Name - A, B, C, ... Specimens A & B, C & D, E & F, etc. are identical specimens and form one set.
2. Second character: M = Monolithic, P = Precast
3. Third & fourth characters: Z2 = Zone 2, Z4 = Zone 4.

The precast concrete elements were connected by two 25 mm (1.0 in) diameter post-tensioning bars having an ultimate strength of 1034 MPa (150 ksi). Figs. 1.1 and 1.2 show the reinforcement details for the specimens tested in Phase I. The inch wide construction joint between the beam and column was filled with a fiber reinforced grout and the post-tensioning ducts were grouted after tensioning. Commercially available pre-mixed grout and straight steel fibers 19 mm (0.75 in) long were used. Results from the monolithic tests are used as a benchmark reference for both present and future precast concrete tests.

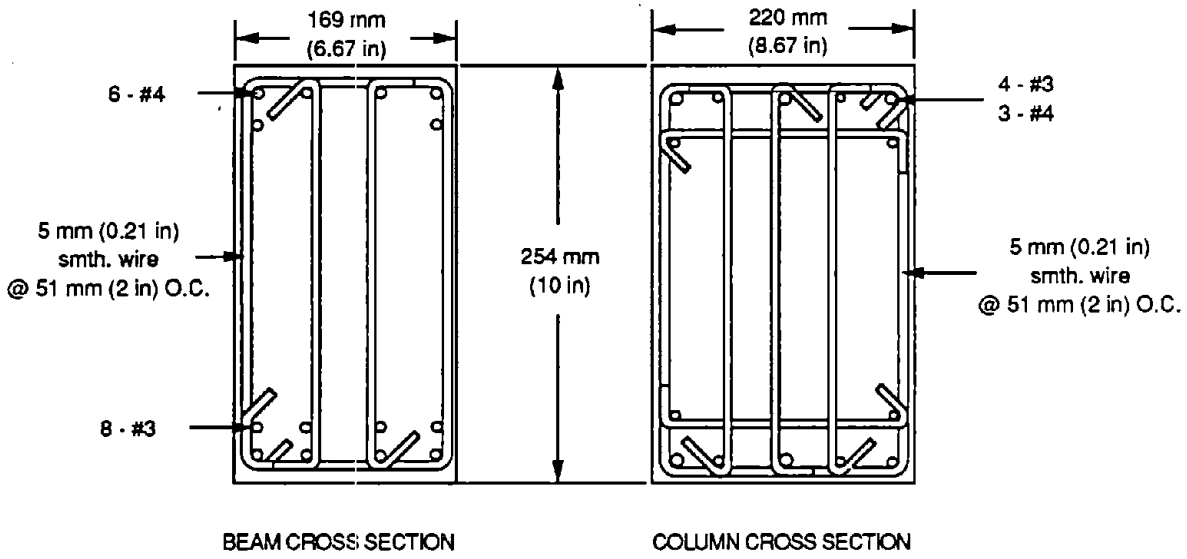

Fig. 1.1 Reinforcement details for monolithic Zone 2 specimens.

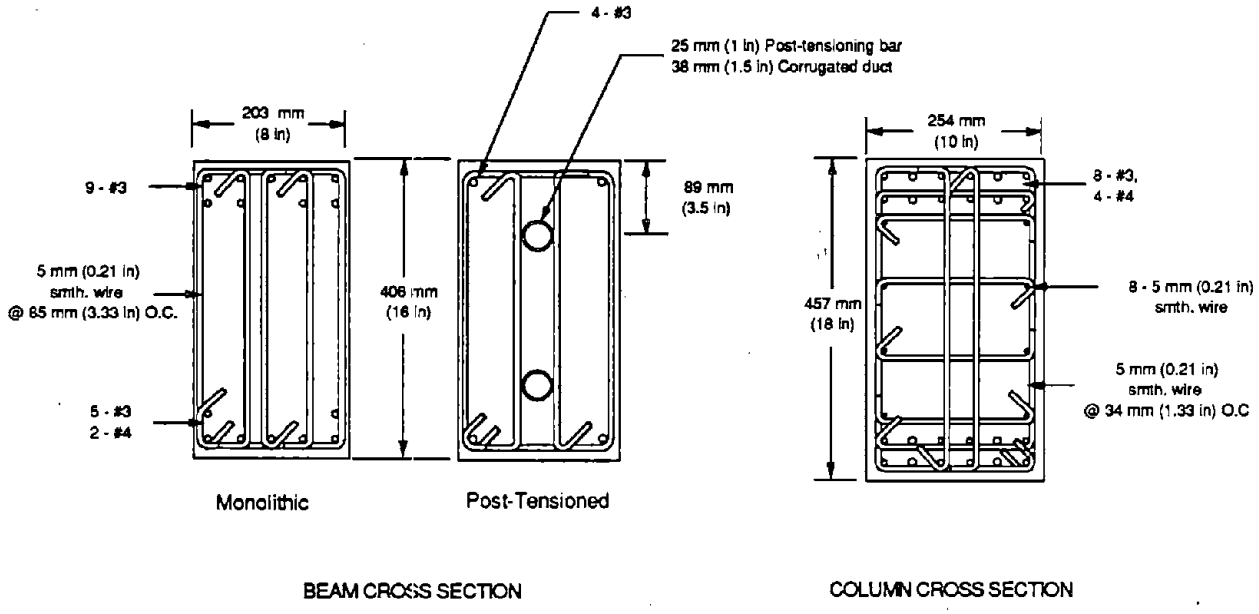

Fig. 1.2 Reinforcement details for monolithic Zone 4 specimens and precast concrete specimens A & B.

Failure of the monolithic Zone 2 specimens occurred in the joint region due to a combination of high joint stresses and inadequate confinement. The monolithic Zone 4 specimens failed as a result of beam hinging and deterioration. Failure of the post-tensioned specimens was characterized by plastic elongation, 12.7 mm (0.5 in), of the post-tensioning bars and crushing and spalling of the concrete cover in the beams. Joint shear stresses for the Zone 4 specimens were below the ACI-ASCE Committee 352 recommended value of 20 $\sqrt{f'_c}$ (f'_c in psi).

The ultimate displacement ductilities for the monolithic Zone 2 specimens were 6 (see section 4.1). These ductilities corresponded to story drifts of 4.1% and 4.3%. The ultimate displacement ductility for the post-tensioned specimens were higher than for their companion monolithic specimens - 10 vs. 6. However, since the post-tensioned specimens were stiffer than the monolithic specimens, the story drift at failure for the Zone 4 post-tensioned and monolithic specimens were almost identical. The story drifts at failure for the Zone 4 specimens ranged from 3.0% - 3.4%. The post-tensioned specimens were approximately twice as stiff as the monolithic Zone 4 specimens and fives times as stiff as the monolithic Zone 2 specimens.

The post-tensioned connections were slightly stronger than the monolithic specimens. The ultimate beam moments were on average 18% greater than the calculated moments for the post-tensioned specimens and 13% greater for the monolithic Zone 4 specimens. The monolithic Zone 2 specimens achieved maximum measured beam moments that were on average 8% greater than the calculated moment.

When comparing the energy absorbed per cycle, the behavior of the post-tensioned specimens was more similar to the monolithic Zone 2 specimens than to the monolithic Zone 4 specimens. On a per cycle basis, the post-tensioned specimens absorbed about 30% of the energy absorbed by the monolithic Zone 4 specimens. However, since the post-tensioned specimens achieved higher displacement ductilities than the monolithic specimens, the average of the cumulative energy absorbed up to failure by the post-tensioned specimens was approximately 80 % of that for the monolithic Zone 4 specimens. The average of the cumulative energy absorbed up to failure by the monolithic Zone 2 specimens is about 33% of that absorbed by the monolithic Zone 4 specimens.

Based on the results of the Phase I test program, it would appear that a post-tensioned precast concrete beam-column connection is a candidate for use in high seismic regions. However, the energy dissipation characteristics for this type of precast connection need to be improved and will thus be the focus of Phase II of the test program.

2.0 SPECIMEN DESIGN, CONSTRUCTION AND TEST PROCEDURE

2.1 Specimen Design

The results of Phase I tests indicated that a post-tensioned connection designed based on the 1985 UBC seismic Zone 4 criteria was as strong as the monolithic Zone 4 specimens. However, the cumulative energy absorbed by the precast concrete Zone 4 specimens was 20% lower and the per cycle energy absorbed by the precast concrete Zone 4 specimens was 70% lower than the monolithic Zone 4 specimens. It was determined through discussions with the project steering committee that a possible method of improving the energy absorption characteristics of the precast concrete connection was to move the post-tensioning bars closer towards the beam center. By doing this, the post-tensioning bars/prestressing strands would experience less strain and would therefore retain their post-tensioning force for a longer period.

Also, as mentioned in Ref. 1, prestressing strands are used more commonly than post-tensioning bars in practice due mainly to the lengths required when post-tensioning several bays at a time. It was also felt that the use of six strands instead of two post-tensioning bars would help the energy absorption characteristics. This was because of a more evenly distributed load and increased bond area with six strands as opposed to two bars. As a result, two sets of precast concrete Zone 4 specimens were tested. Post-tensioning bars were used to connect one set of specimens while prestressing strands were used in the other set. In both sets, the centroid of the steel was moved closer to the beam centroid. In addition, one set of precast concrete Zone 2 specimens was constructed and tested.

The Phase II specimens were designed similarly to the Phase I precast concrete specimens. The required amount of post-tensioning steel was computed so that the strength of the precast concrete connection was as strong as the monolithic concrete connection. Reinforcement details for the precast columns, both Zones 2 and 4, were the same as those of the corresponding monolithic specimens. The reinforcement details for the Zone 4 precast concrete beams were identical to those of the Phase I precast concrete specimens except for the location of the post-tensioning bars/prestressing strands. Fig. 2.1 shows the reinforcement details for the precast concrete Zone 4 specimens and Fig. 2.2 shows the reinforcement details for the precast concrete Zone 2 specimens. The reinforcing bars located in the corners of the ties in the beams were used mainly to hold the ties together. The main resistance to the applied loads was provided by the post-tensioning bars/prestressing strands. Figs. 2.3 and 2.4 show the steel cages for the Zone 4 and Zone 2 specimens, respectively.

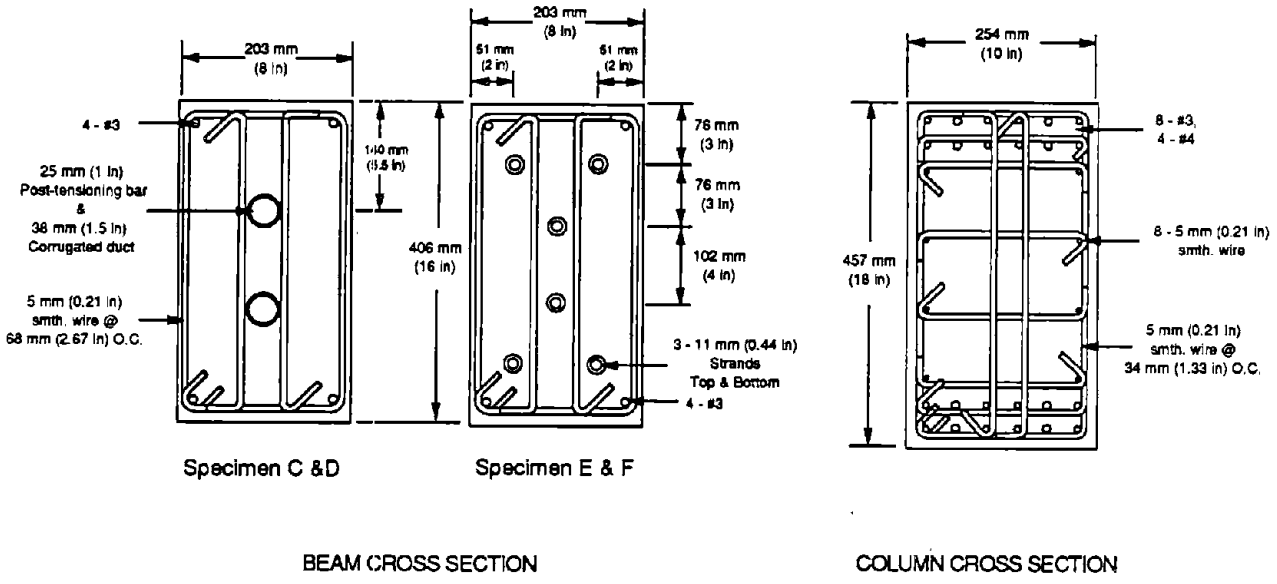

Fig. 2.1 Reinforcement details for precast concrete Zone 4 specimens.

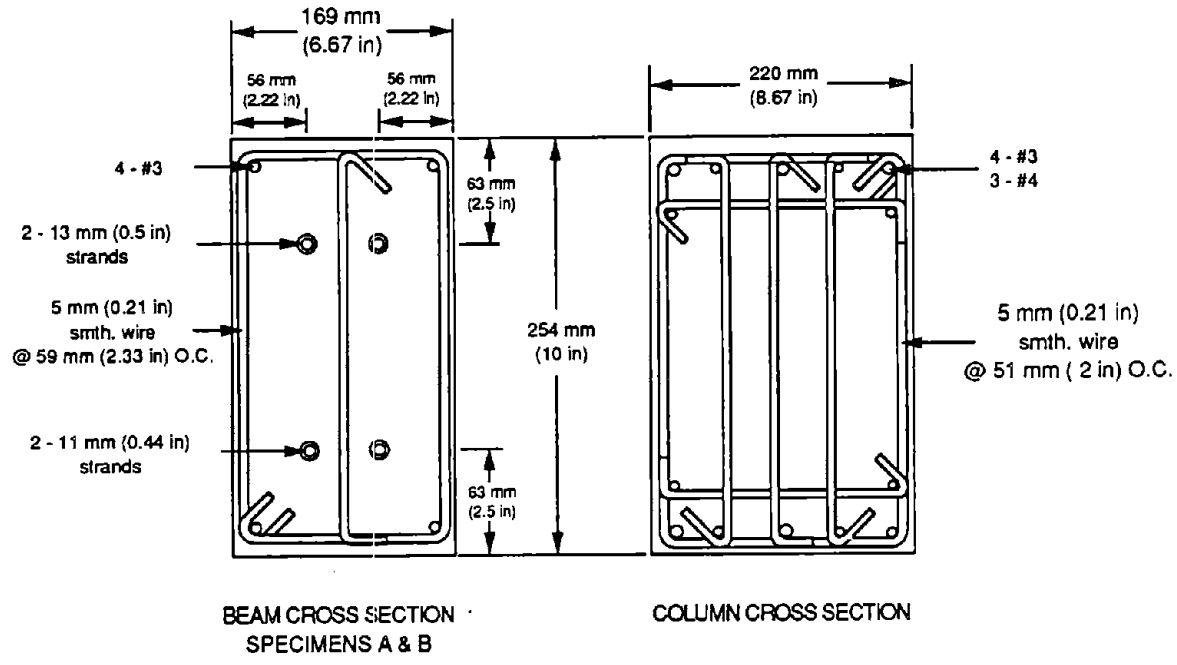

Fig. 2.2 Reinforcement details for precast concrete Zone 2 specimens.

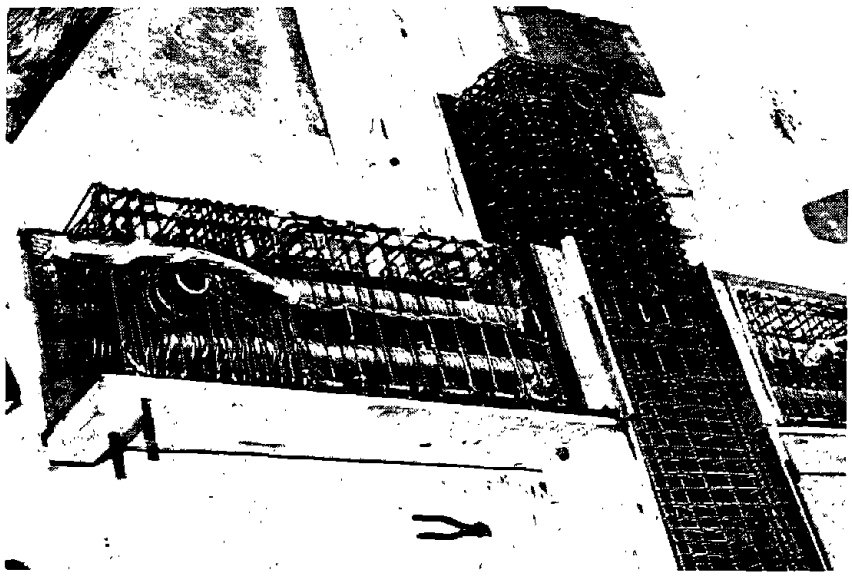

Fig. 2.3 Steel cages for specimen C-P-Z4 and D-P-Z4.

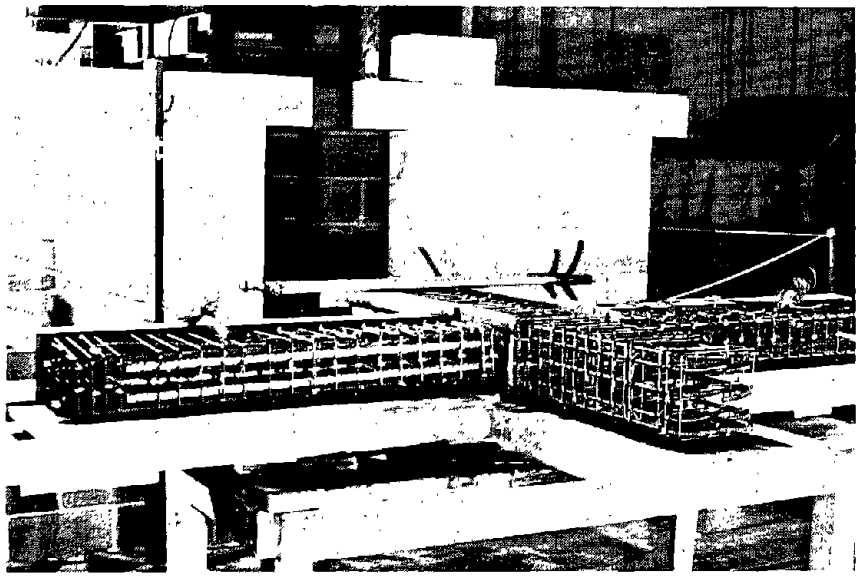

Fig. 2.4 Steel cages for A-P-Z2 and B-P-Z2.

A summary of the specimens tested to date (Phase I and II) is given in Table 2.1.

Table 2.1 Specimen Description.

Test Phase	Specimens	Description
I	A-M-Z2 & B-M-Z2	Monolithic Zone 2 specimens. Used as a reference for precast Zone 2 specimens.
II	A-P-Z2 & B-P-Z2	Precast Zone 2 specimens. Post-tensioned with 4 prestressing strands located 63 mm (2.5 in) from beam top/bottom.
I	A-M-Z4 & B-M-Z4	Monolithic Zone 4 specimens. Used as a reference for precast Zone 4 specimens.
I	A-P-Z4 & B-P-Z4	Precast Zone 4 specimens. Post-tensioned with 2 post-tensioning bars located 89 mm (3.5 in) from beam top/bottom.
II	C-P-Z4 & D-P-Z4	Precast Zone 4 specimens. Post-tensioned with 2 post-tensioning bars located 138 mm (5.5 in) from beam top/bottom.
II	E-P-Z4 & F-P-Z4	Precast Zone 4 specimens. Post-tensioned with 6 prestressing strands. Steel centroid located 102 mm (4.0 in) from beam top/bottom.

2.2 Material and Construction

The construction of the precast concrete specimens was similar to construction of the precast concrete specimens in Phase I. As shown in Figs. 2.3 and 2.4, the specimens were cast on their sides. A 25 mm (1.0 in) wide construction joint between the beam and column was filled with a fiber reinforced grout. The fibers used were 19 mm (0.75 in) long straight steel fibers. Roughening of the beam and column surfaces to approximately 6 mm (0.25 in) amplitude was done prior to post-tensioning the precast concrete elements. As in Phase I, corrugated ducts were used. The initial beam prestress was 10.5 MPa (1.5 ksi) and 7.0 MPa (1.0 ksi) for the precast concrete Zone 2 and Zone 4 specimens, respectively.

The non-prestressed reinforcement conformed to ASTM A706/A 706M requirements. The post-tensioning bars used conform to ASTM A-722 requirements and the low relaxation prestressing strands conform to ASTM A-416. The ties and crossties were made from smooth wire. As with the Phase I specimens, the design concrete strength was 34.5 MPa (5000 psi). Material properties are given in Tables 2.2 and 2.3.

Table 2.2 Steel Properties.

Specimen	f_y MPa [ksi]				f_u MPa [ksi]			
	Wire	#3	#4	PT	Wire	#3	#4	PT
C-P-Z4	574	466	419	1024[a]	627	620	669	1103
	[83]	[68]	[61]	[149]	[91]	[90]	[97]	[160]
D-P-Z4	574	466	419	1024[a]	627	620	669	1103
	[83]	[68]	[61]	[149]	[91]	[90]	[97]	[160]
E-P-Z4	543	512	419	1824[b]	593	772	669	1917
	[79]	[74]	[61]	[265]	[86]	[112]	[97]	[278]
F-P-Z4	543	512	419	1824[b]	593	772	669	1917
	[79]	[74]	[61]	[265]	[86]	[112]	[97]	[278]
A-P-Z2	543	466	419	1824[b]	593	510	669	1917
	[79]	[68]	[61]	[265]	[86]	[74]	[97]	[278]
				1717[c]				1917
				[249]				[278]
B-P-Z2	543	466	419	1824[b]	593	510	669	1917
	[79]	[68]	[61]	[265]	[86]	[74]	[97]	[278]
				1717[c]				1917
				[247]				[278]

a 25 mm (1.0 in) post-tensioning bar.
b 11 mm (0.44 in) prestressing strand at 1% strain.
c 13 mm (0.5 in) prestressing strand at 1% strain.

Table 2.3 Concrete and Grout Strengths.

Specimen	f'_c MPa [psi]		Duct Grout MPa [psi]		Joint Grout MPa [psi]	
	28-day	Test Date[a]	28-day	Test Date[a]	28-day	Test Date[a]
C-P-Z4	45.7 [6630]	46.8 [6780]	86.7 [12,570]	77.9 [11,290]	86.3 [12,510]	92.1 [13,360]
D-P-Z4	45.7 [6630]	44.9 [6510]	86.7 [12,570]	81.9 [11,890]	86.3 [12,150]	88.6 [12,850]
E-P-Z4	32.4 [4700]	29.2 [4230]	72.7 [10,540]	78.8 [11,430]	79.8 [11,570]	97.3 [14,110]
F-P-Z4	32.4 [4700]	27.7 [4020]	72.7 [10,540]	83.2 [12,060]	79.8 [[11,570]	101.4 [14,710]
A-P-Z2	31.1 [4510]	34.0 [4930]	62.6 [9,070]	68.3 [9,910]	75.7 [10,980]	87.4 [12,670]
B-P-Z2	31.1 [4510]	36.4 5280]	62.2 [9,070]	70.2 [10,180]	75.7 [10,980]	88.3 [12,810]

a These cylinders and cubes were stripped at the same time as the test specimens and allowed to cure in the same environment as the test specimens. The cylinders were 102 mm x 203 mm (4 in x 8 in) and the cubes were 51 mm x 51 mm (2 in x 2 in).

A major concern at the beginning of this phase of the test was the load loss in the strands due to seating of the chucks. This loss would be significant due to the short lengths of strand involved. As a result, several trial runs were made prior to post-tensioning the specimens to determine the amount of load loss and means to minimize this loss. As in the actual run, three strands were pulled at the same time in the trial runs. The procedure used was as follows:

1. Pull all three strands so that the total load was equal to 0.8 F_{pu}.
2. Seat the chucks and release the load.
3. Reload the strands to 0.8 F_{pu} and shim the chucks.
4. Release the load.

The basic setup of the jacking assembly for the Zone 4 specimens is shown in Fig. 2.5. In the trial runs, three load cells (one per strand) were used to monitor the loads in the strands. The steel box beam shown in Fig. 2.5 was cut to the same length as the specimens. Another area of concern was that all three strands be evenly loaded when pulled at the same time. Therefore, the hole in Plate A, as shown in Fig. 2.5, was chamfered so as to negate any misalignments of the jack. A 534 kN (60 ton) capacity, center-hole jack was used.

Five trial runs were made using 3 - 11 mm (0.44 in.) strands and one was made using 3 - 13 mm (0.5 in.) strands. The loads in the strands as obtained from the load cells indicated that the strands were evenly loaded. The results from these runs are given in Table 2.4. The loads given in Table 2.4 for the load cells were the sum of all three load cells. The individual load cell readings, 18 total, ranged from 0.58 F_{pu} to 0.77 F_{pu} with a mean of 0.69 F_{pu} and a standard deviation of 0.048 F_{pu}. On two of the runs, 4 and 6, the loads in the strands after 1 day (Run 4) and after 4 days (Run 6) showed a load drop of approximately 1% when compared with the loads read immediately after Step 4.

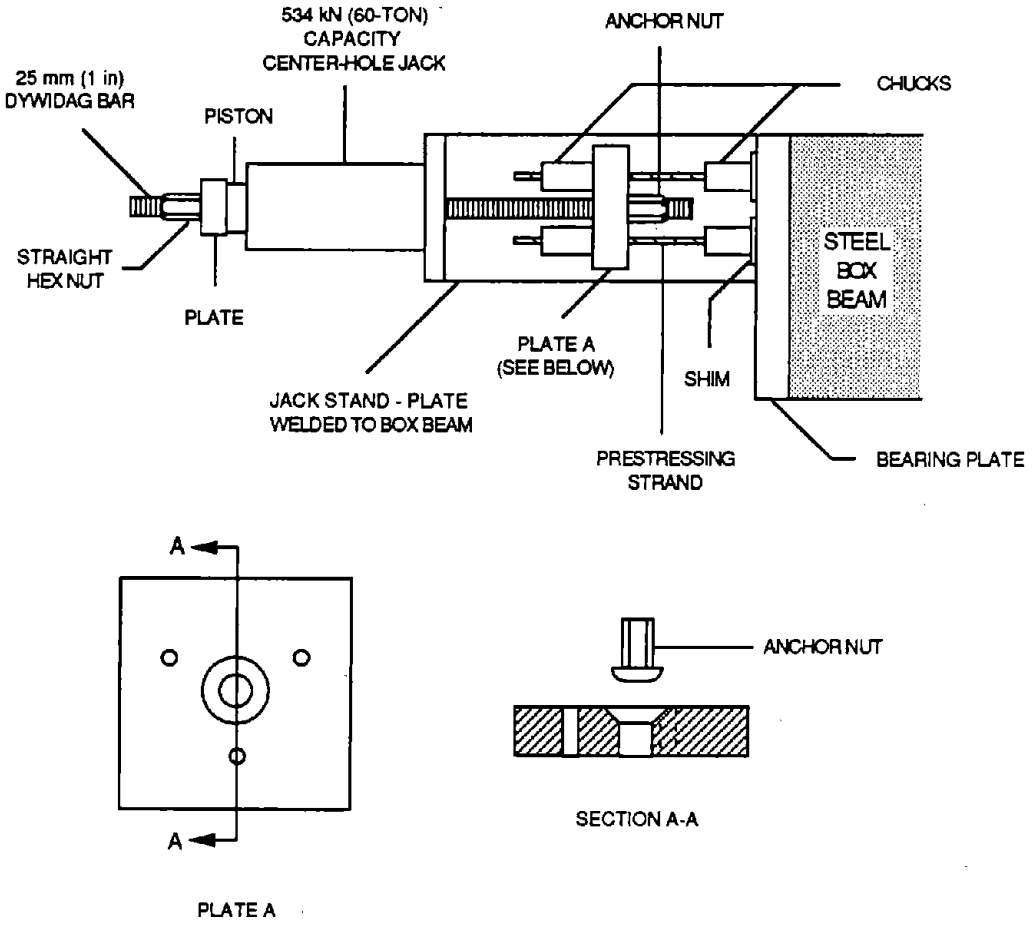

Fig. 2.5 Jacking assembly for precast concrete Zone 4 specimens.

Table 2.4 Prestress Losses.

Run	Step 1[a]		Step 2	Step 3		Step 4
	Jack[b]	Load Cell[c]	Load Cell	Jack	Load Cell	Load Cell
1	0.8 F_{pu}	0.78 F_{pu}	0.57 F_{pu}	0.8 F_{pu}	0.78 F_{pu}	0.66 F_{pu}
2	0.8	0.76	0.58	0.8	0.77	0.67
3	0.8	0.77	0.59	0.8	0.78	0.70
4	0.8	0.77	0.57	0.8	0.77	0.73
5	0.8	0.77	0.59	0.8	0.77	0.69
6[d]	0.8	0.76	0.59	0.8	0.76	0.69

a These step numbers refer to the post-tensioning trial run procedure described previously.
b Jacking load as read from a calibrated pressure transducer.
c Sum of the load from all three strands as read from individual load cells.
d Run in which 13 mm (0.5 in) strands were used.

The method used to post-tension the precast Zone 2 specimens was somewhat different from that used for the Zone 4 specimens. As shown in Fig. 2.2, two strands each top and bottom were used for the Zone 2 specimens. It was decided that the simplest way to post-tension the specimens was to use two jacks (one jack per strand) and pull both strands (top or bottom) simultaneously. Due to the limited space available at the end of the specimen, one jack was set up at one end of the specimen and the other at the opposite end as shown in Fig. 2.6. A 267 kN (30-ton), center-hole jack was used on each end of the specimen.

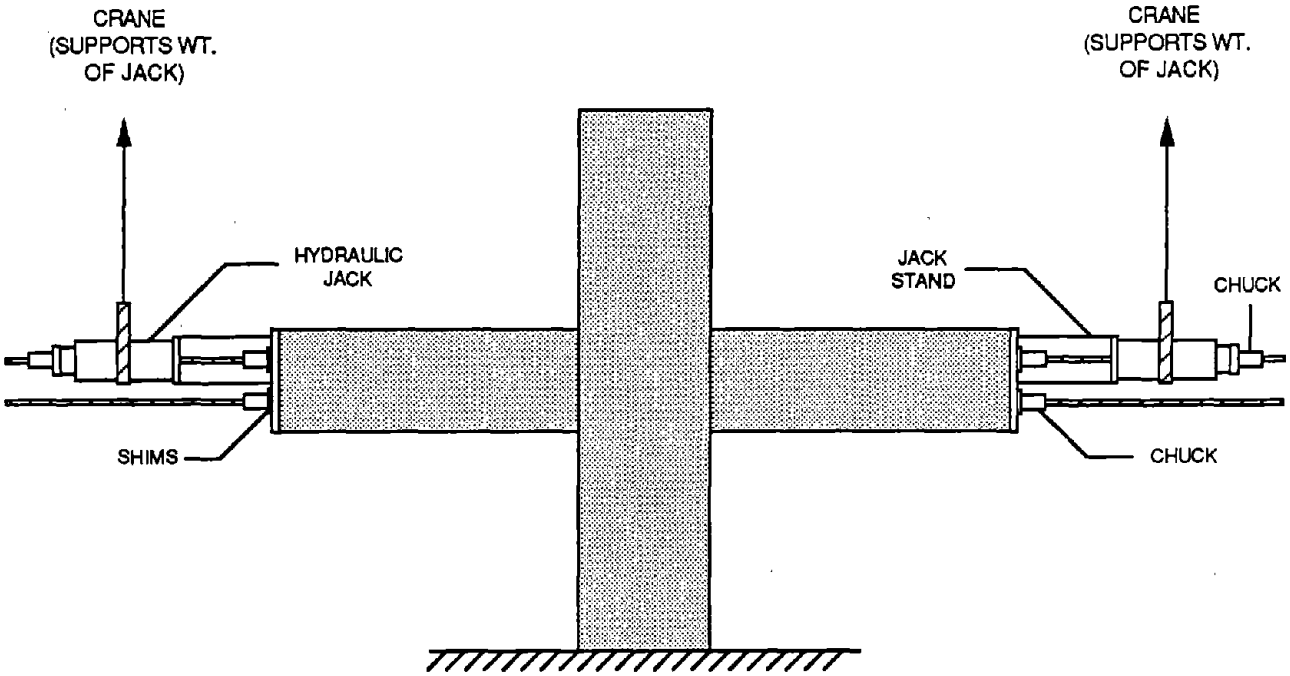

Fig. 2.6 Set-up for post-tensioning precast concrete Zone 2 specimens.

When the test specimens were post-tensioned, only two load cells were used - one top and one bottom. The Zone 4 specimens were post-tensioned in eight stages and the Zone 2 in ten stages. These stages were as follows:

Zone 2

1. Pull bottom strands to 0.4 F_{pu}.
2. Seat chucks and release load.
3. Pull top strands to 0.8 F_{pu}.
4. Seat chucks and release load.
5. Pull bottom strands to 0.8 F_{pu}.
6. Seat chucks and release load.
7. Pull bottom strands to 0.8 F_{pu}
8. Shim chucks and release load.
9. Pull top chucks to 0.8 F_{pu}.
10. Shim chucks and release load.

Zone 4

1. Pull top strands to 0.4 F_{pu}.
2. Seat chucks and release load.
3. Pull bottom strands to 0.8 F_{pu}.
4. Seat chucks and release load.
5. Pull bottom strands to 0.8 F_{pu}.
6. Shim chucks and release load.
7. Pull top strands to 0.8 F_{pu}.
8. Shim chucks and release load.

The loads in the two load cells after post-tensioning four of the specimens are given in Table 2.5 As seen in Table 2.5, the loads in the individual load cells were within one standard deviation of the mean as obtained in the trial runs.

Table 2.5 Load Cell Readings After Post-Tensioning.

Specimen	Load Cell 1[a]	Load Cell 2[b]
E-P-Z4	0.65 F_{pu}	0.65 F_{pu}
F-P-Z4	0.65 F_{pu}	0.67 F_{pu}
A-P-Z2	0.71 F_{pu}	0.67 F_{pu}
B-P-Z2	0.69 F_{pu}	0.70 F_{pu}

a Top set of strands.
b Bottom set of strands.
c 13 mm (0.5 in) Prestressing strands.

2.3 Instrumentation and Test Procedure

The same type of instrumentation was used in the Phase II tests as was used for the Phase I tests. This included load cells on the ends of the beams, LVDTs for displacement measurements and strain gages on the beam reinforcement. The LVDTs were used to measure column displacements, openings between the beam and column, and displacements at various locations on the beam. These beam displacements were used to compute the strain along the beam. However, rotation of the beams made such strain calculations erroneous.

Boundary conditions for the test specimens were as follows: pinned at the column bottom and roller supported at the column top and beam ends as shown in Fig. 2.7. The test set-up and test facility are shown in Fig. 2.8. Further details of the test facility may be found in Ref. 2.

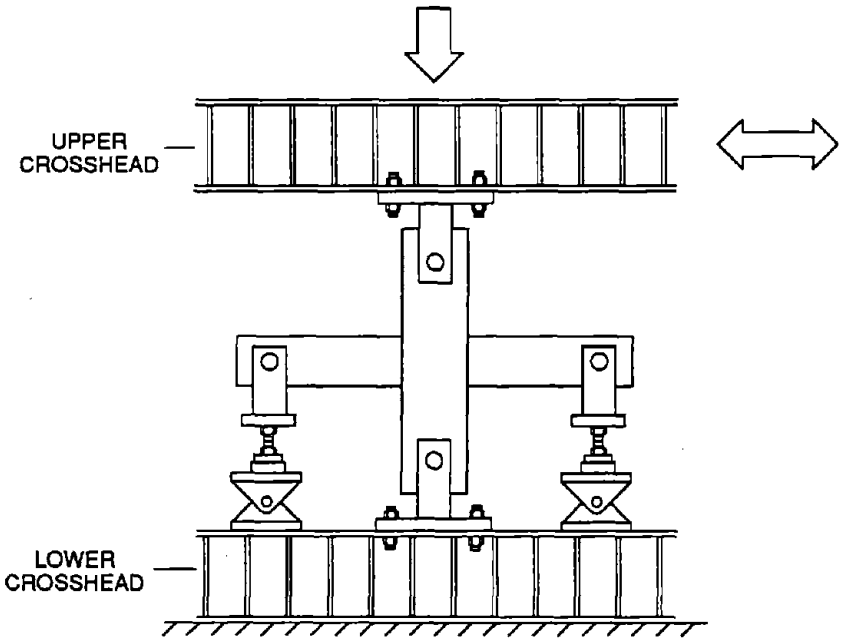

Fig. 2.7 Boundary conditions for the test specimens.

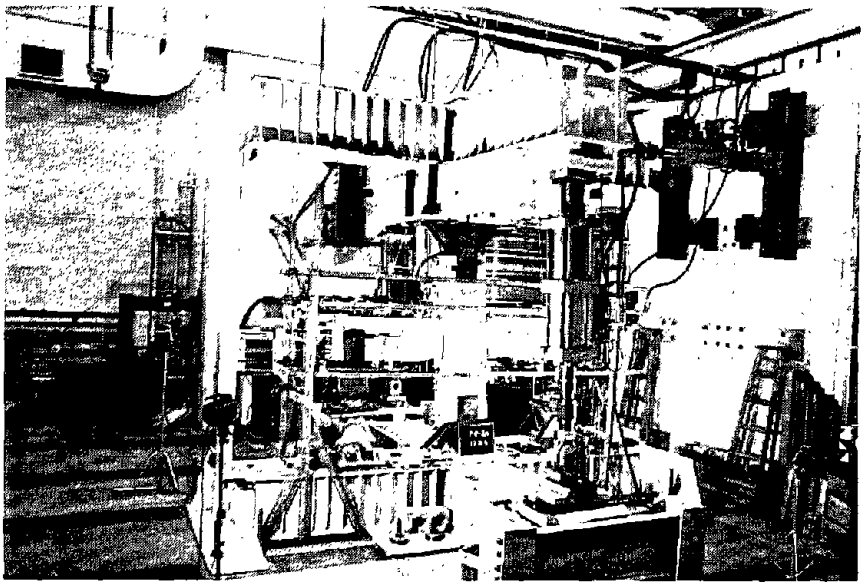

Fig. 2.8 Test set-up and test facility.

An axial load equal to 0.1 $f'_c A_g$ was applied to the column at the beginning of the test. The concrete strength was that obtained from the 28-day cylinder tests. The column was then laterally loaded at the column top for the initial elastic cycle. This initial elastic cycle was designed to develop a load equal to 75% of the calculated ultimate capacity of the monolithic beam. The top column displacements in the forward (south) and reverse (north) directions were measured. The yield displacement, Δ_y, was then defined as the average of these two displacements divided by 0.75. The specimen was then cycled in increments of Δ_y as described below.

The loading history for the precast Zone 4 specimens was two cycles each at $\pm$ 2 Δ_y and $\pm$ 4 Δ_y, three cycles each at $\pm$ 6 Δ_y and $\pm$ 8 Δ_y, two cycles at $\pm$ 10 Δ_y, and three cycles at $\pm$ 12 Δ_y. The loading sequence for the precast Zone 2 specimens was two cycles at $\pm$ 2 Δ_y, three cycles at $\pm$ 4 Δ_y, and two cycles at $\pm$ 6 Δ_y. These loading histories matched those for the corresponding monolithic specimens.

Displacement ductility, μ, is defined as the ratio of the maximum displacement achieved in any cycle to the yield displacement. Ultimate displacement ductility, μ_u, is defined as the ratio of the maximum displacement achieved for a specimen to the yield displacement. Failure was considered to have occurred when the lateral load dropped below 80% of the maximum load that was achieved in the first cycle at 2 Δ_y.

3.0 TEST OBSERVATIONS AND RESULTS

3.1 Precast Concrete Specimens C-P-Z4 and D-P-Z4

Specimens C-P-Z4 and D-P-Z4 were the precast Zone 4 specimens post-tensioned with two 25 mm (1 in.) post-tensioning bars and were detailed as shown in Fig. 2.1. The loading history for both specimens is shown in Fig. 3.1. The axial load on the column was 529 kN [119 kips] (0.1 $f'_c A_g$, based on a 28-day strength of 45.7 MPa [6628 psi]).

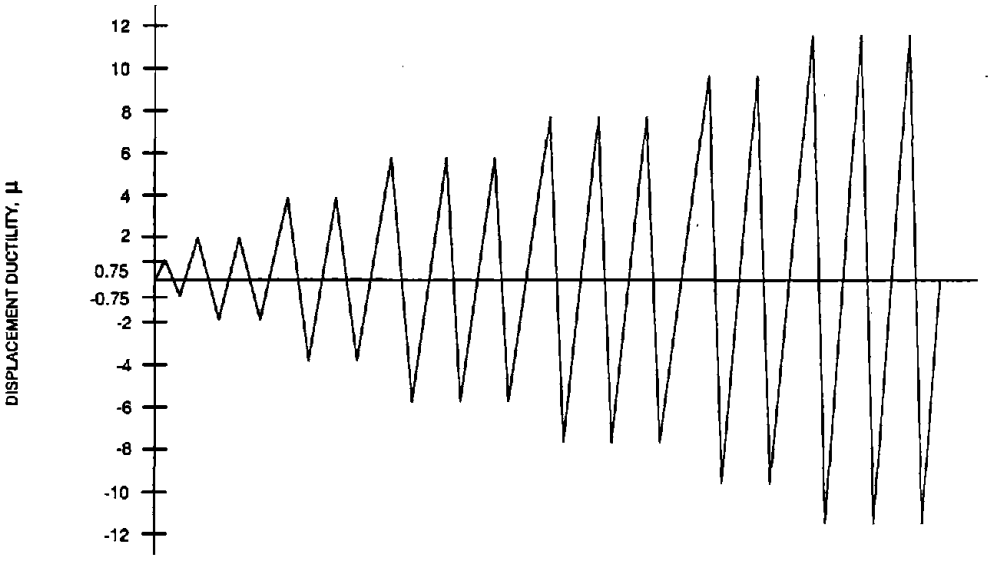

Fig. 3.1 Loading sequence for specimens C-P-Z4 through F-P-Z4.

In the initial elastic cycle, no cracks were observed in either specimen. This was also the case for the precast concrete specimens in Phase I. At 2 Δ_y, a few flexure and shear cracks were observed in this series of specimens. Very minor crushing of the beams was also noted at this ductility level. The crack between the beam and the construction joint was approximately 1 mm (0.04 in). Further cracking, shear and flexure, of both beams and columns was observed at 4 Δ_y. The crack pattern is shown in Fig. 3.2. Some minor spalling and crushing of the beams occurred at this stage of the test. The opening between the beam and construction joint as shown in Fig. 3.3 was approximately 4 mm (0.2 in). Additional cracking of the specimens was observed at 6 Δ_y with the majority of the cracks occurring in the first cycle at 6 Δ_y. The crack pattern in the joint region is shown in Fig. 3.4. Continued crushing of the beams and widening of the opening between the beam and the construction joint were noted at this ductility level. The total opening between the beam and column was approximately 9 mm (0.4 in). Henceforth, the "beam-column opening" shall be defined as the sum of the opening between the beam and the grout joint and the grout joint and the column. The extent of crushing in the beam and the beam-column opening are shown in Figs. 3.5 and 3.6, respectively.

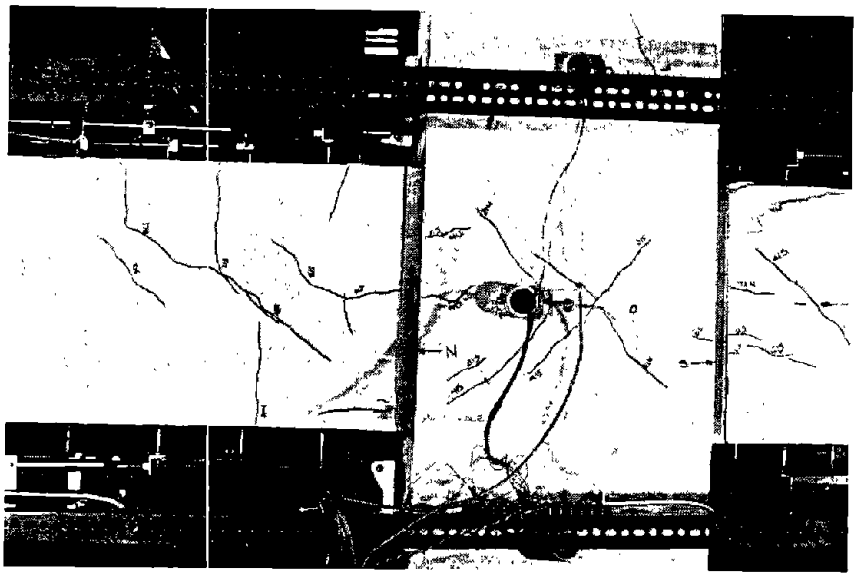

Fig. 3.2 Crack pattern for specimen C-P-Z4 at 4 Δ_y.

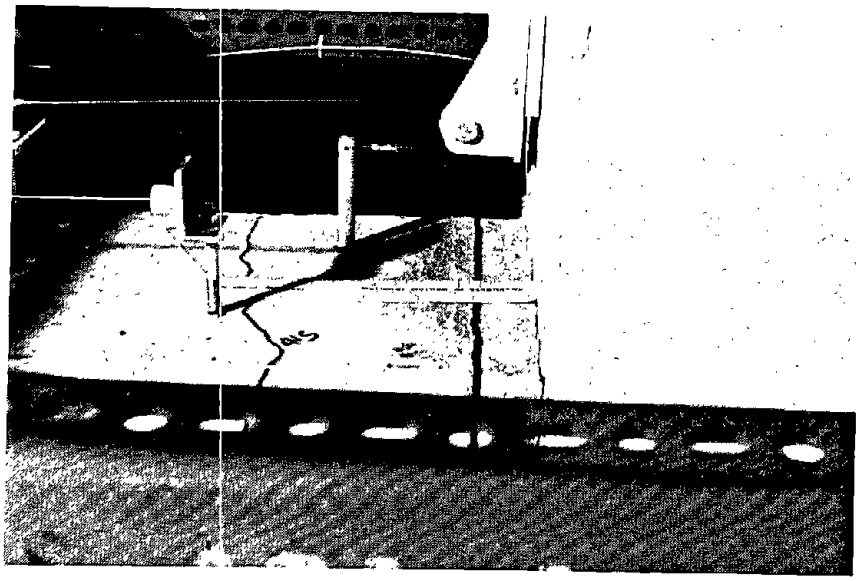

Fig. 3.3 Opening between the beam and construction joint at 4 Δ_y.

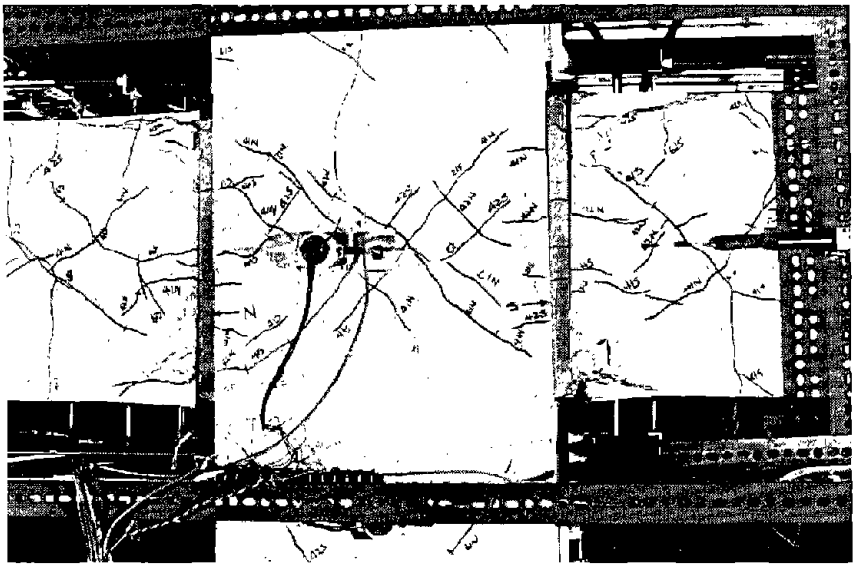

Fig. 3.4 Crack pattern for C-P-Z4 at 6 Δ_y.

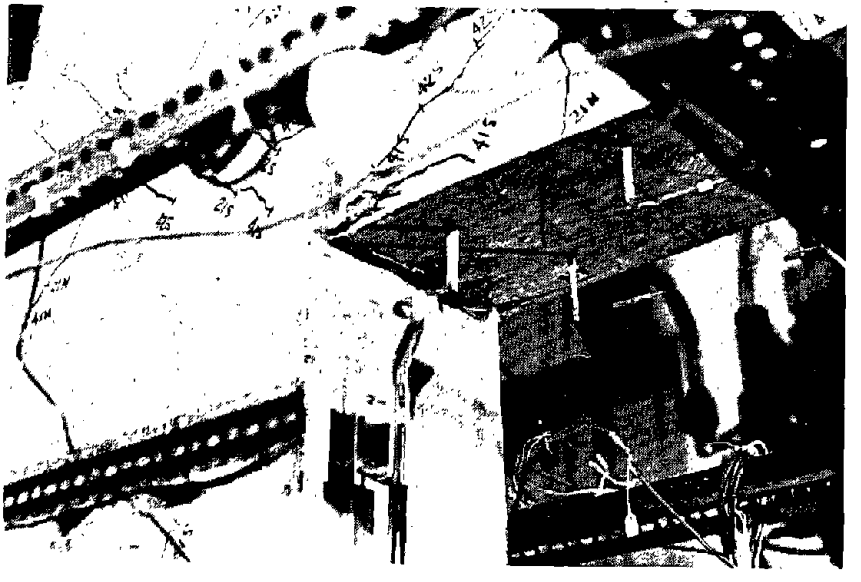

Fig. 3.5 Crushing of the beam at 6 Δ_y - C-P-Z4.

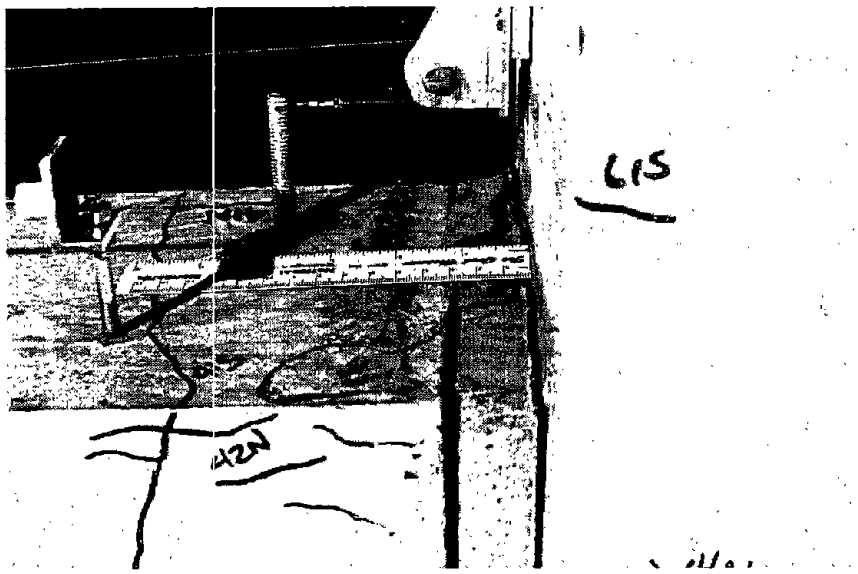

Fig. 3.6 Opening between the beam and column at 6 Δ_y - C-P-Z4.

No significant change in the crack pattern was observed at 8 Δ_y. Some splitting cracks (cracking of the beam top/bottom longitudinally) in the beams were noticed at this ductility level. At this point in the test, only additional beam crushing and widening of the beam-column opening were observed as depicted in Fig. 3.7. The beam-column opening was approximately 16 mm (0.6 in). The crack widths in the column joint region and in the beams were still small. Crack propagations, continued crushing and spalling of the beams, and widening of the beam-column joint were noted at 10 Δ_y. The beam-column opening was approximately 20 mm (0.8 in) at 10 Δ_y.

Both connections failed at 12 Δ_y. Views of the overall connection and close-ups of the beams for specimen C-P-Z4 are shown in Fig. 3.8, 3.9, and 3.10. Fig. 3.11 shows an overall view of specimen D-P-Z4 at failure, μ = 12 Δ_y. As seen in Fig. 3.9, extensive crushing and spalling of the beams occurred at 12 Δ_y. Also, as seen in Fig. 3.10, other than sustaining minor crushing and spalling, the grout joint performed well throughout the test. The beam-column opening at failure was approximately 25 mm (1.0 in). Spalling of beams occurred over an area which averaged 241 mm (9.5 in) from the column face.

Fig. 3.7 Beam damage at 8 Δ_y - C-P-Z4.

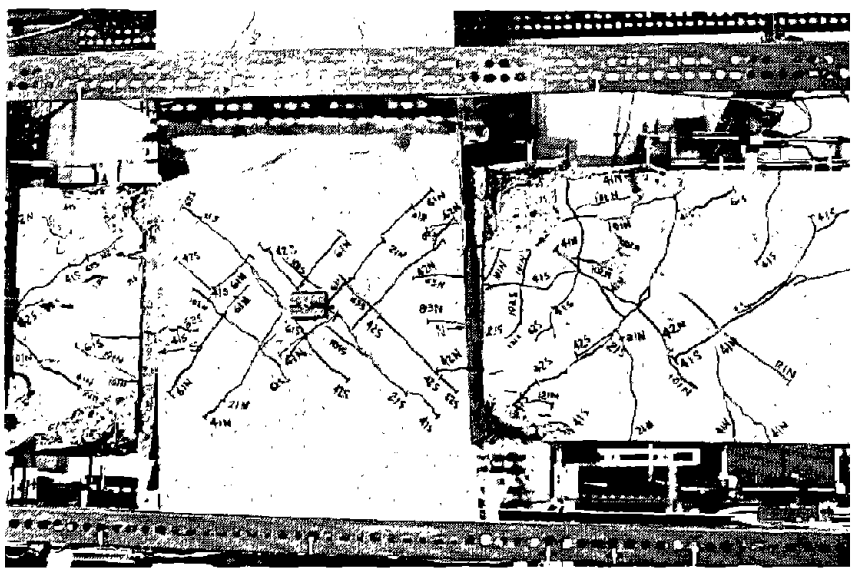

Fig. 3.8 Specimen C-P-Z4 at failure - 12 Δ_y.

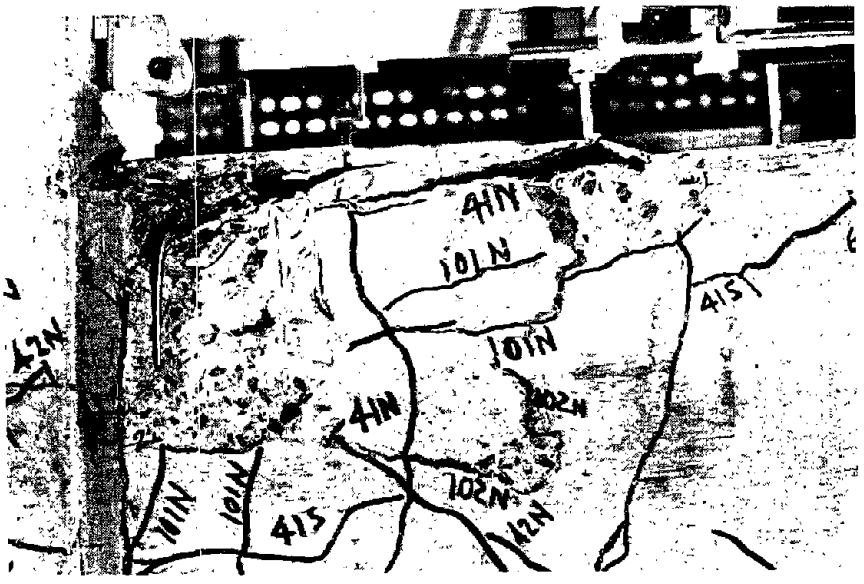

Fig. 3.9 Crushing of beams at 12 Δ_y - C-P-Z4.

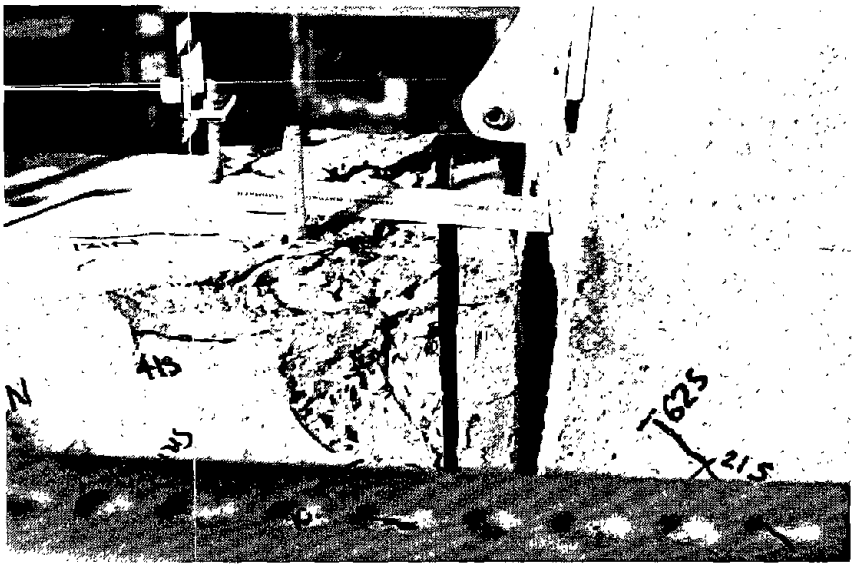

Fig. 3.10 Opening between beam and column - C-P-Z4.

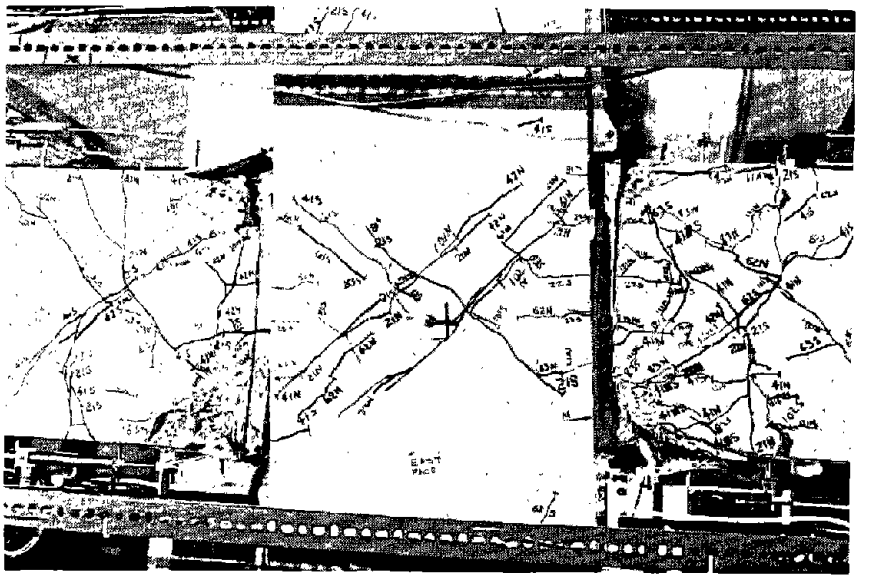

Fig. 3.11 Specimen D-P-Z4 at failure - 12 Δ_y.

The load displacement plots for C-P-Z4 and D-P-Z4 are given in Figs. 3.12 and 3.13, respectively. The load in the figures is the lateral load at the top of the column and the displacement is the displacement of the column top. As seen in the figures, the specimens exhibited stable behavior until failure and severely pinched hysteresis curves. The experimental yield displacement was 5.3 mm (0.209 in) and 5.4 mm (0.213 in) for specimens C-P-Z4 and D-P-Z4, respectively. As was mentioned earlier, the ultimate displacement ductility for both specimens was 12.

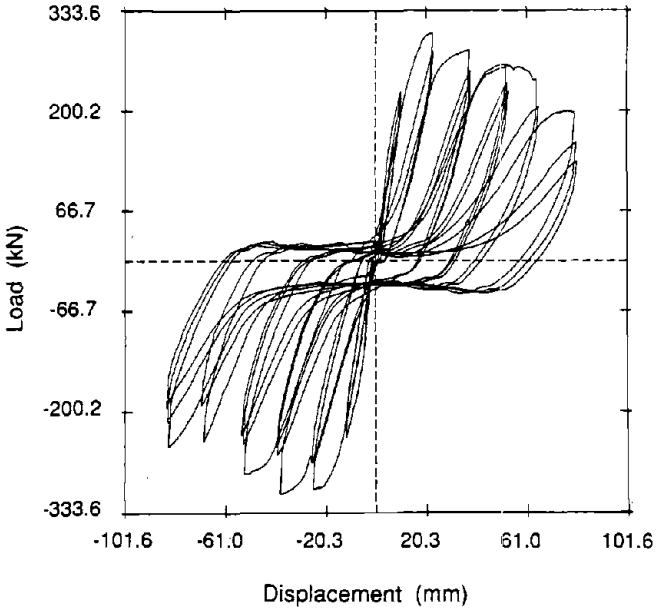

Fig. 3.12 Hysteresis curves for C-P-Z4.

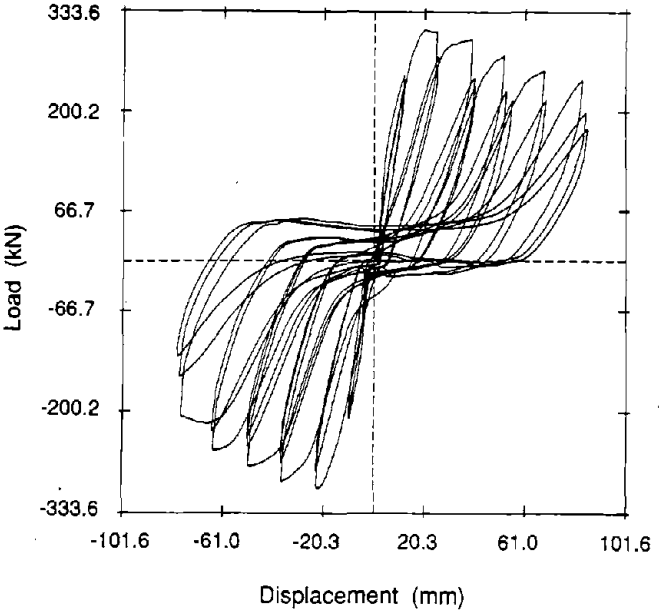

Fig. 3.13 Hysteresis curves for D-P-Z4.

The experimental ultimate moments for C-P-Z4 were 169 kN-m (125 k-ft) and 171 kN-m (126 k-ft) at the face of the column. The first value was obtained in the first cycle at 6 Δ_y and the second in the first cycle at 4 Δ_y. Similar values, 165 kN-m (122 k-ft) and 169 kN-m (125 k-ft), were obtained for specimen D-P-Z4. Both of these values were obtained in the first cycle at 4 Δ_y.

A comparison of the energy absorbed by each specimen on a per cycle basis is shown in Fig. 3.14. The energy absorbed is defined as the area enclosed by the load displacement curve. As indicated by Figs. 3.12 and 3.13 and as seen in Fig. 3.14, both specimens behaved in a very similar fashion. The cumulative energy absorbed to failure by specimen C-P-Z4 was 93.9 kN-m (831 k-in) and by specimen D-P-Z4 was 92.9 kN-m (822 k-in).

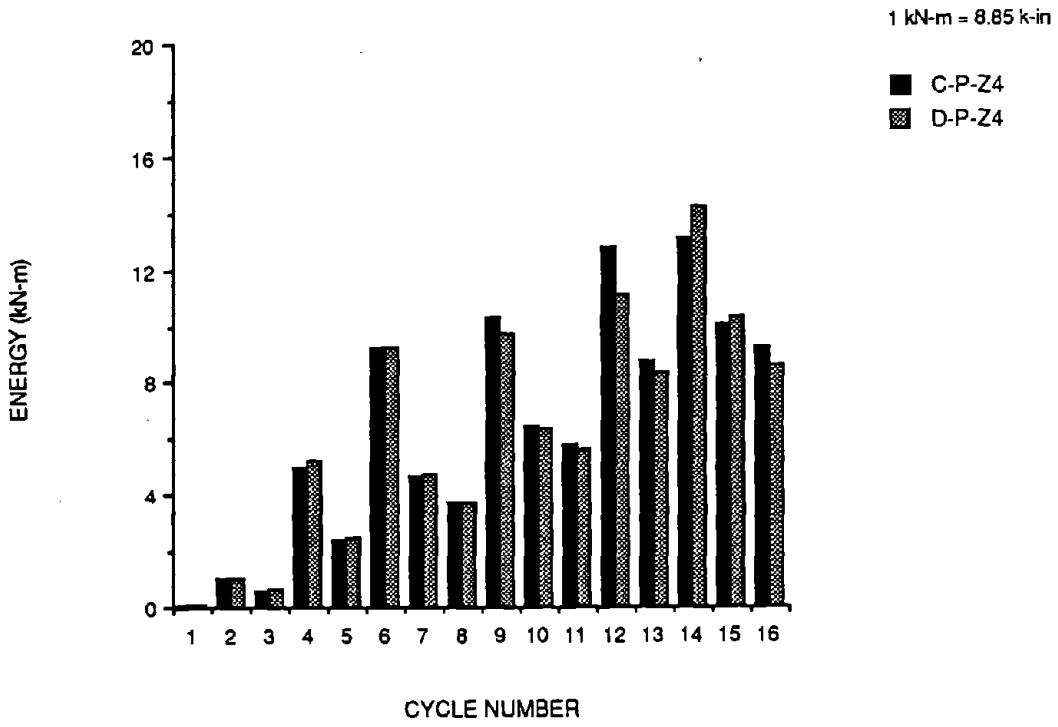

Fig. 3.14 Energy absorbed per cycle by specimens C-P-Z4 and D-P-Z4.

The maximum strains in the reinforcing bars are shown in Figs. 3.15 through 3.30. In these figures, the term "11 S" refer to the first cycle at $\mu = 0.75\ \Delta_y$ on the excursion to the south, "41 S" refer to the first cycle at $\mu = 4\ \Delta_y$ on the excursion south, "122 N" refer to the second cycle at $\mu = 12\ \Delta_y$ on the excursion north, and so forth. Recall that the precast concrete beams have four #3 reinforcing bars located in the corners of the ties. In the following and subsequent figures which show the extent of reinforcing bar yielding, the term "northeast" refers to a reinforcing bar located on the east side of the north beam, "southwest" refers to a reinforcing bar located on the west side of the south beam, etc. Also, "top" refers to the top of the beam. The average extent of reinforcing bar yielding was 393 mm (15 in) for C-P-Z4 and 337 mm (13 in) for D-P-Z4. These average values were determined from Figs. 3.15 through 3.30. The yield length for each bar was defined as the length at which the strain in the reinforcing bar was greater than or equal to the yield strain. However, as observed during the tests and from Figs. 3.15 through 3.30, the yielding in the beam reinforcement was not extensive. Also from Figs. 3.15 through 3.30, it can be seen that the highest strains recorded in the reinforcement occurred at $\mu = 4\ \Delta_y$. In the following cycles, the strains in the beam reinforcement decreased indicating that debonding of the post-tensioning bars occurred at this stage and that the main load resistance to the applied loads was provided by the post-tensioning bars.

Three ties in the beams were instrumented with strain gages. Of the three, only the first tie, located 42 mm (1.7 in) away from the column face, yielded. The other two ties were located 110 mm (4.3 in) and 245 mm (9.7 in) away from the column face. The highest recorded strains in these ties were approximately half of the yield strain or less.

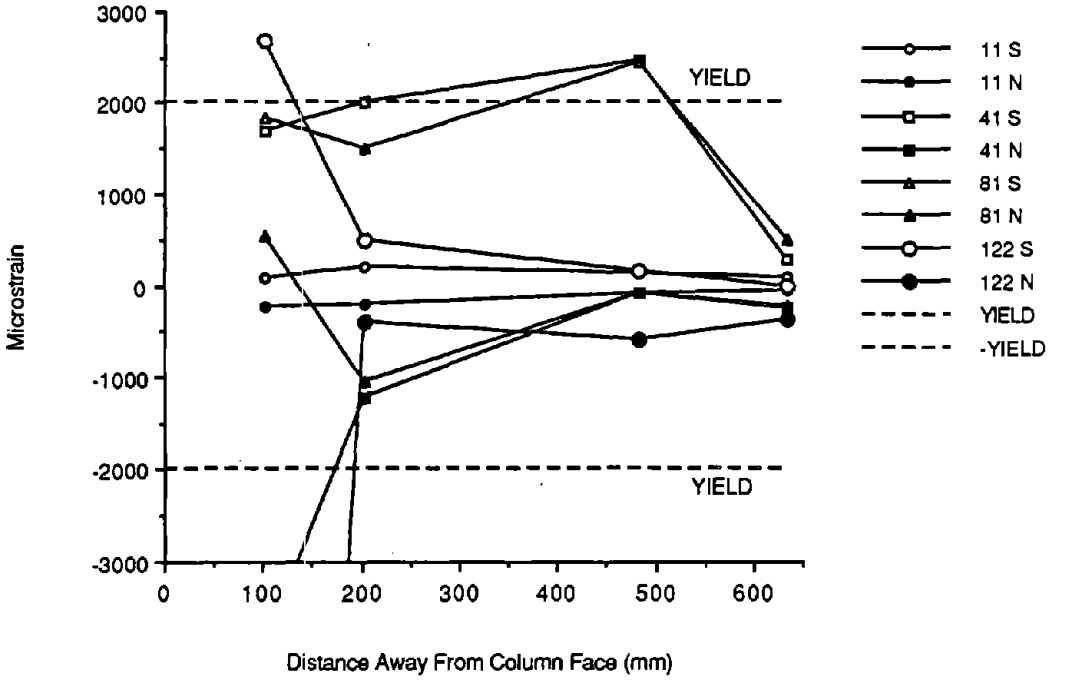

Fig. 3.15 Top northeast reinforcing bar strains - C-P-Z4.

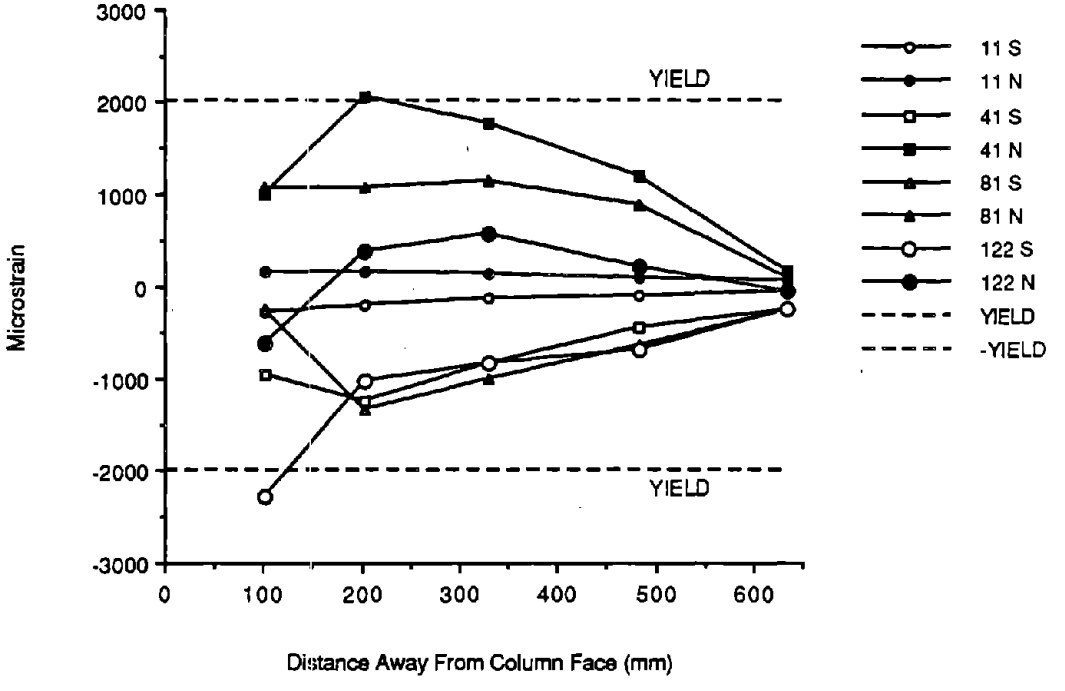

Fig. 3.16 Bottom northeast reinforcing bar strains - C-P-Z4.

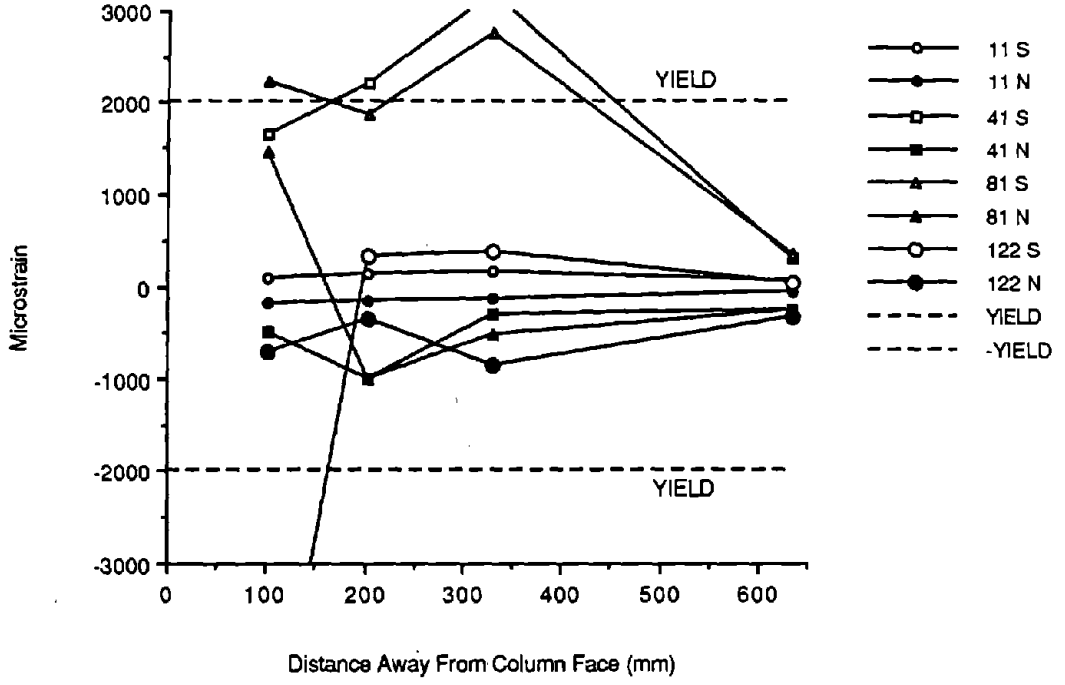

Fig. 3.17 Top northwest reinforcing bar strains - C-P-Z4.

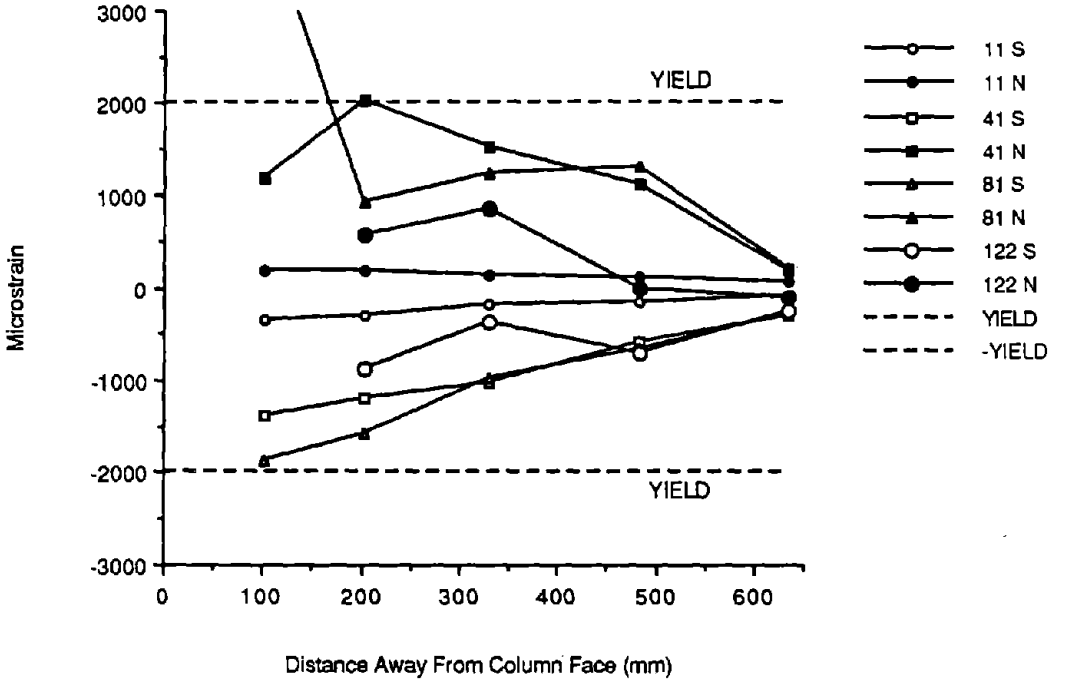

Fig. 3.18 Bottom northwest reinforcing bar strains - C-P-Z4.

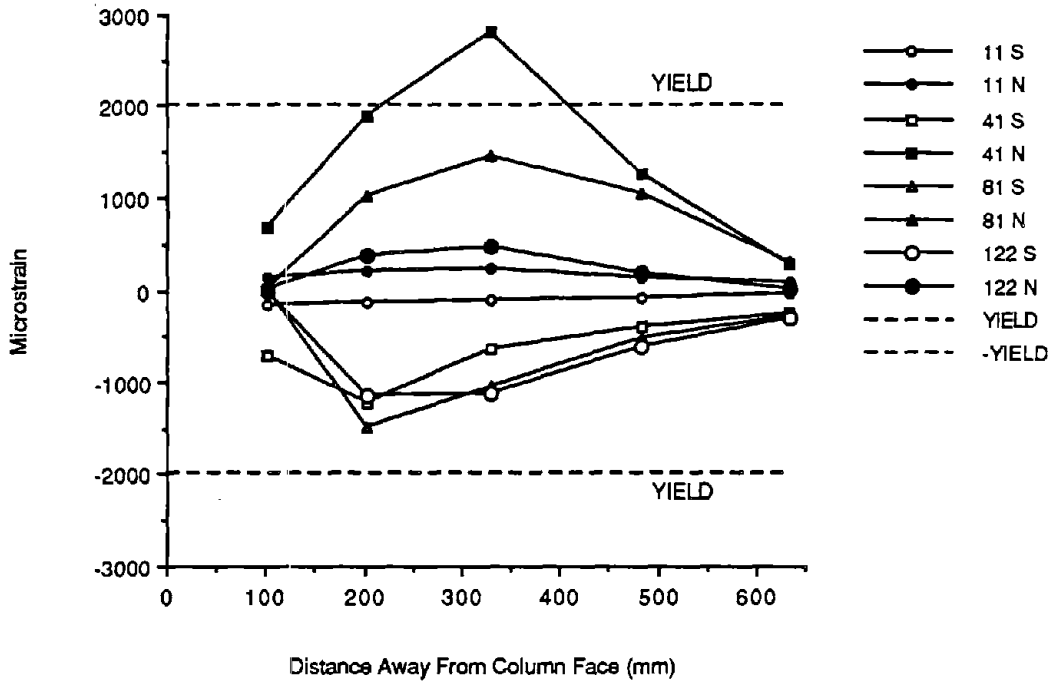

Fig. 3.19 Top southeast reinforcing bar strains - C-P-Z4.

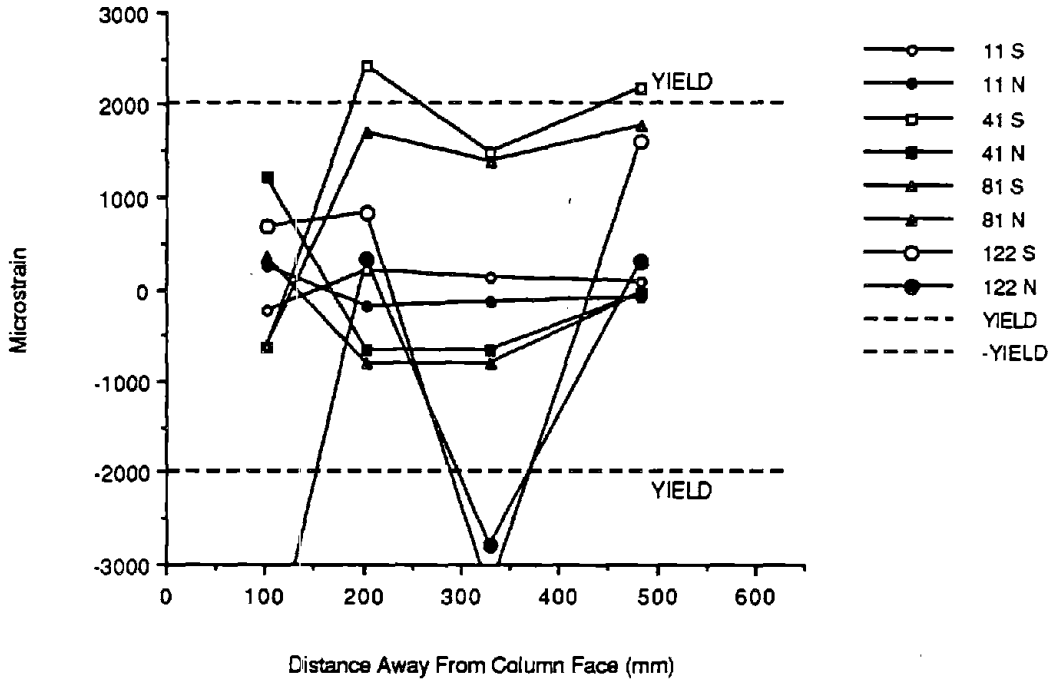

Fig. 3.20 Bottom southeast reinforcing bar strains - C-P-Z4.

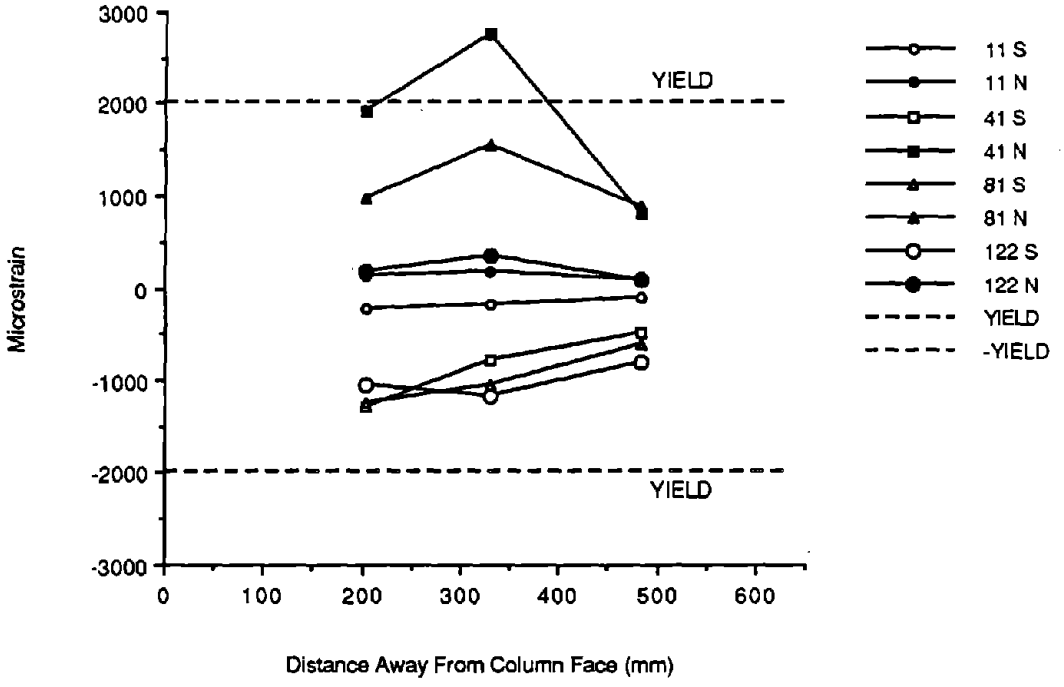

Fig. 3.21 Top southwest reinforcing bar strains - C-P-Z4.

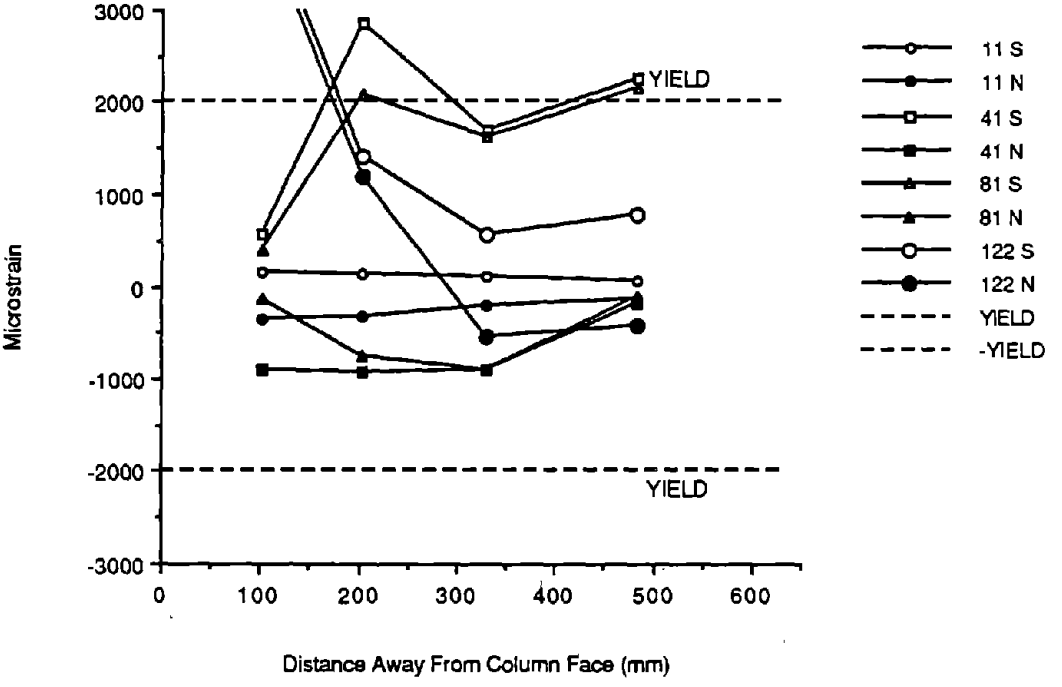

Fig. 3.22 Bottom southwest reinforcing bar strains - C-P-Z4.

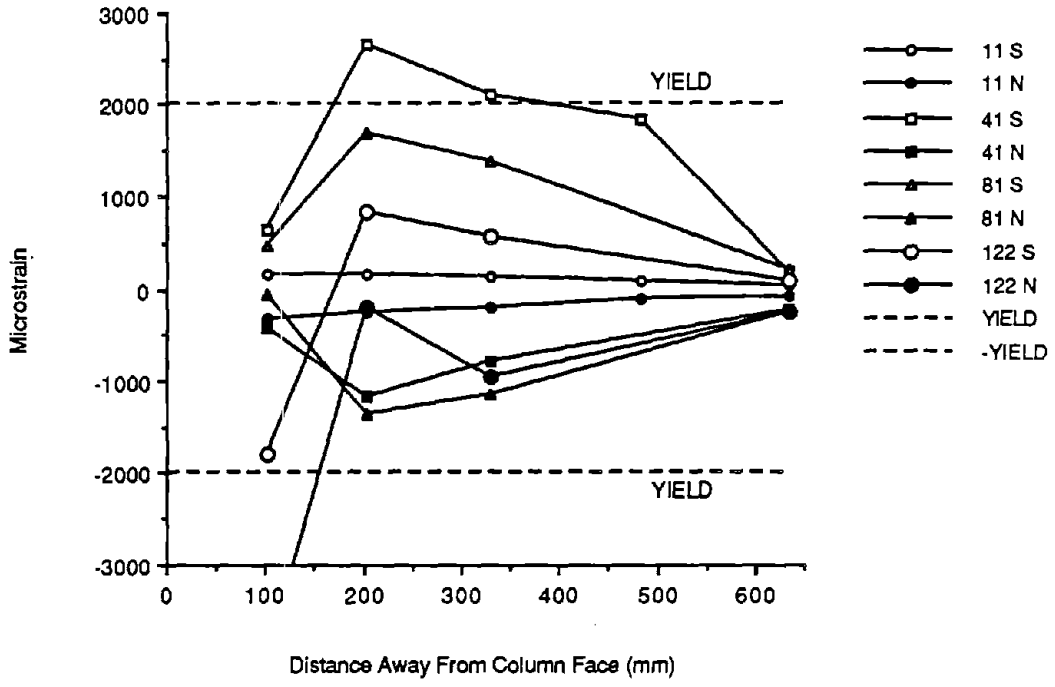

Fig. 3.23 Top northeast reinforcing bar strain - D-P-Z4.

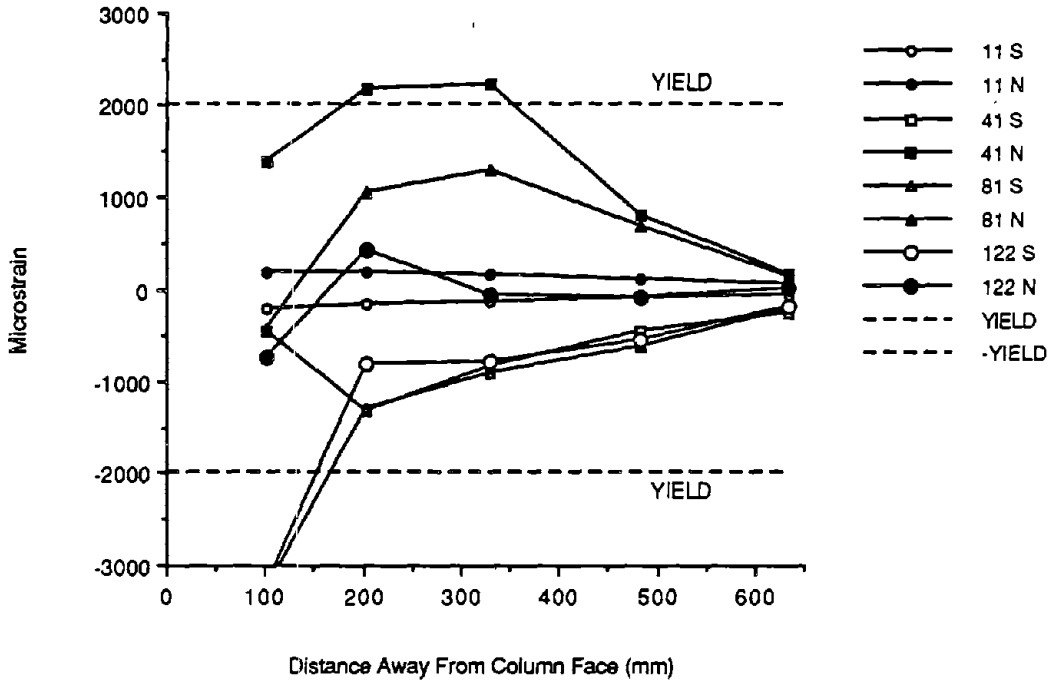

Fig. 3.24 Bottom northeast reinforcing bar strains - D-P-Z4.

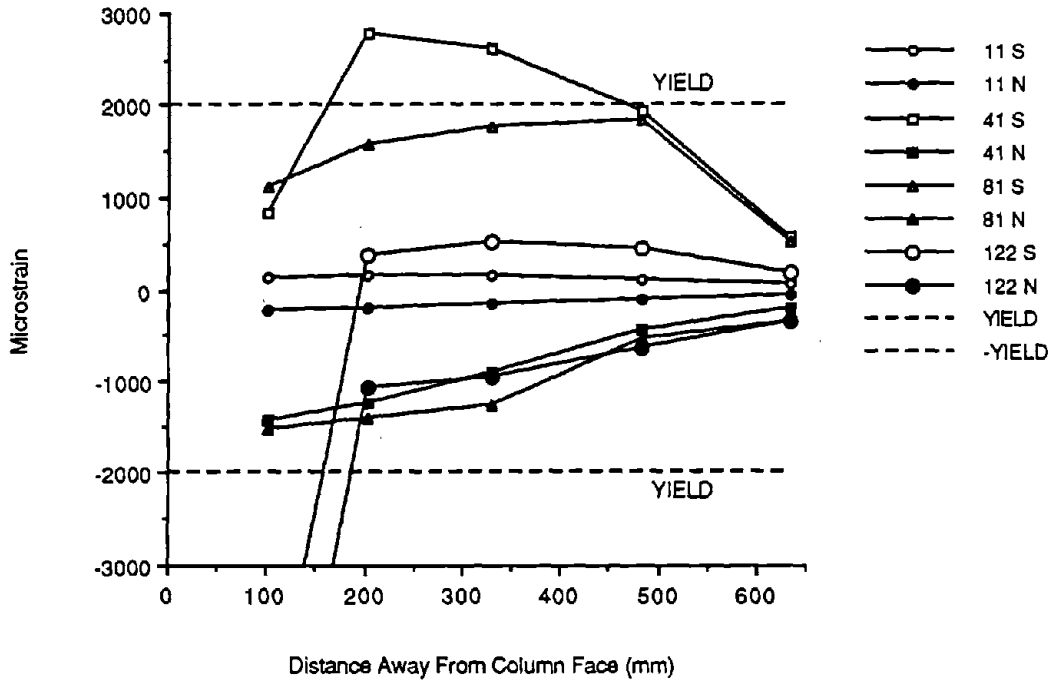

Fig. 3.25 Top northwest reinforcing bar strains - D-P-Z4.

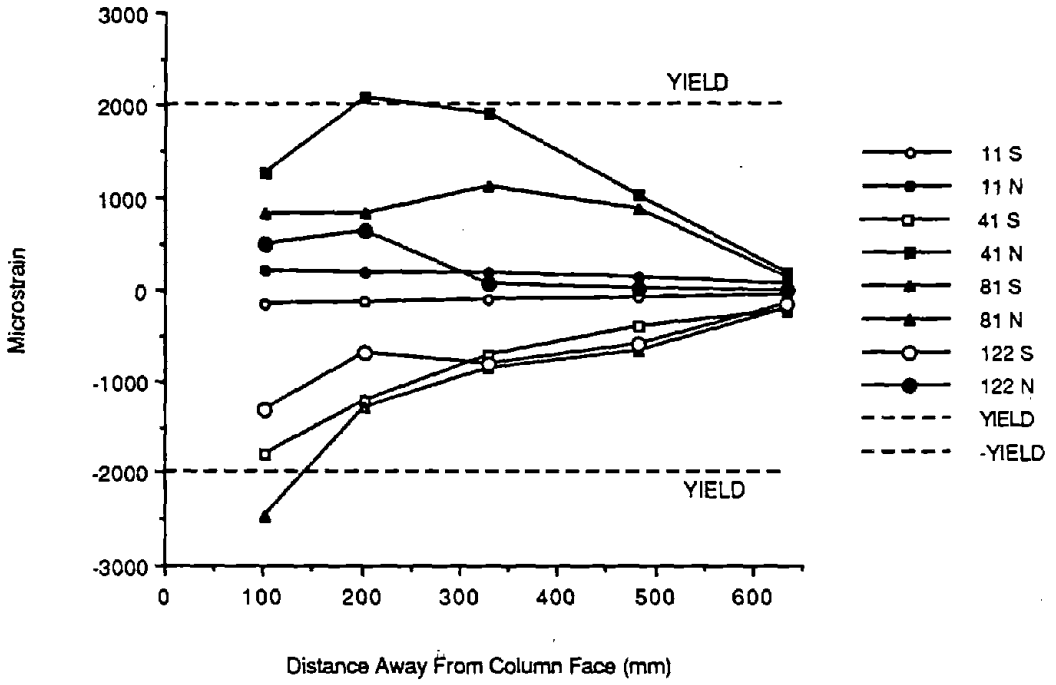

Fig. 3.26 Bottom northwest reinforcing bar strains - D-P-Z4.

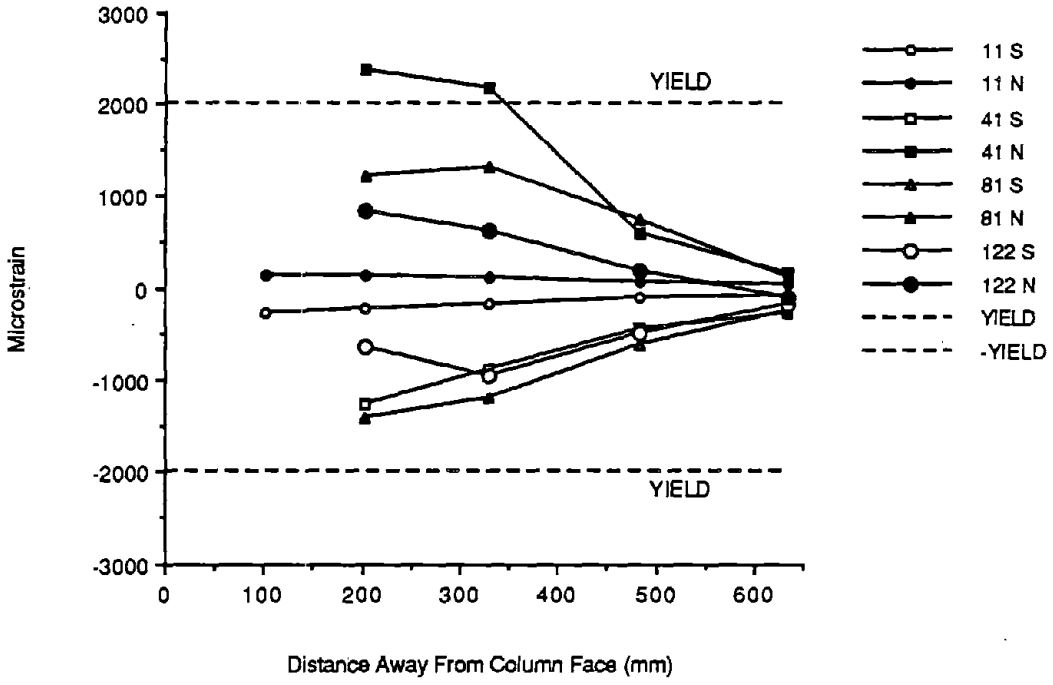

Fig. 3.27 Top southeast reinforcing bar strains - D-P-Z4.

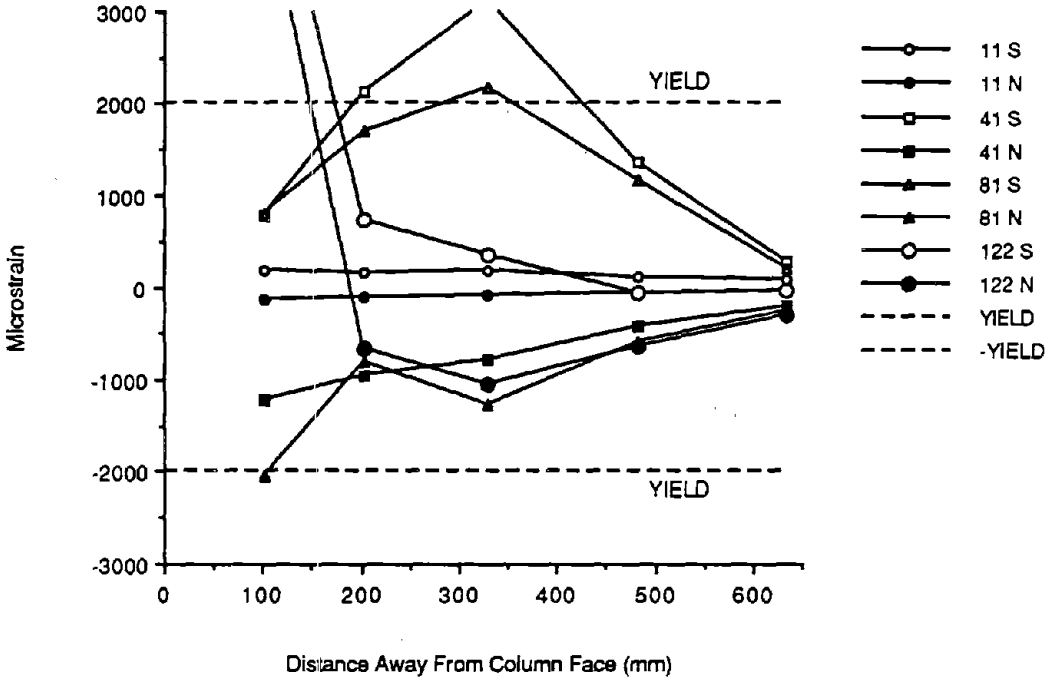

Fig. 3.28 Bottom southeast reinforcing bar strains - D-P-Z4.

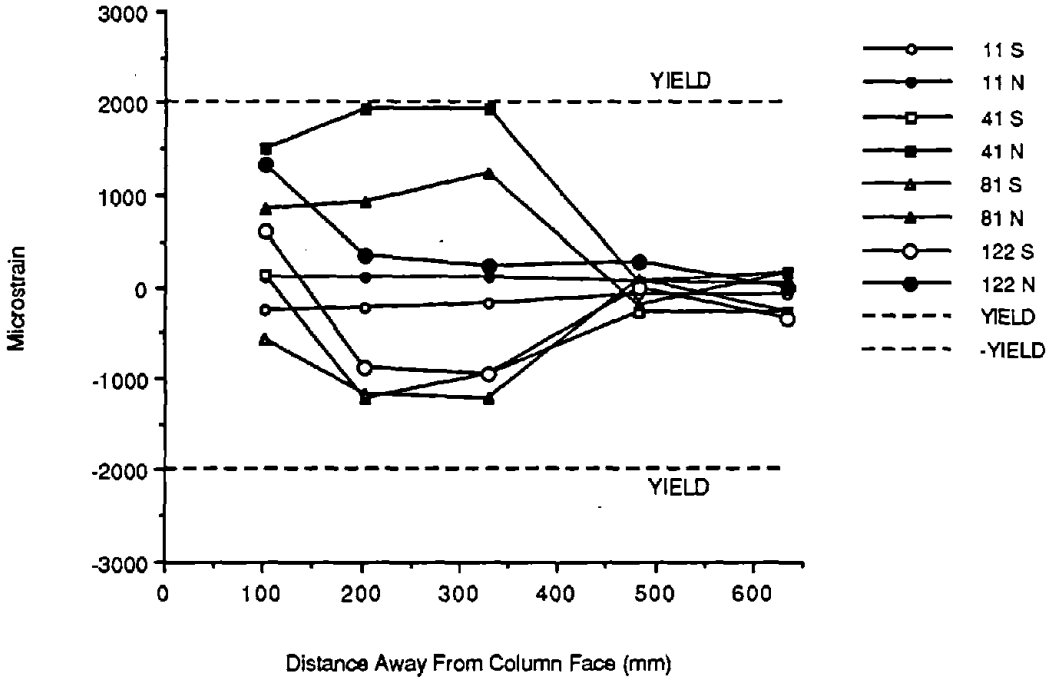

Fig. 3.29 Top southwest reinforcing bar strains - D-P-Z4.

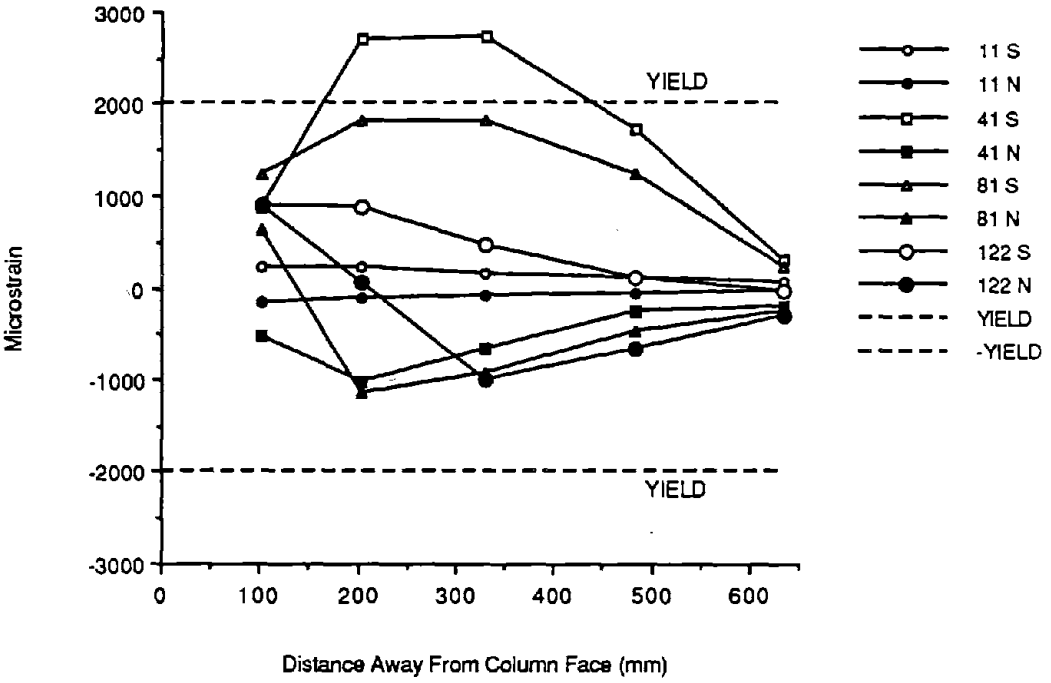

Fig. 3.30 Bottom southwest reinforcing bar strains - D-P-Z4.

3.2 Precast Concrete Specimens E-P-Z4 and F-P-Z4

Specimens E-P-Z4 and F-P-Z4 are the Zone 4 precast concrete specimens which were post-tensioned using 6 - 11 mm (0.44 in) prestressing strands as shown in Fig. 2.1. The loading histories for specimens E-P-Z4 and F-P-Z4 were identical to those for the previous precast concrete specimens as shown in Fig. 3.1. The applied axial load was 376 kN [84.5 kips] (0.1 f'_c A_g based on a 28-day strength of 32.4 MPa [4698 psi]).

In the initial elastic cycle, no cracks were noted in either specimen as was the case for the previous four precast concrete specimens. At 2 Δ_y, a few flexure and shear cracks were observed in the beams and in the column. Very minor crushing in the beams was noted in F-P-Z4 at 2 Δ_y. The shear cracks in the column of F-P-Z4, Fig. 3.31, differed slightly from those in specimen E-P-Z4 in that the cracks in F-P-Z4 started out as flexure cracks, then became shear cracks and were slightly shallower than those in specimen E-P-Z4. The shear cracks in specimen E-P-Z4 are shown in Fig. 3.32. This slight variation in the shear cracks could a result of one of the ducts in specimen F-P-Z4 not being completely grouted. More cracking and crack propagation occurred at 4 Δ_y. Additional beam crushing also occurred at this stage. The opening between the beam and column was approximately 5 mm (0.2 in) as shown in Fig. 3.33. The extent of beam crushing is shown in Fig. 3.34.

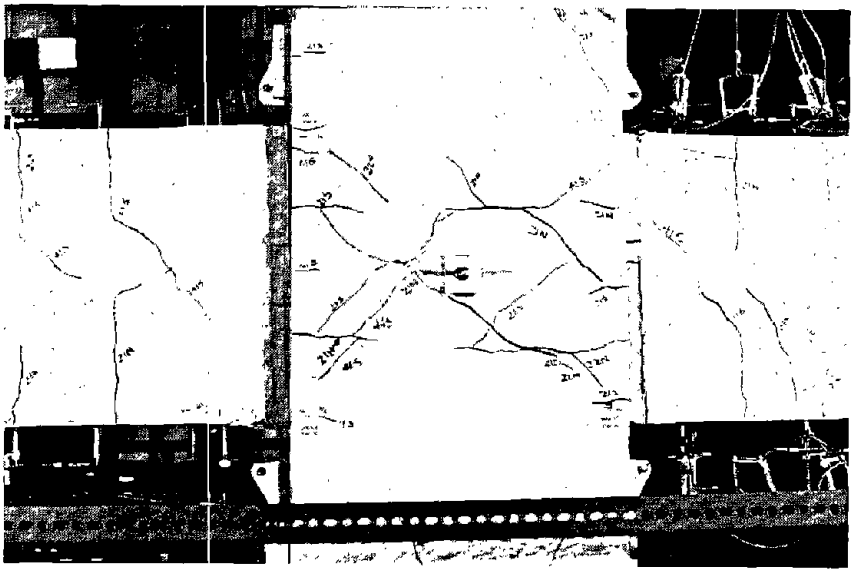

Fig. 3.31 Shear cracks in F-P-Z4 at 4 Δ_y.

Fig. 3.32 Shear cracks in E-P-Z4 at 4 Δ_y.

Fig. 3.33 Opening between beam and column at 4 Δ_y, F-P-Z4.

Fig. 3.34 Crushing of beam at 4 Δ_y, F-P-Z4.

Minor cracking and crack extensions were noted at both 6 Δ_y and 8 Δ_y. Continued beam crushing and spalling also occurred at these ductility levels. The opening between the beam and column was approximately 11.5 mm (0.45 in) at 6 Δ_y and 15.5 mm (0.61 in) at 8 Δ_y. The crack pattern, beam opening and crushing for specimen F-P-Z4 at 8 Δ_y are shown in Fig. 3.35. No significant change in the crack pattern occurred at the next two ductility levels, 10 Δ_y and 12 Δ_y. Further widening of the opening between the beam and the column and crushing of the beams took place at these ductility levels. The openings between the beam and column were approximately 21.5 mm (0.85 in) at 10 Δ_y and 27 mm (1.06 in) at 12 Δ_y. Fig. 3.36 shows the opening in which the strands are visible at 12 Δ_y and Fig. 3.37 shows an overall view of the connection at 12 Δ_y. Fig. 3.38 shows specimen E-P-Z4 at 12 Δ_y. The average extent of the spalling was approximately 206 mm (8.11 in) for specimen E-P-Z4 and 248 mm (9.76 in) for specimen F-P-Z4. Both specimens failed at 12 Δ_y. The cracks in the column joint region were still fine at failure and the fiber reinforced construction joints held together very well throughout the test.

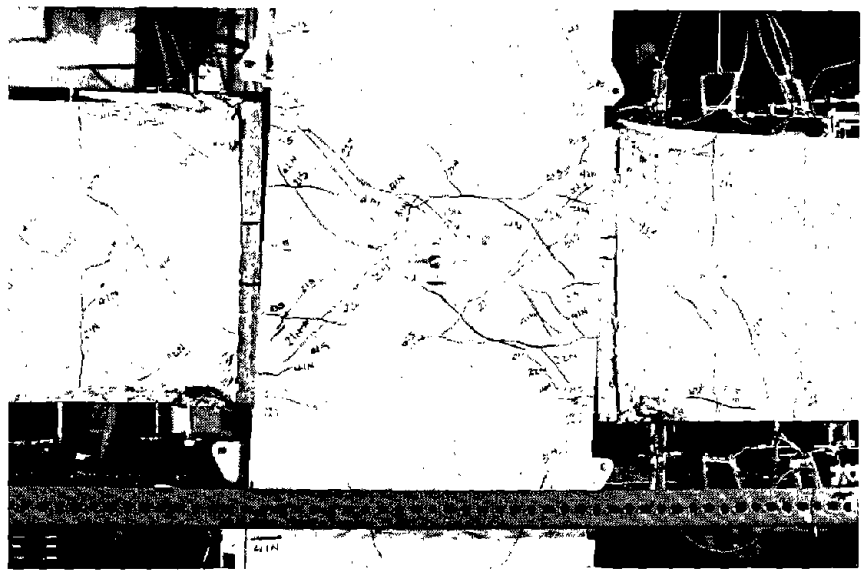

Fig. 3.35 Connection F-P-Z4 at 8 Δ_y.

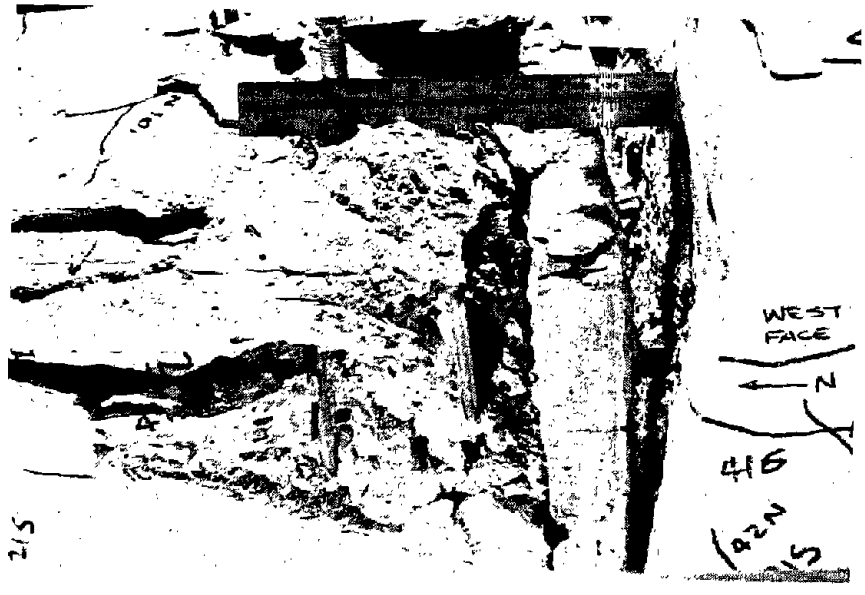

Fig. 3.36 Opening between the beam and column at 12 Δ_y, F-P-Z4.

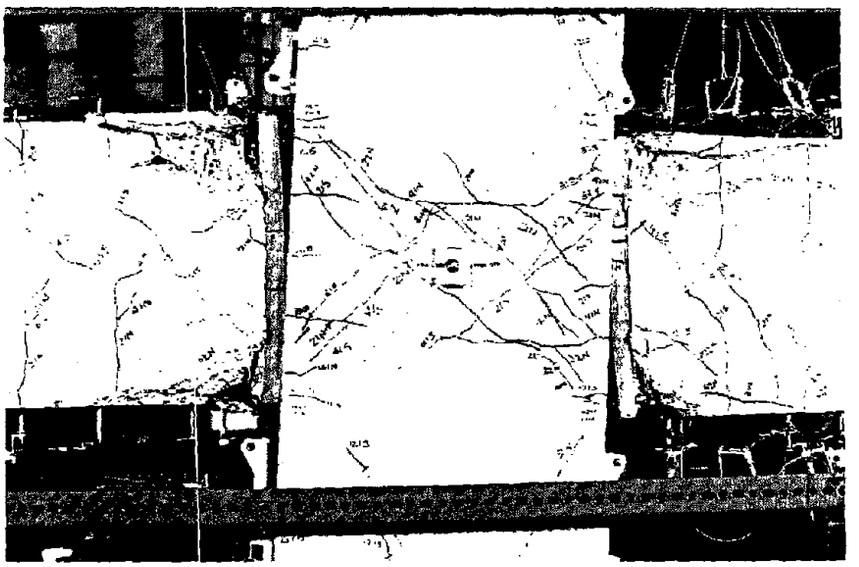

Fig. 3.37 Specimen F-P-Z4 at failure - 12 Δ_y.

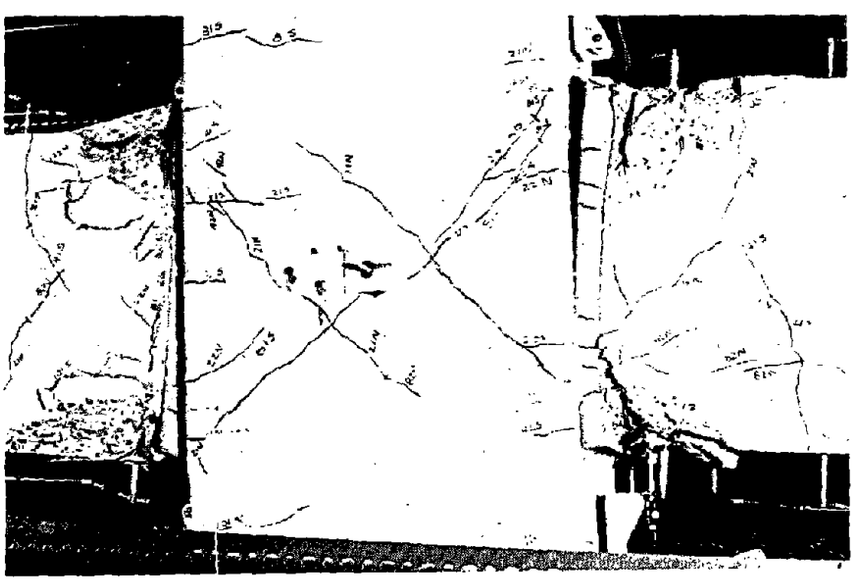

Fig. 3.38 Specimen E-P-Z4 at failure - 12 Δ_y.

The hysteresis curves for E-P-Z4 and F-P-Z4 are shown in Figs. 3.39 and 3.40. Again, both specimens behaved very similarly and exhibited severly pinched hysteresis curves. The yield displacement was 5.7 mm (0.225 in) for specimen E-P-Z4 and 5.5 mm (0.218 in) for specimen F-P-Z4. The ultimate displacement ductility for both specimens was 12.

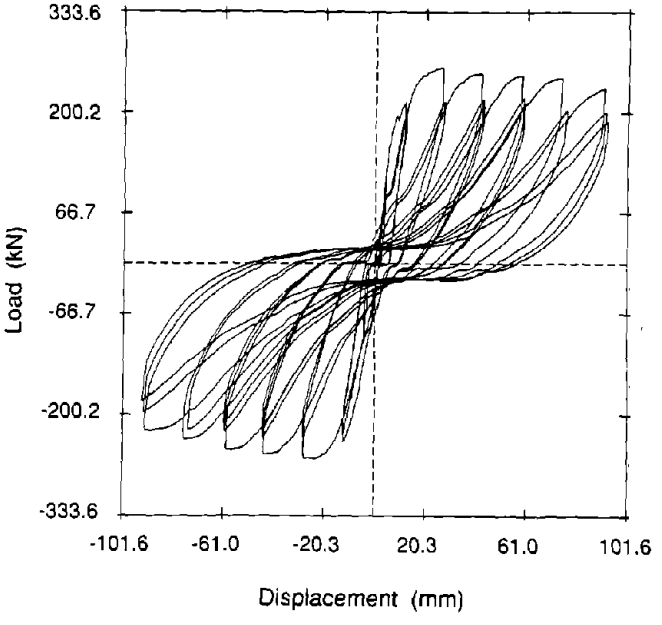

Fig. 3.39 Hysteresis curves for E-P-Z4.

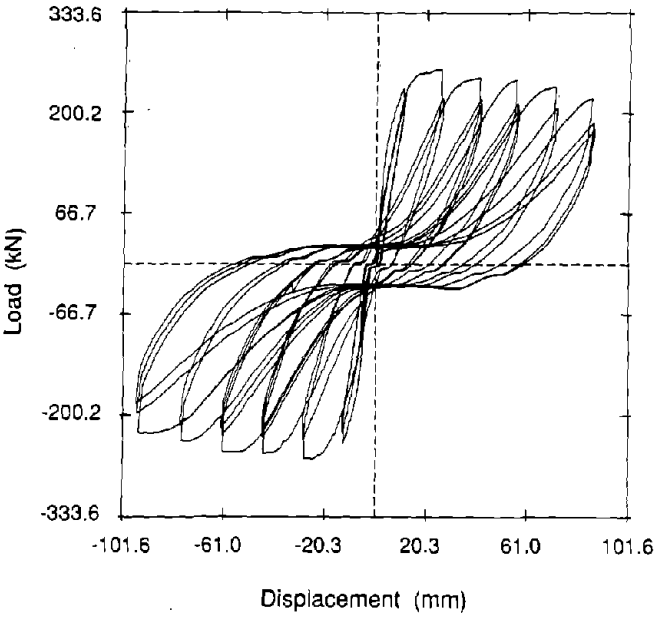

Fig. 3.40 Hysteresis curves for F-P-Z4.

The experimental ultimate beam moments at the column face were 146 kN-m (108 k-ft) and 137 kN-m (101 k-ft) for E-P-Z4 and 139 kN-m (102 k-ft) and 135 kN-m (100 k-ft) for F-P-Z4. The values for E-P-Z4 were obtained in the first cycle at 8 Δ_y and those for F-P-Z4 were obtained in the first cycle at 4 Δ_y.

A comparison of the per cycle energy absorbed for the two specimens is given in Fig. 3.41. The cumulative energy absorbed to failure was 110.76 kN-m (980 k-in) for E-P-Z4 and 109.39 kN-m (968 k-in) for F-P-Z4.

The maximum strains in the reinforcing bars are given in Figs. 3.42 through 3.57. The average extent of reinforcing bars yielding was 95 mm (3.7 in) for E-P-Z4 and 148 mm (5.8 in) for F-P-Z4. Again, as with the previous precast specimens, the highest recorded strains occurred at 4 Δ_y and decreased thereafter. Only the first tie (42.3 mm [1.7 in] from the column face) in the beams yielded. Two other ties, located 110 mm (4.3 in) and 245 mm (9.7 in) from the column face, registered strains of the order of half the yield strain or less.

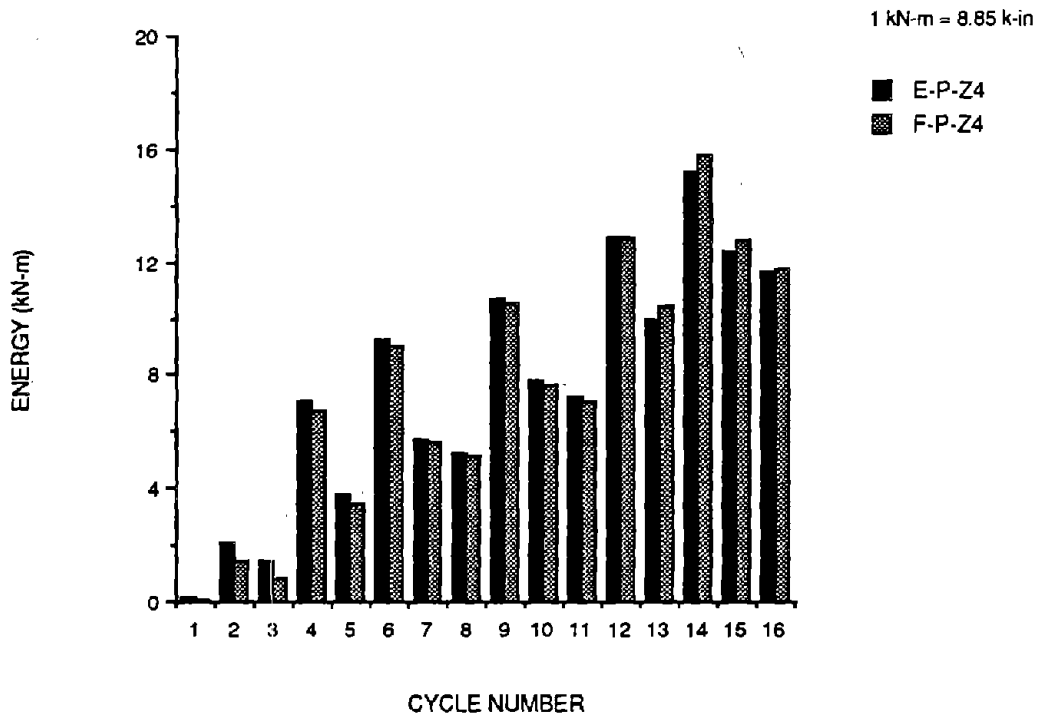

Fig. 3.41 Energy absorbed by specimens E-P-Z4 and F-P-Z4.

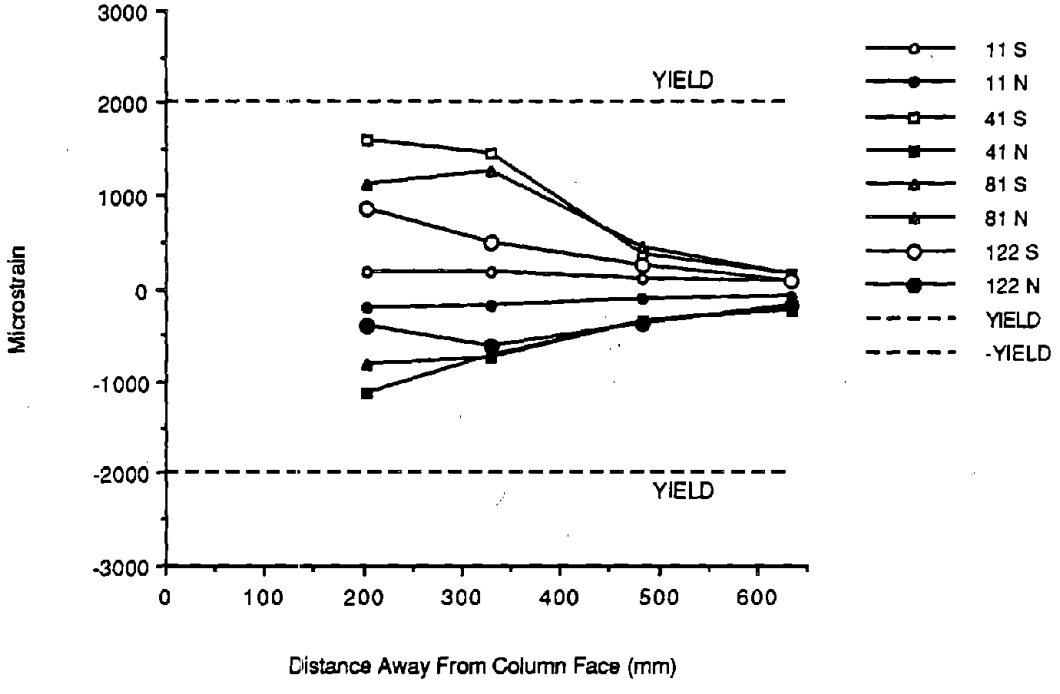

Fig. 3.42 Top northeast reinforcing bar strains - E-P-Z4.

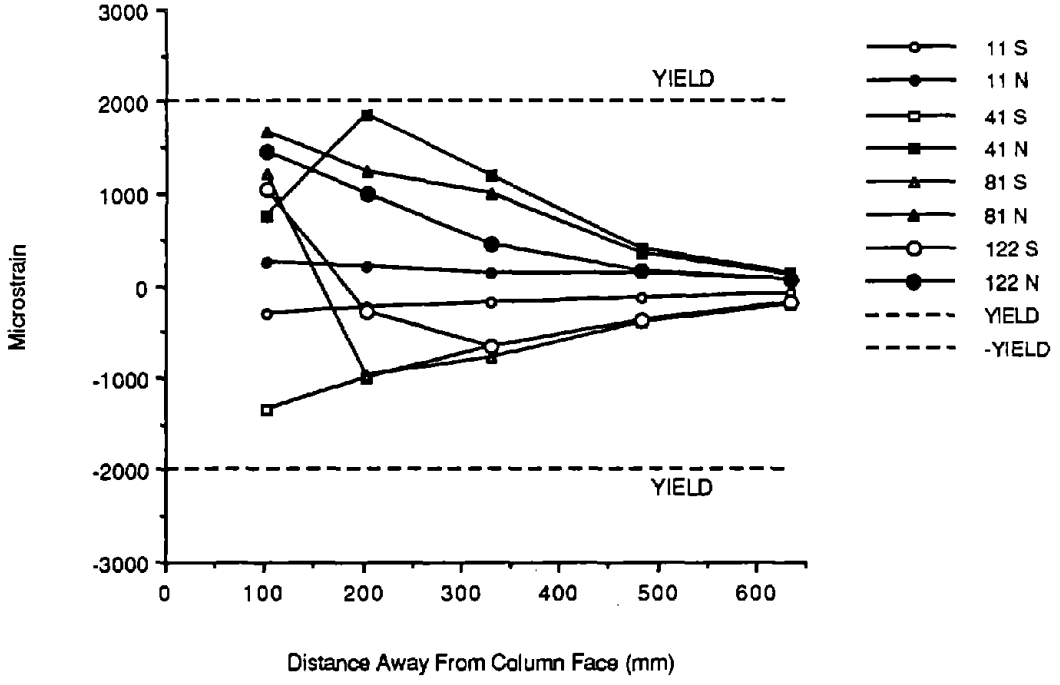

Fig. 3.43 Bottom northeast reinforcing bar strains - E-P-Z4.

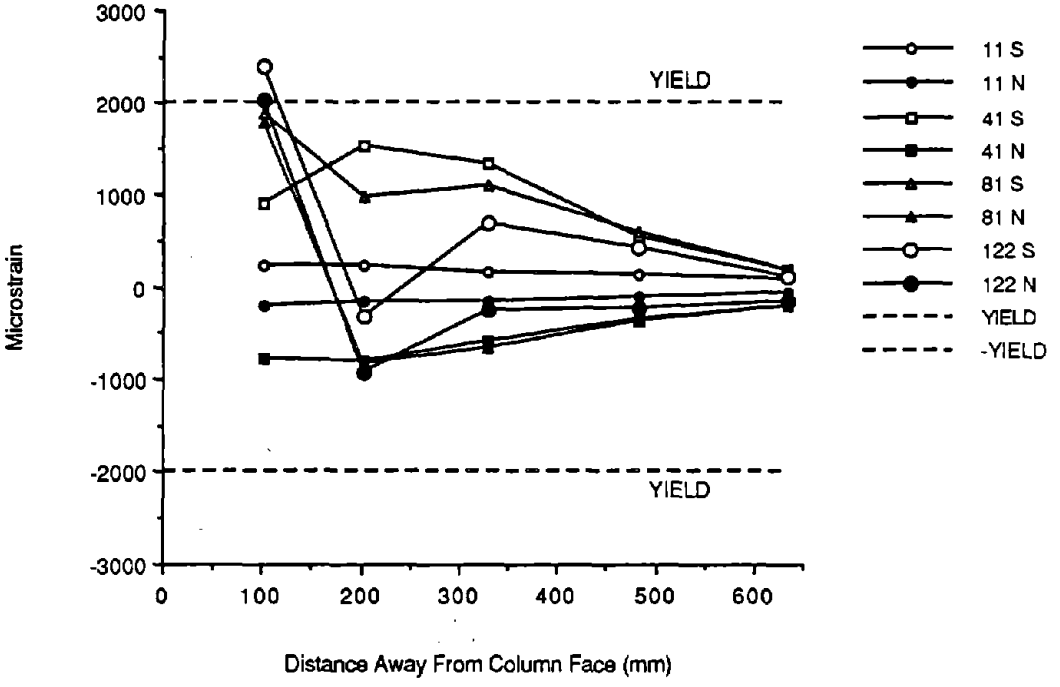

Fig. 3.44 Top northwest reinforcing bar strains - E-P-Z4.

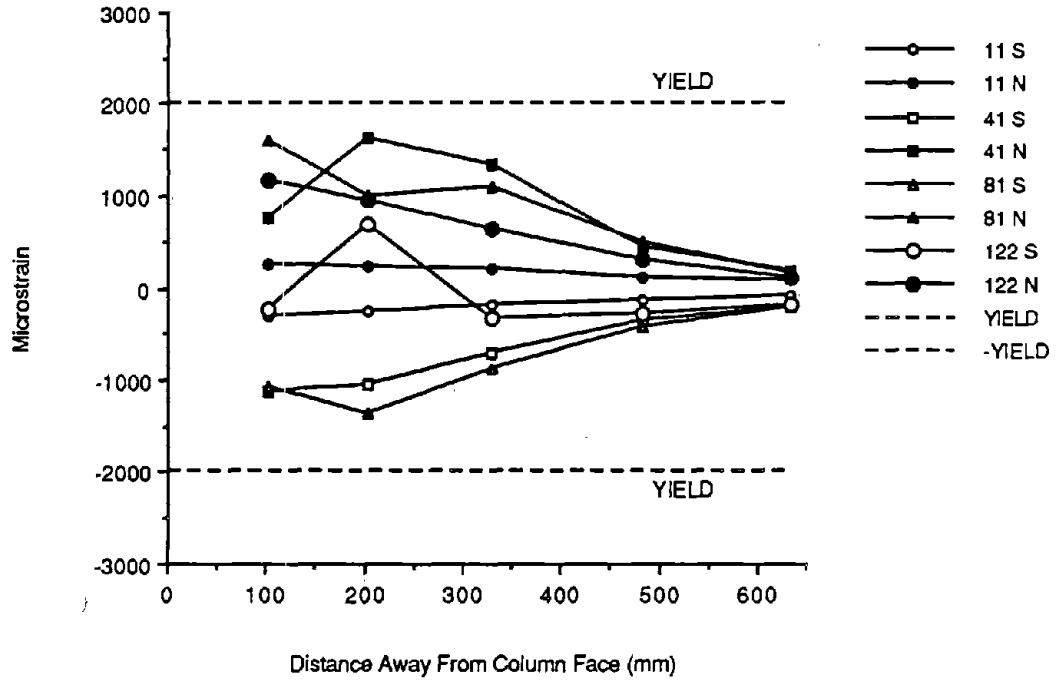

Fig. 3.45 Bottom northwest reinforcing bar strains - E-P-Z4.

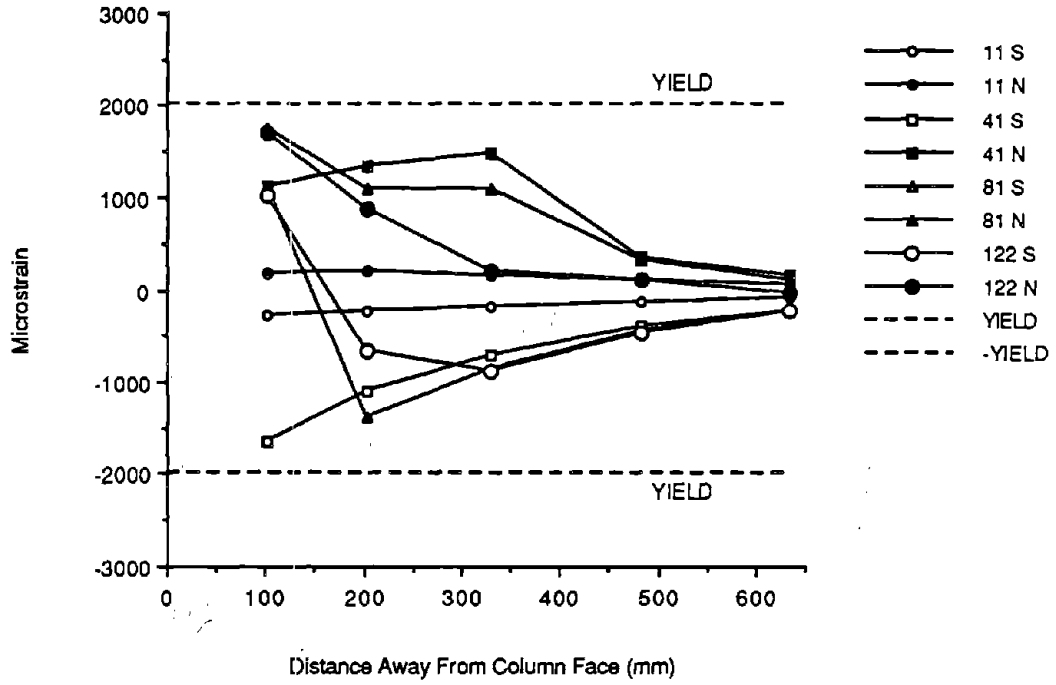

Fig. 3.46 Top southeast reinforcing bar strains - E-P-Z4.

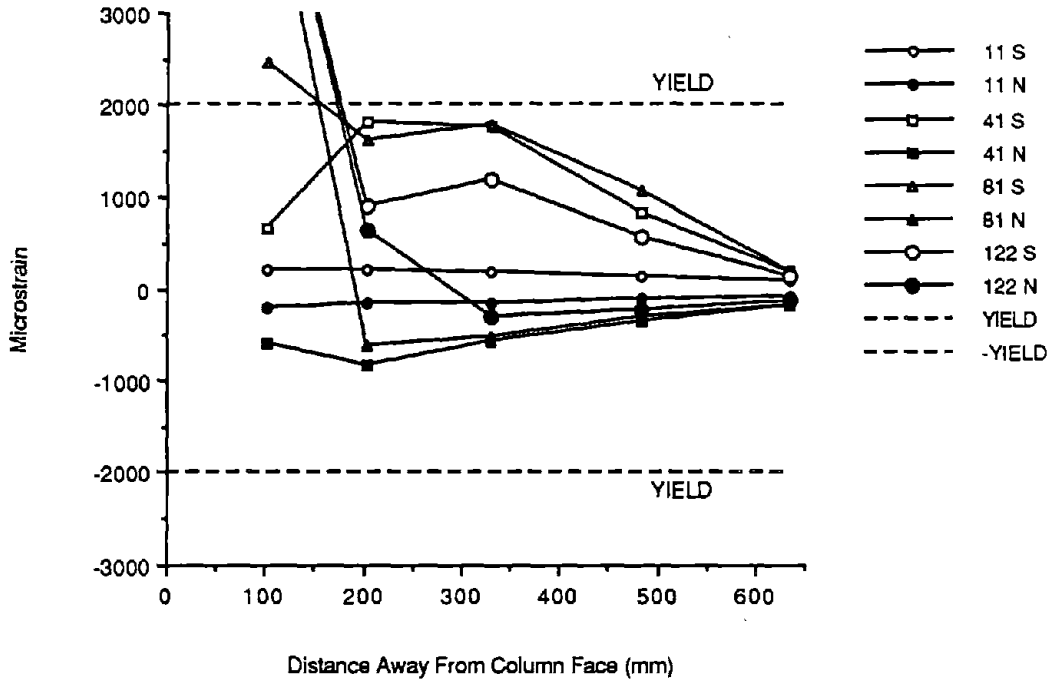

Fig. 3.47 Bottom southeast reinforcing bar strains - E-P-Z4.

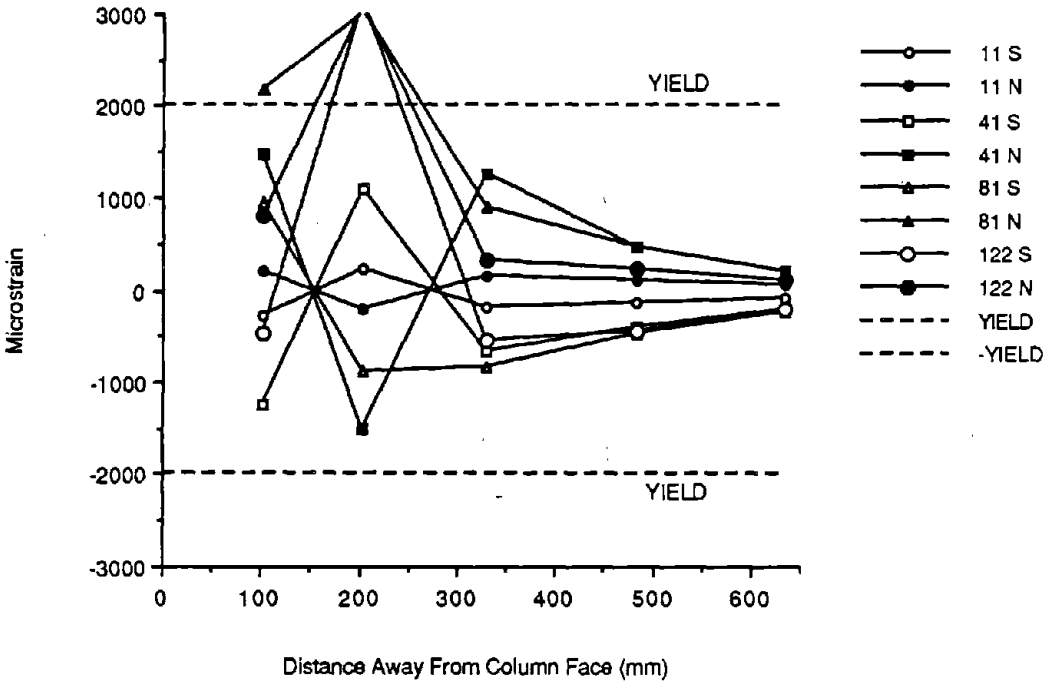

Fig. 3.48 Top southwest reinforcing bar strains - E-P-Z4.

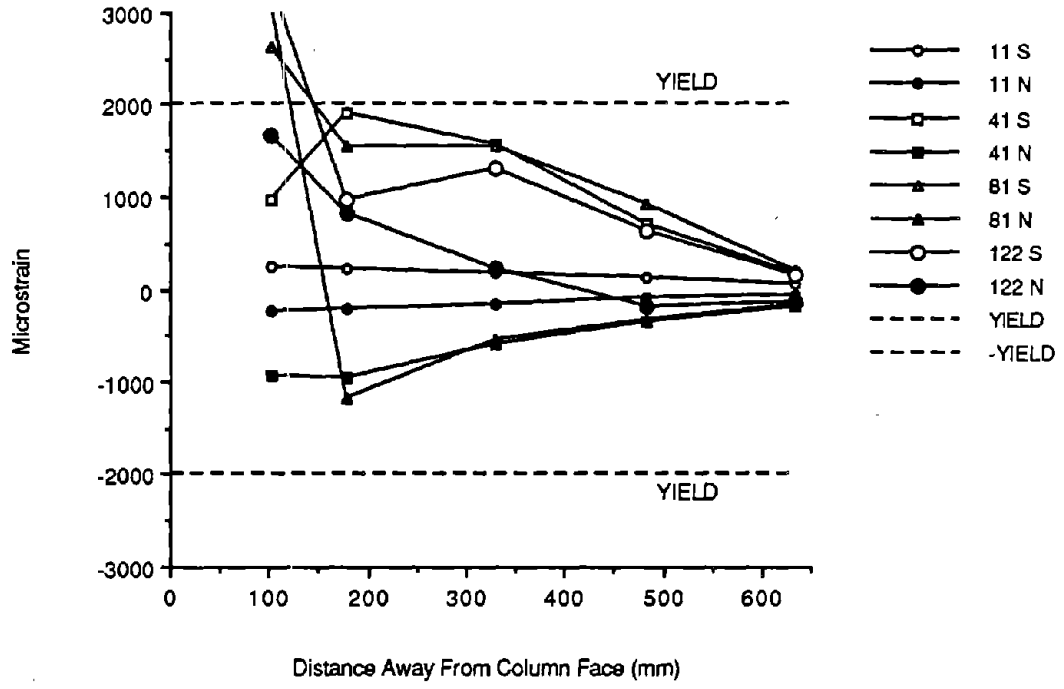

Fig. 3.49 Bottom southwest reinforcing bar strains - E-P-Z4.

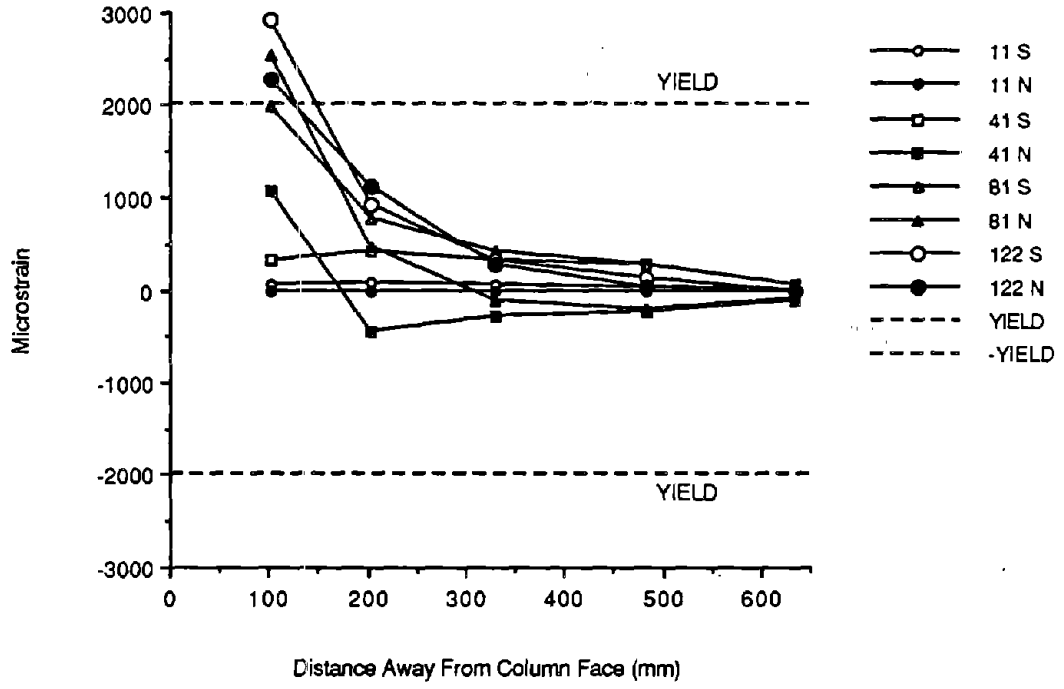

Fig. 3.50 Top northeast reinforcing bar strains - F-P-Z4.

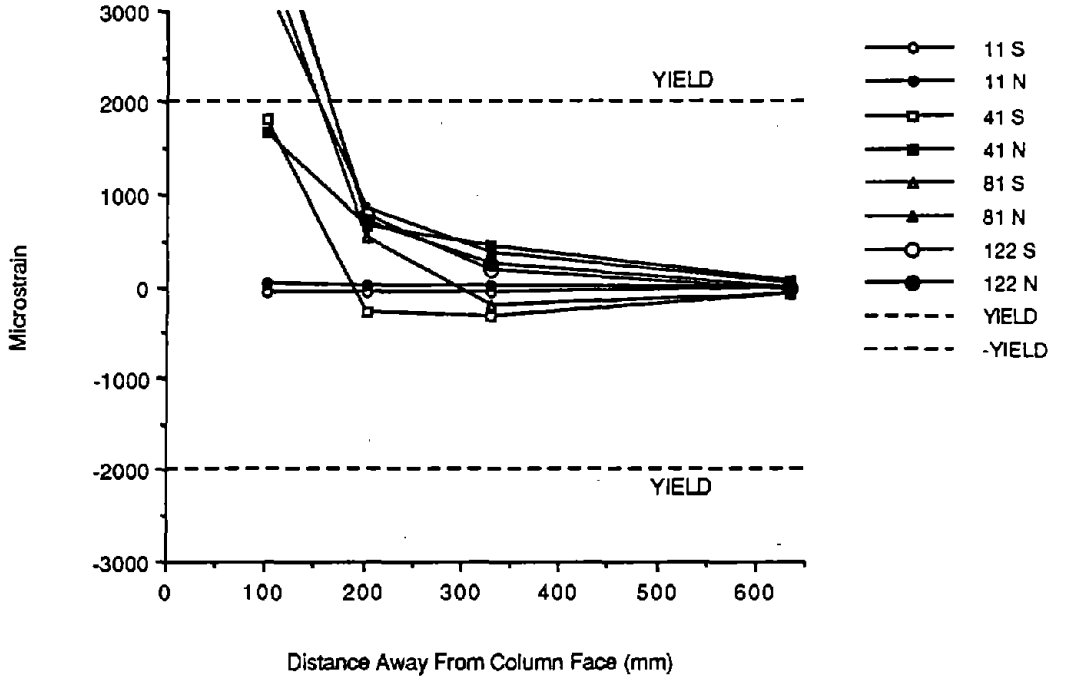

Fig. 3.51 Bottom northeast reinforcing bar strains - F-P-Z4.

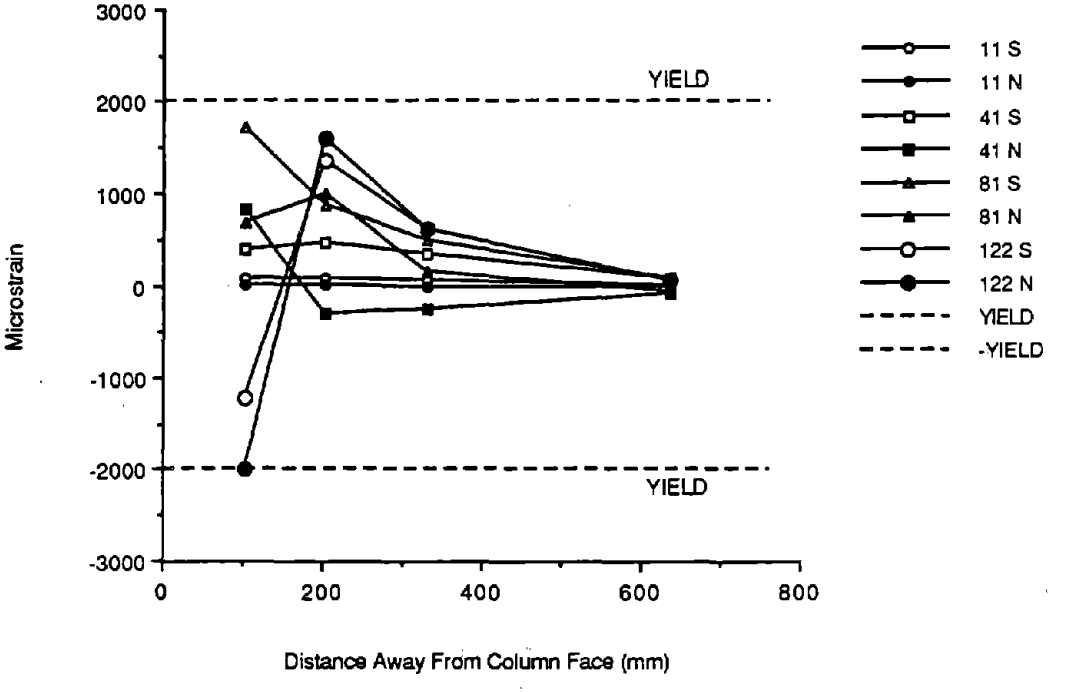

Fig. 3.52 Top northwest reinforcing bar strains - F-P-Z4.

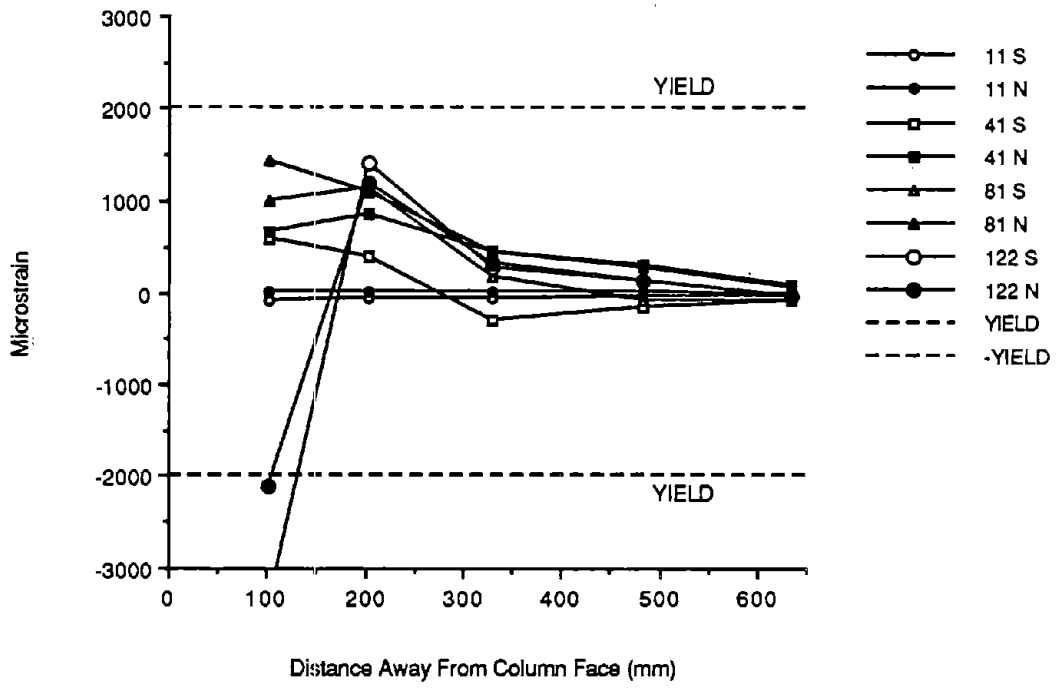

Fig. 3.53 Bottom northwest reinforcing bar strains - F-P-Z4.

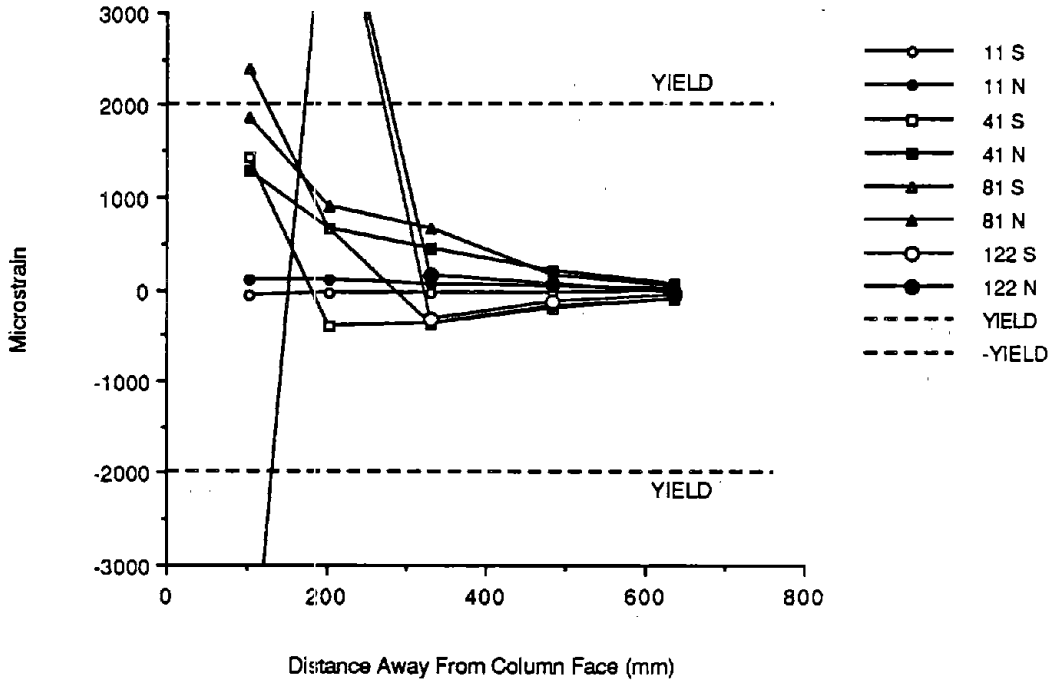

Fig. 3.54 Top southeast reinforcing bar strains - F-P-Z4.

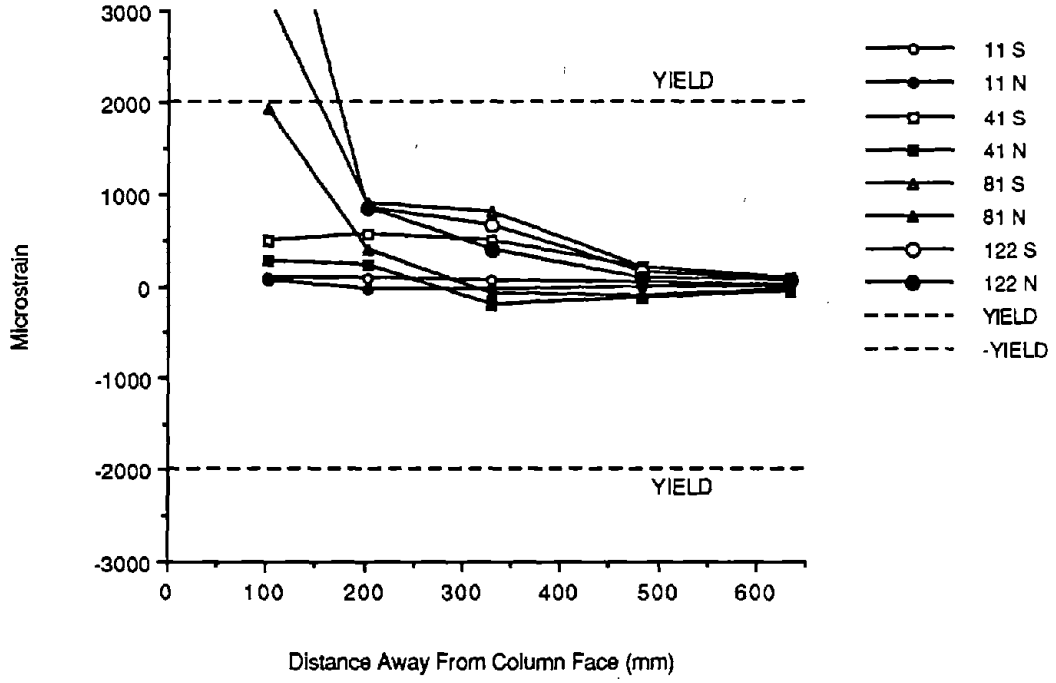

Fig. 3.55 Bottom southeast reinforcing bar strains - F-P-Z4.

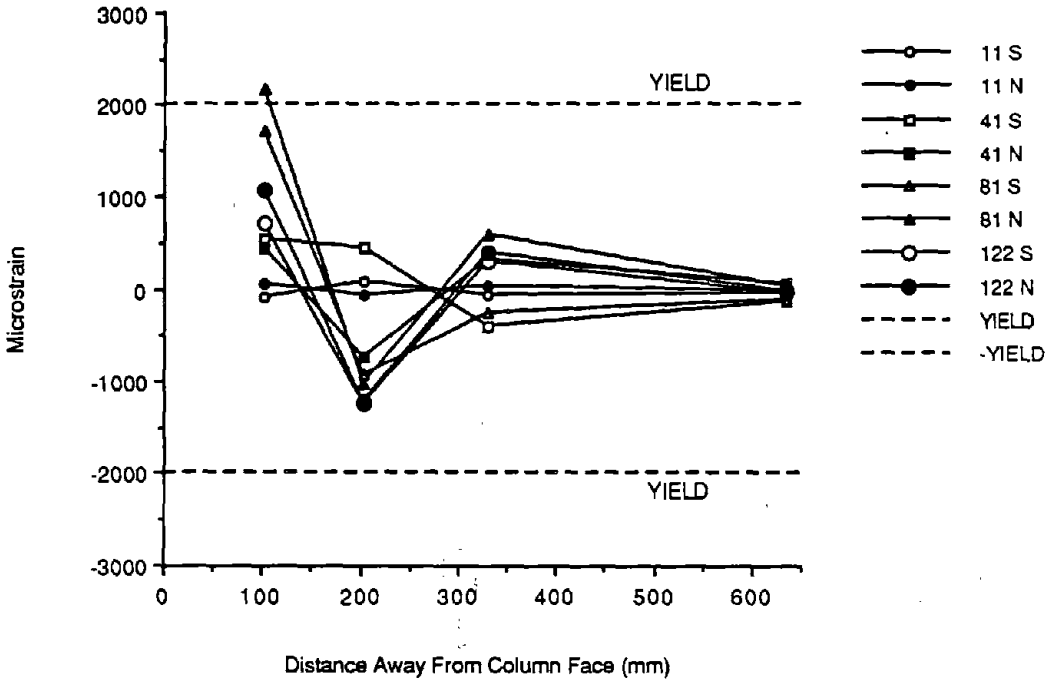

Fig. 3.56 Top southwest reinforcing bar strains - F-P-Z4.

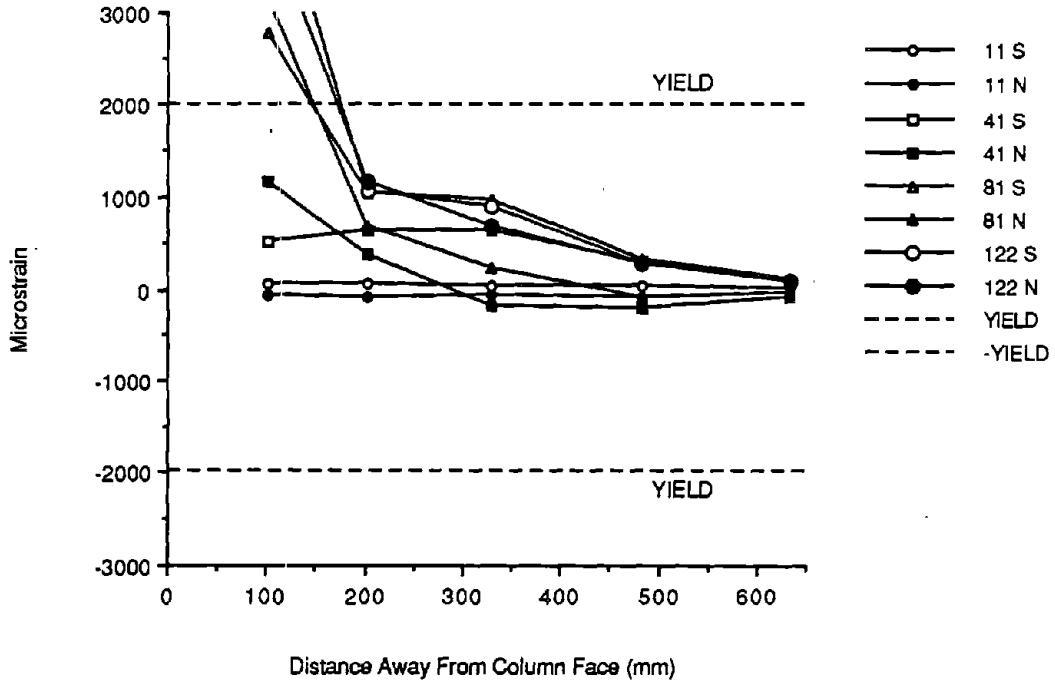

Fig. 3.57 Bottom southwest reinforcing bar strains - F-P-Z4.

3.3 Precast Concrete Specimens A-P-Z2 and B-P-Z2

Specimens A-P-Z2 and B-P-Z2 were the precast concrete Zone 2 specimens and were detailed as shown in Fig. 2.2. The loading history is shown in Fig. 3.58. The column axial load was 173.9 kN (39.1 k) [0.1 f'_c A_g based on a 28-day strength of 31.1 MPa (4510 psi)].

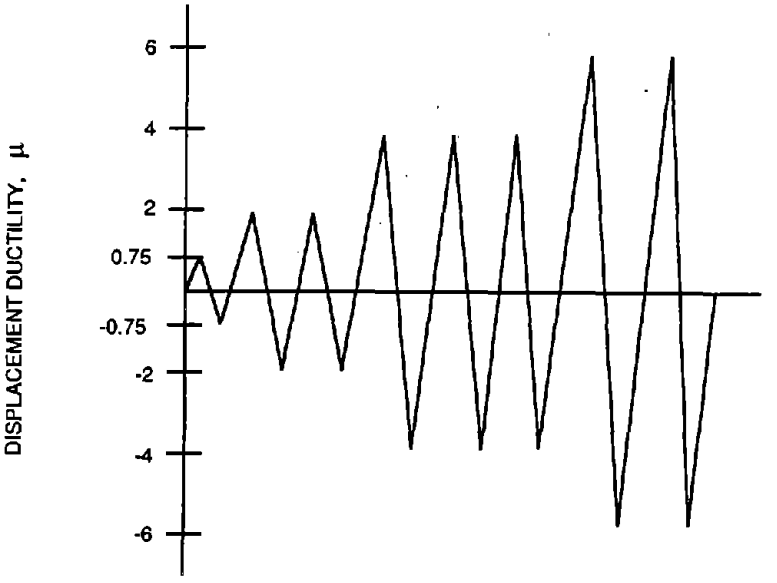

Fig. 3.58 Loading sequence for specimens A-P-Z2 and B-P-Z2.

In the initial elastic cycle, a few short, hairline flexure cracks were noted in the column in specimen A-P-Z2. No cracks were observed in specimen B-P-Z2. However, very minor crushing of the construction joints was noted on the tension side of both beams of specimen B-P-Z2. No obvious explanation was found for this deviation. At 2 Δ_y, flexure cracks were observed in the beams and flexure and shear cracks were observed in the column joint region. Minor crushing of the beams also occurred at this stage. The extent of cracking at 2 Δ_y is shown in Fig. 3.59. More shear cracks in columns and beams developed at 4 Δ_y. In addition, extensive crushing of the beams occurred at 4 Δ_y. The opening between the beam and column was approximately 5 mm (0.2 in). The column joint region was in good condition at this stage with the column crack widths still narrow. The average length of spall in the beams for both specimens was approximately 175 mm (6.9 in). Figs. 3.60 through 3.62 show the crack pattern, crushing and beam opening at 4 Δ_y, respectively. Both specimens were considered to have failed at this stage. Fig. 3.63 shows the joint region of specimen B-P-Z2 at failure.

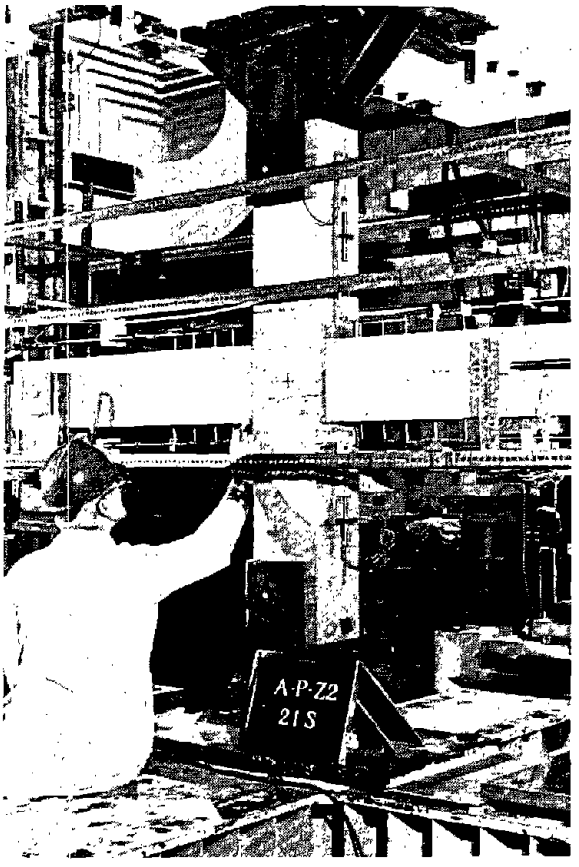

Fig. 3.59 Crack pattern at 2 Δ_y - A-P-Z2.

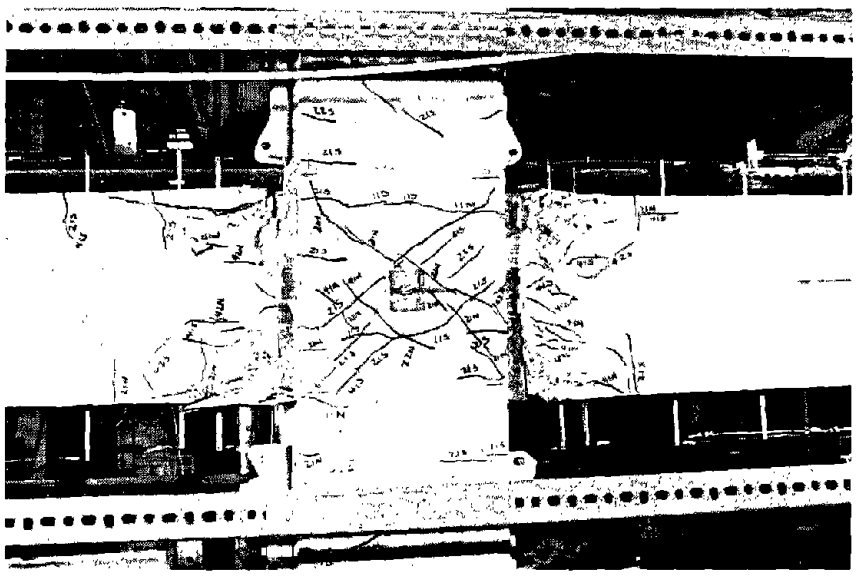

Fig. 3.60 Joint region at failure, 4 Δ_y - A-P-Z2.

Fig. 3.61 Beam crushing at 4 Δ_y - A-P-Z2.

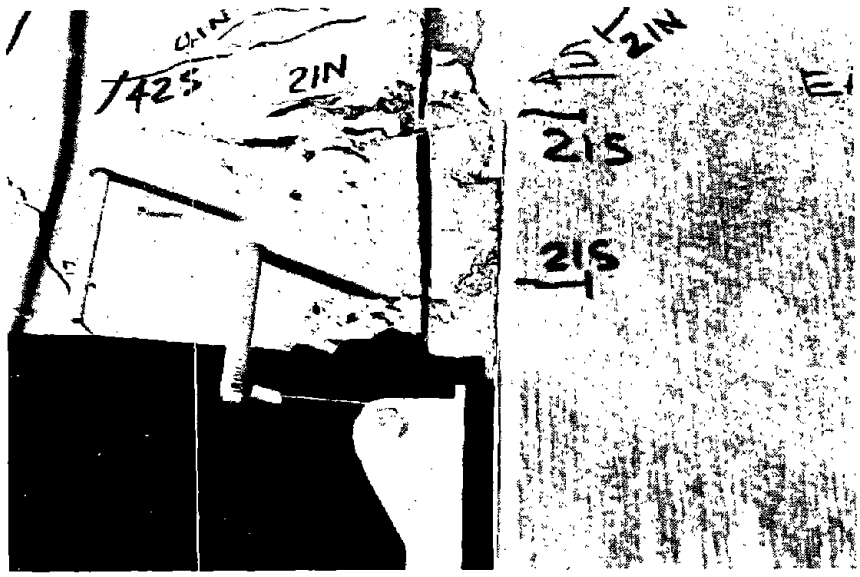

Fig. 3.62 Opening between beam and column at 4 Δ_y - A-P-Z2.

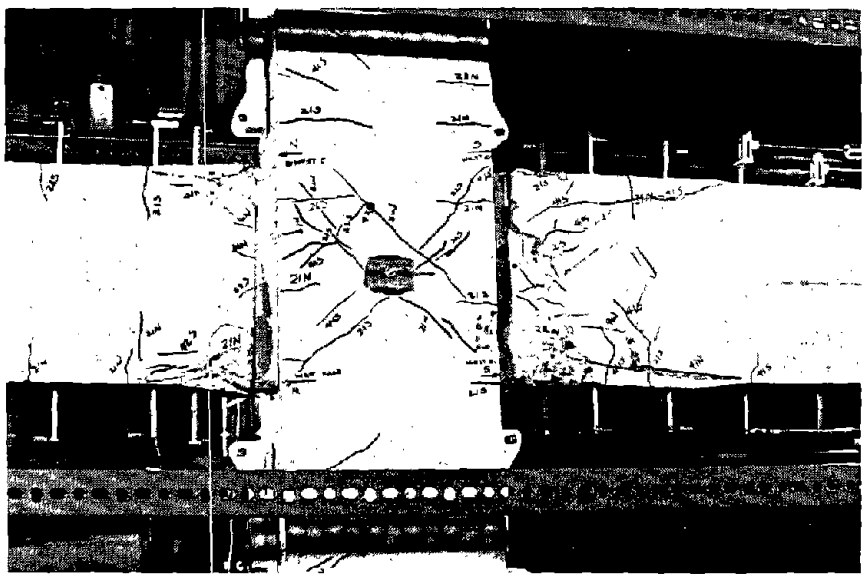

Fig. 3.63 Joint region at failure, 4 Δ_y - B-P-Z2.

The hysteresis curves for specimens A-P-Z2 and B-P-Z2 are shown in Figs. 3.64 and 3.65, respectively. The yield displacements were 8.5 mm (0.333 in) and 8.4 mm (0.330 in) for specimens A-P-Z2 and B-P-Z2, respectively. The ultimate displacement ductility was 4 for both specimens.

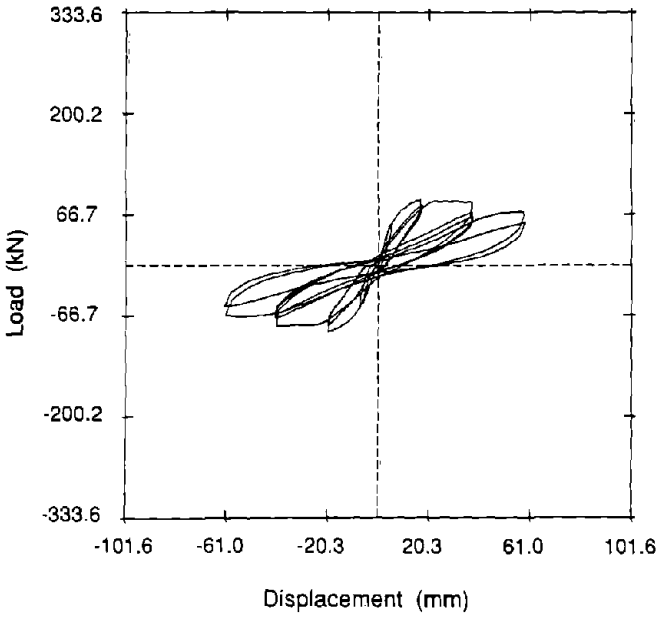

Fig. 3.64 Hysteresis curves for A-P-Z2.

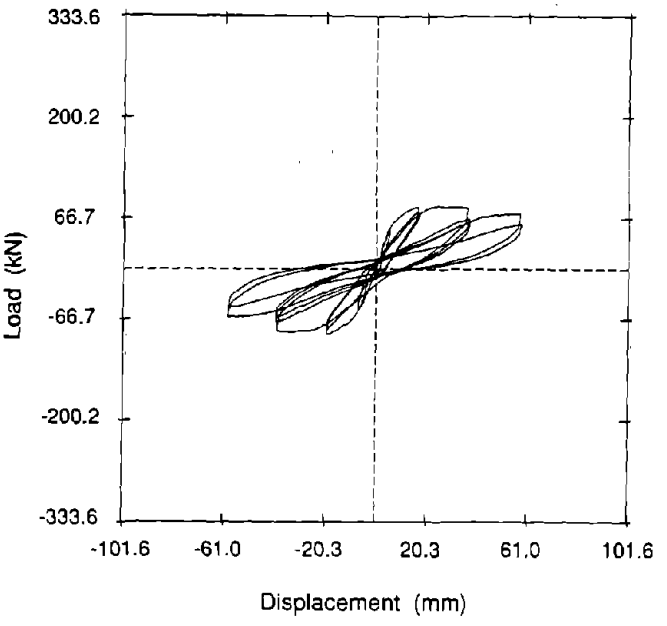

Fig. 3.65 Hysteresis curves for B-P-Z2.

The experimental ultimate moments were 52 kN-m (38 k-ft) and 54 kN-m (40 k-ft) for A-P-Z2 and 51 kN-m (37 k-ft) and 54 kN-m (40 k-ft) for B-P-Z2. Three of these values were obtained in the first cycle at 2 Δ_y and the fourth (54 kN-m [40 k-ft] for B-P-Z2) in the first cycle at 4 Δ_y.

A comparison of the energy absorbed on a per cycle basis is given in Fig. 3.66. The cumulative energy absorbed to failure for specimen A-P-Z2 was 7.4 kN-m (65.2 k-in) and for specimen B-P-Z2 was 8.8 kN-m (78.1 k-in).

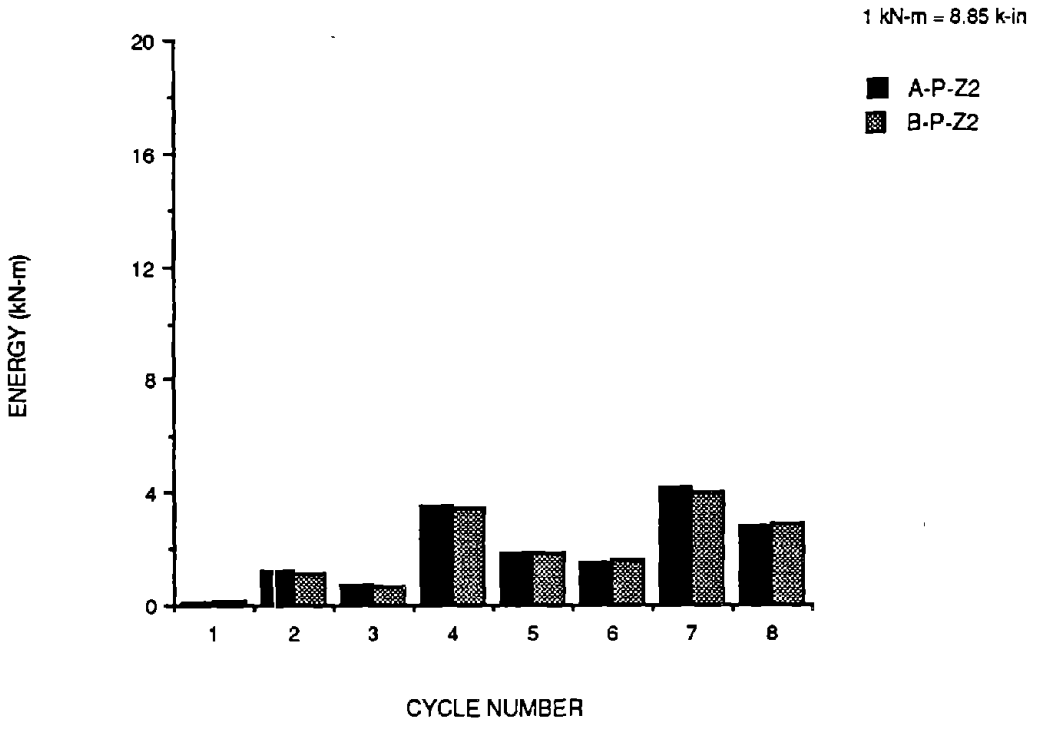

Fig. 3.66 Energy absorbed by specimens A-P-Z2 and B-P-Z2.

The reinforcing bar strains are shown in Figs. 3.67 through 3.82. The average length over which the reinforcing bars yielded was 110 mm (4.3 in) and 112 mm (4.4 in) for specimens A-P-Z2 and B-P-Z2, respectively. The maximum values were obtained at 4 Δ_y. The first two ties located 42 mm [1.7 in] and 110 mm (4.3 in) from the column face in the beams yielded. A third tie located 245 mm (9.7 in) registered low strains throughout the test.

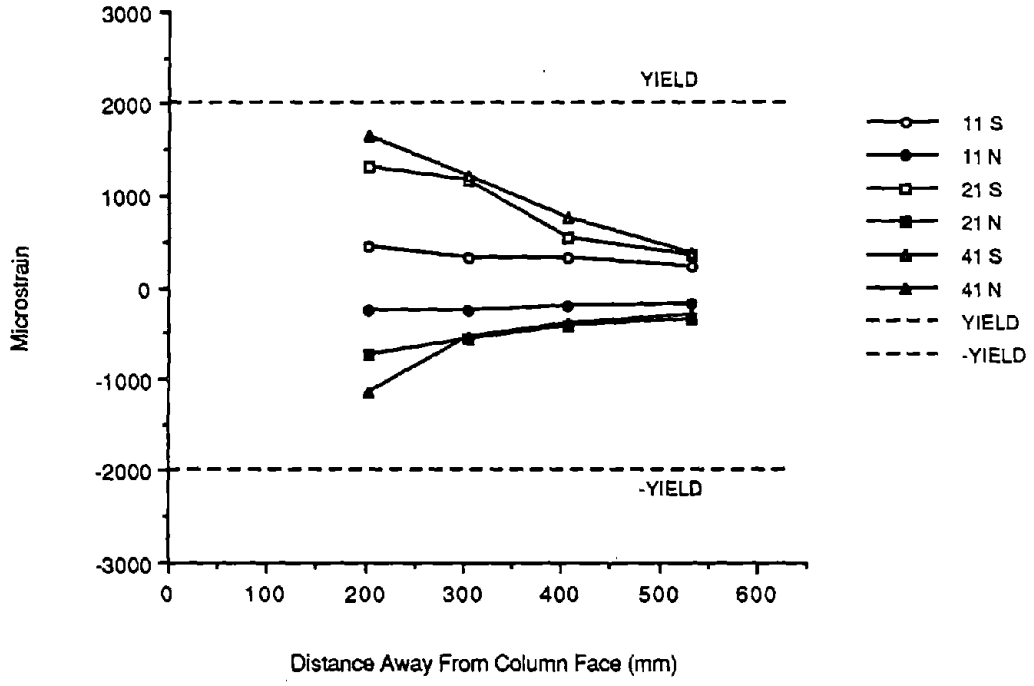

Fig. 3.67 Top northeast reinforcing bar strains - A-P-Z2.

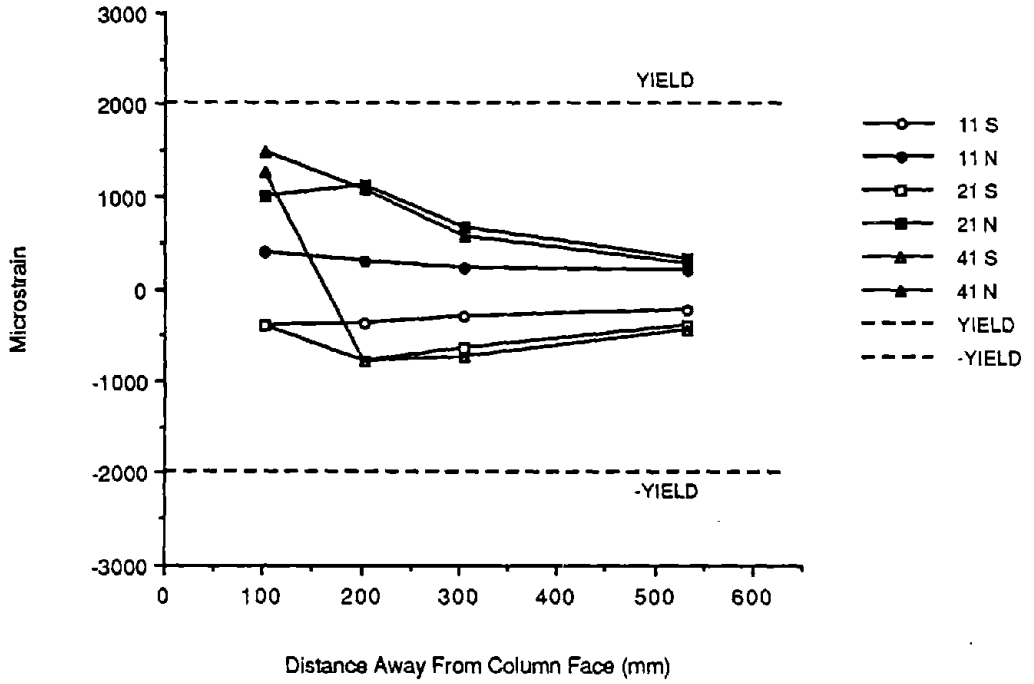

Fig. 3.68 Bottom northeast reinforcing bar strains - A-P-Z2.

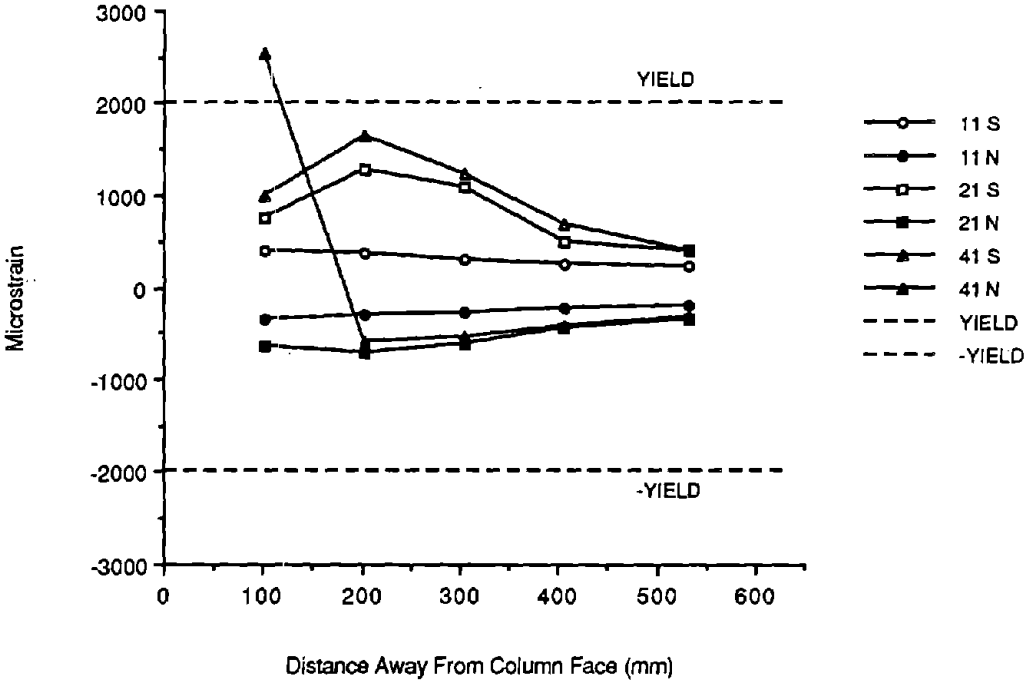

Fig. 3.69 Top northwest reinforcing bar strains - A-P-Z2.

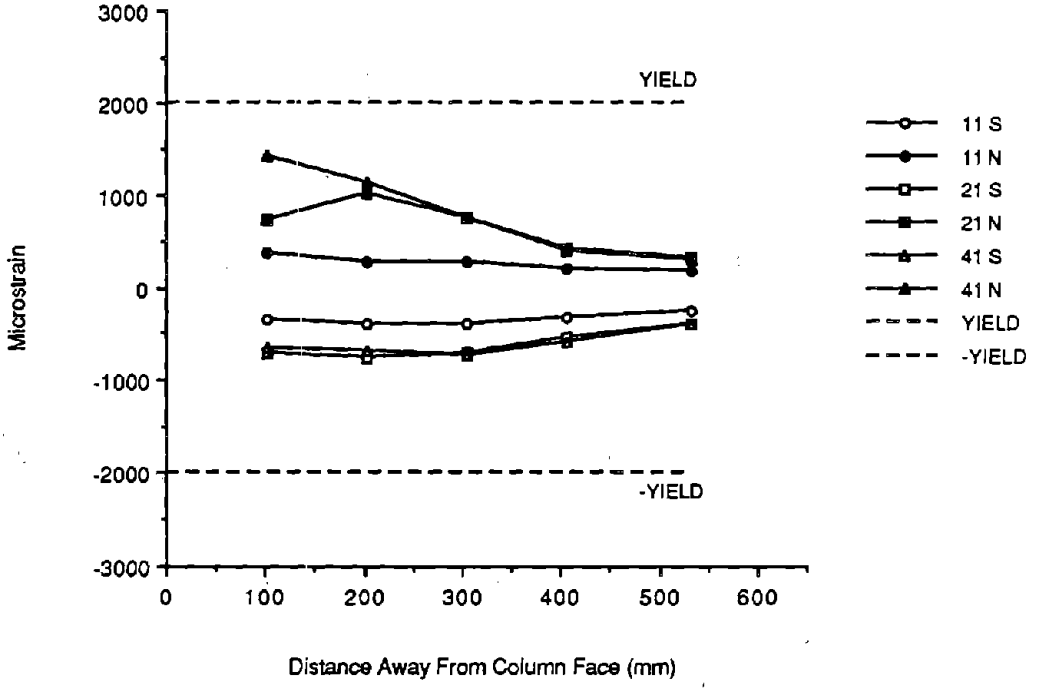

Fig. 3.70 Bottom northwest reinforcing bars strains - A-P-Z2.

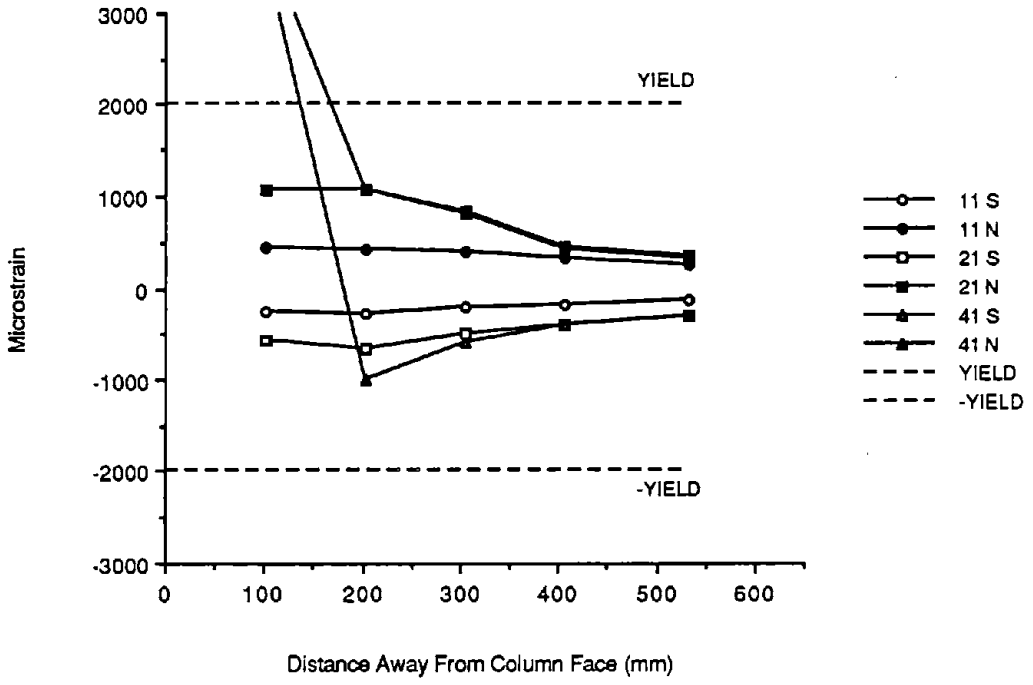

Fig. 3.71 Top southeast reinforcing bar strains - A-P-Z2.

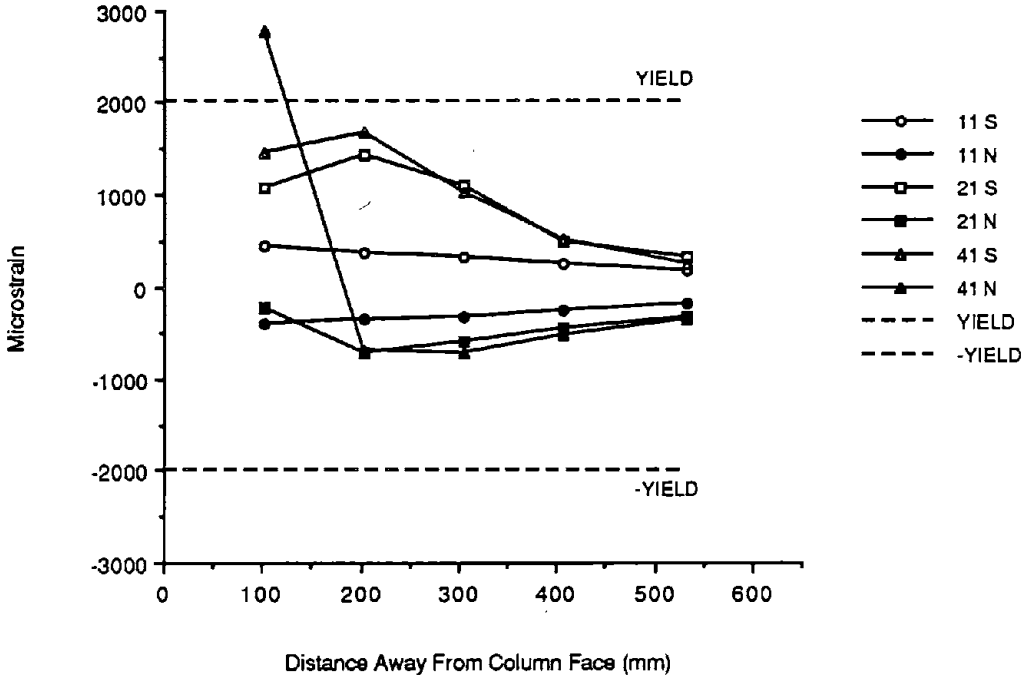

Fig. 3.72 Bottom southeast reinforcing bar strains - A-P-Z2.

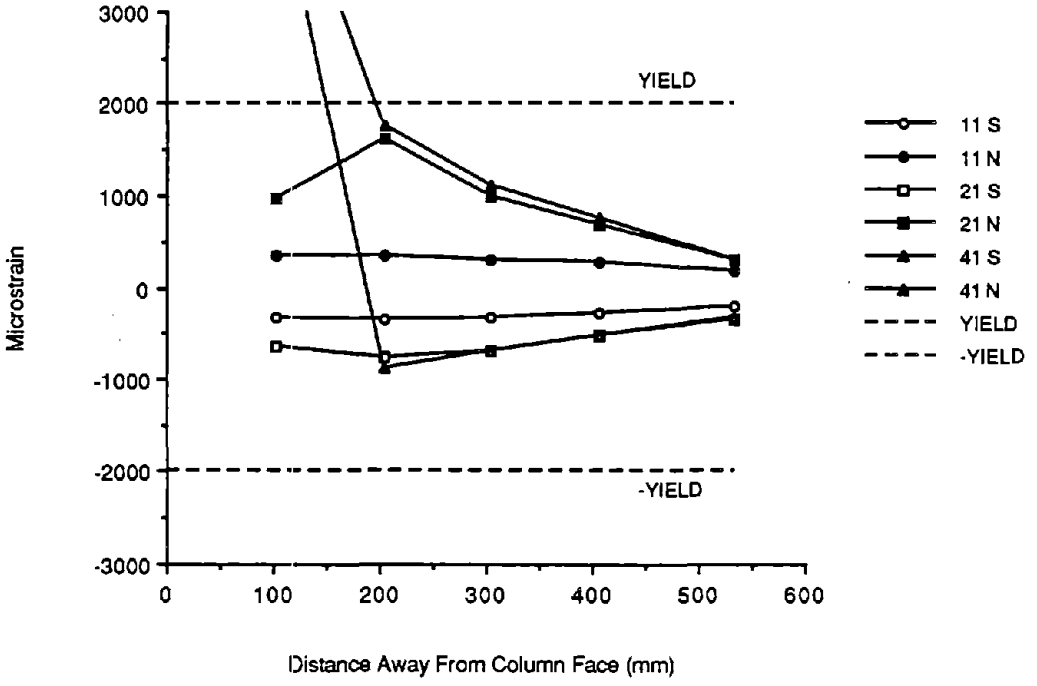

Fig. 3.73 Top southwest reinforcing bar strains - A-P-Z2.

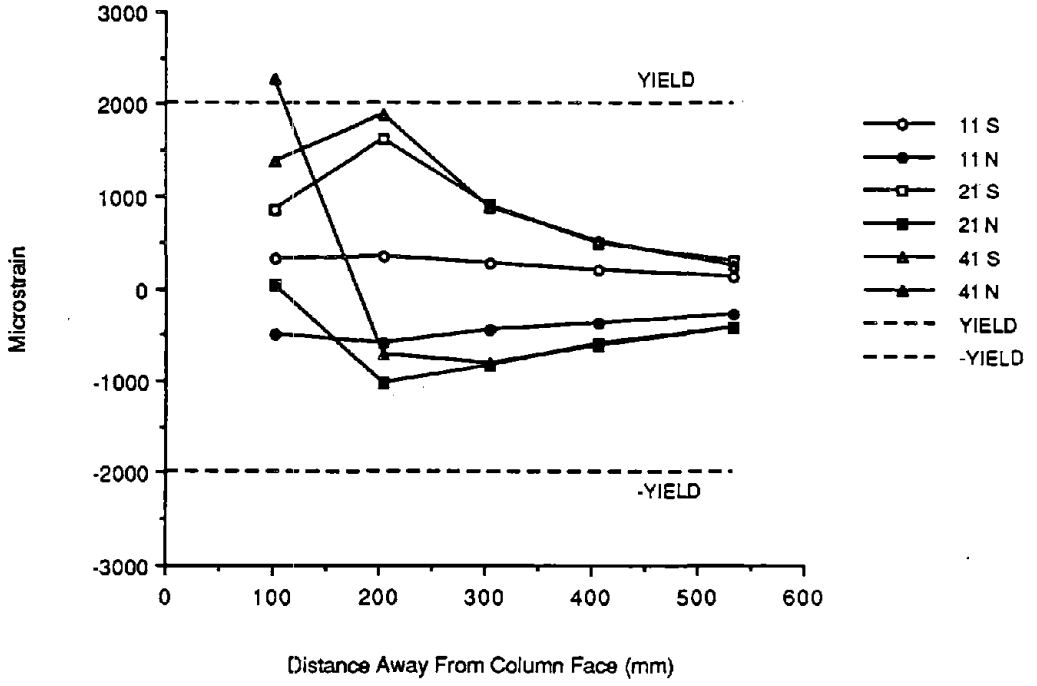

Fig. 3.74 Bottom southwest reinforcing bars strains - A-P-Z2.

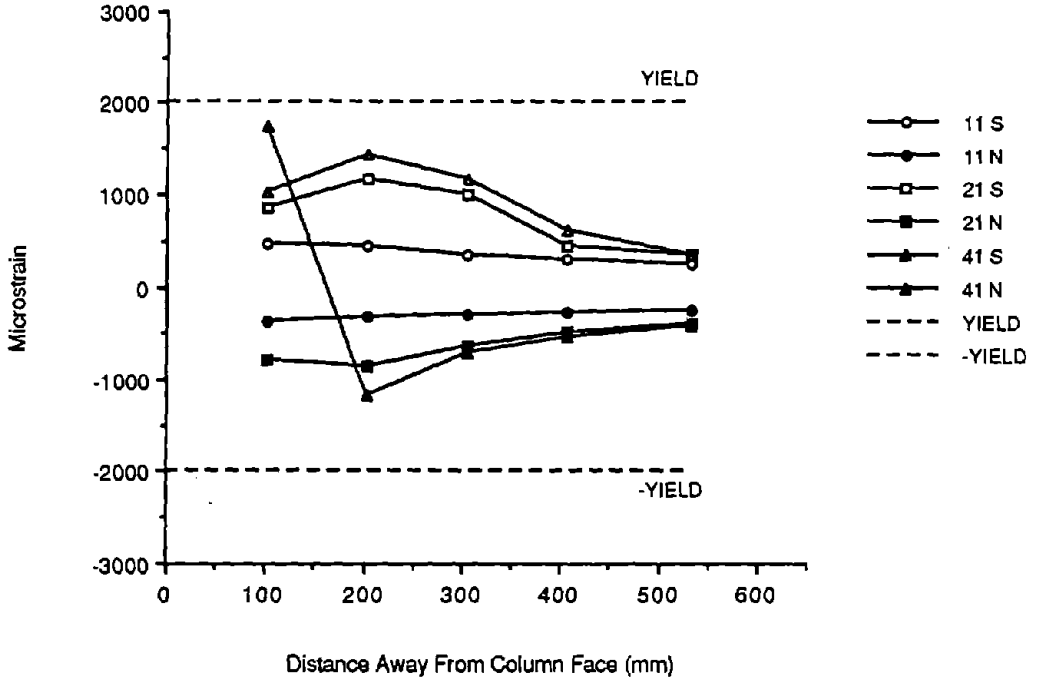

Fig. 3.75 Top northeast reinforcing bar strains - B-P-Z2.

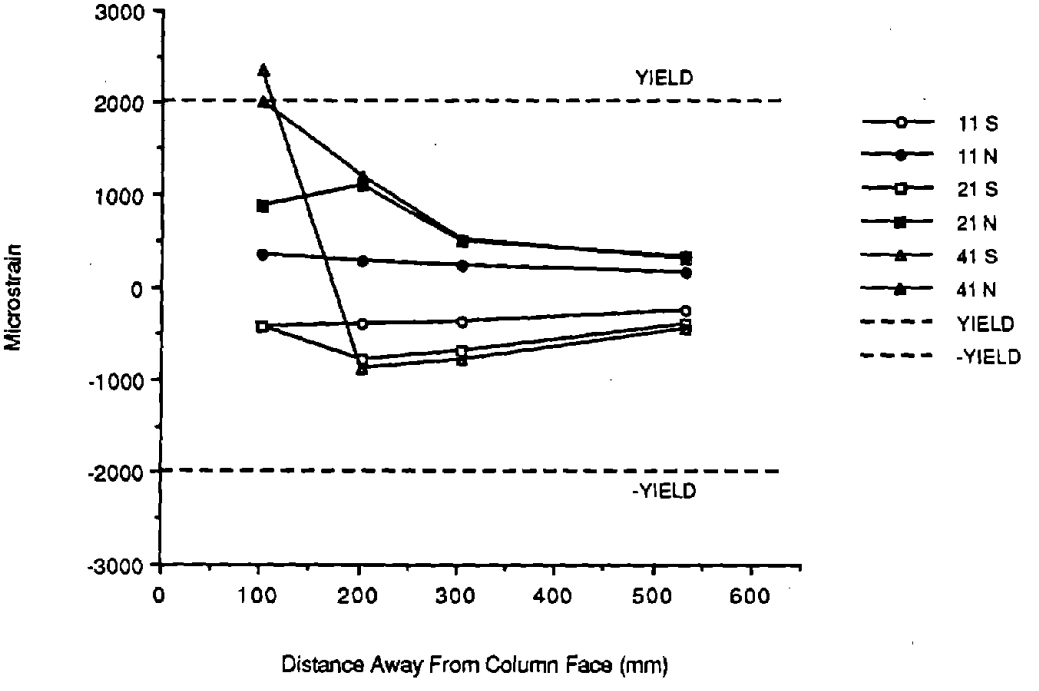

Fig. 3.76 Bottom northeast reinforcing bar strains - B-P-Z2.

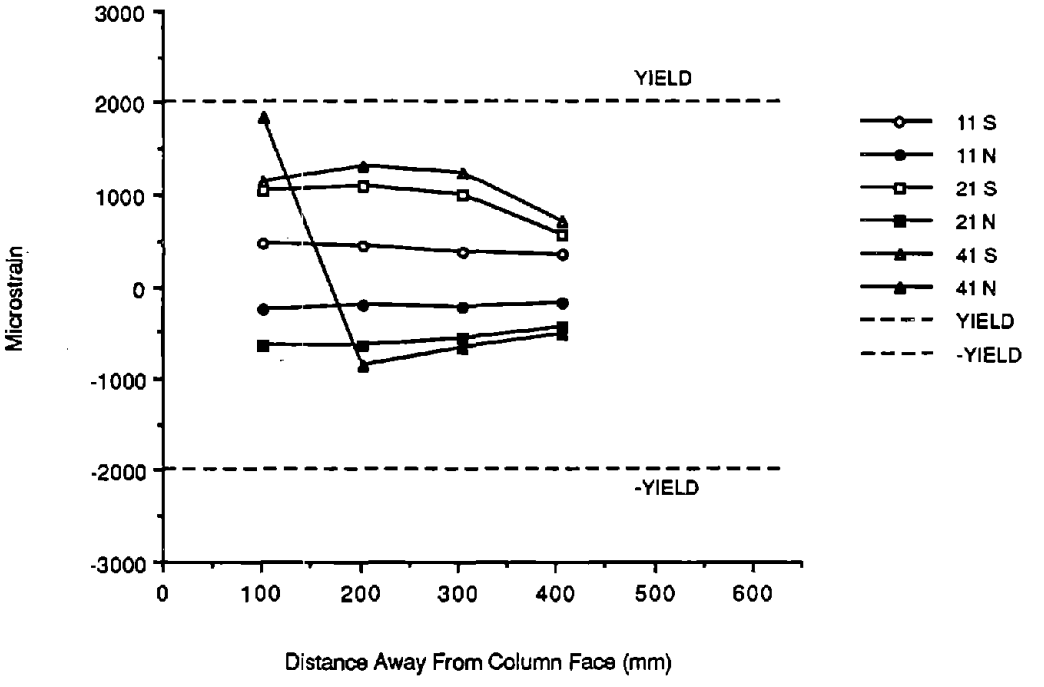

Fig. 3.77 Top northwest reinforcing bars strains - B-P-Z2.

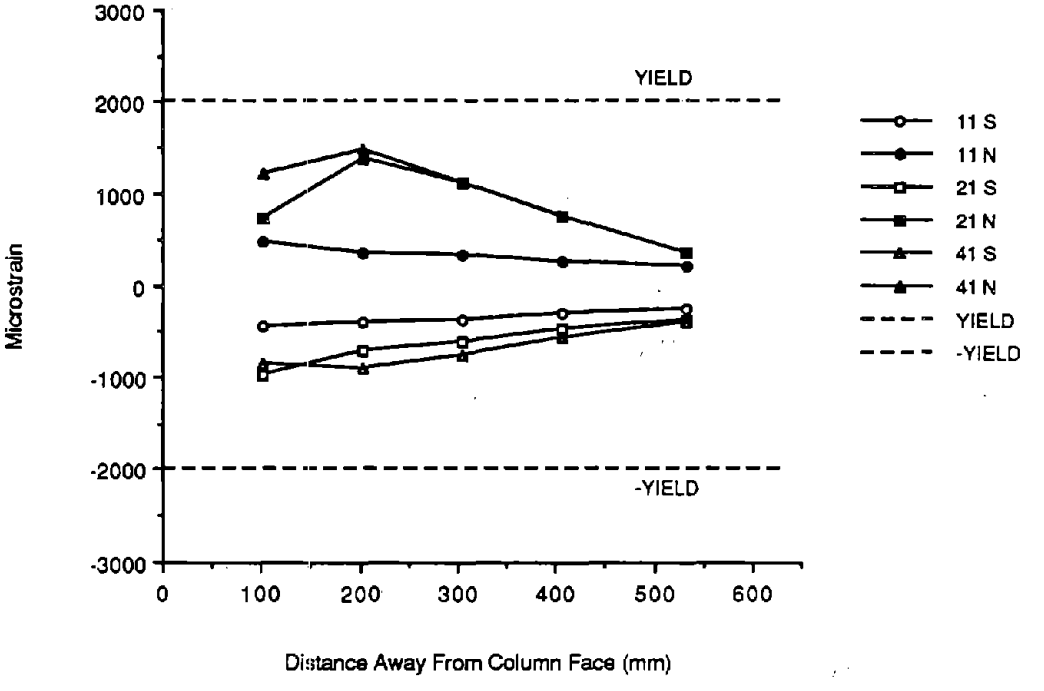

Fig. 3.78 Bottom northwest reinforcing bar strains - B-P-Z2.

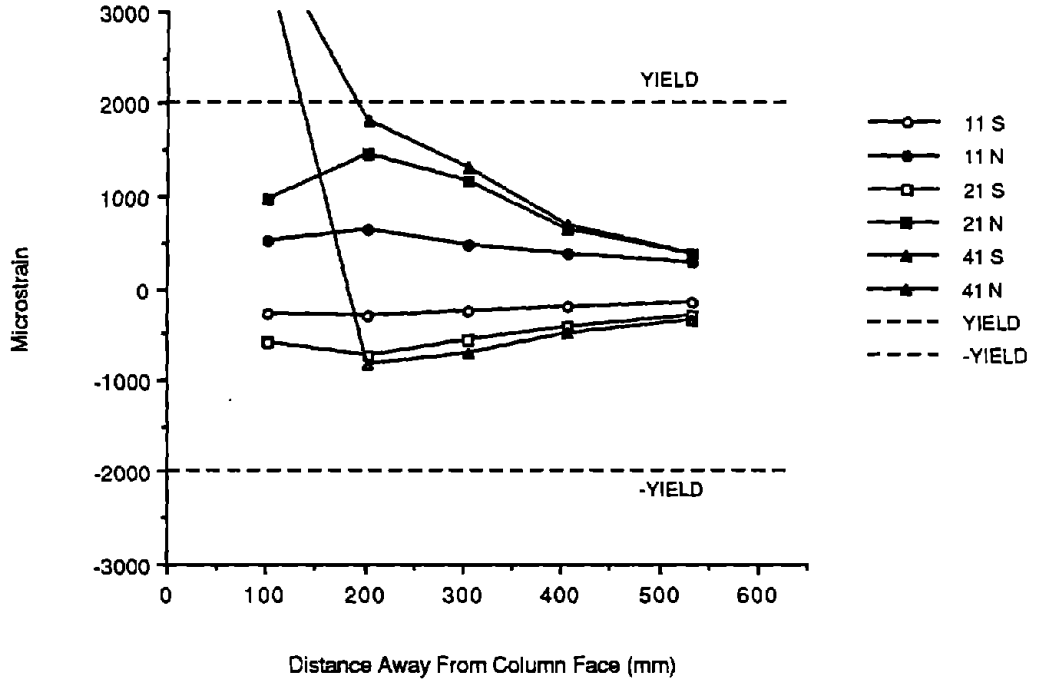

Fig. 3.79 Top southeast reinforcing bar strains - B-P-Z2.

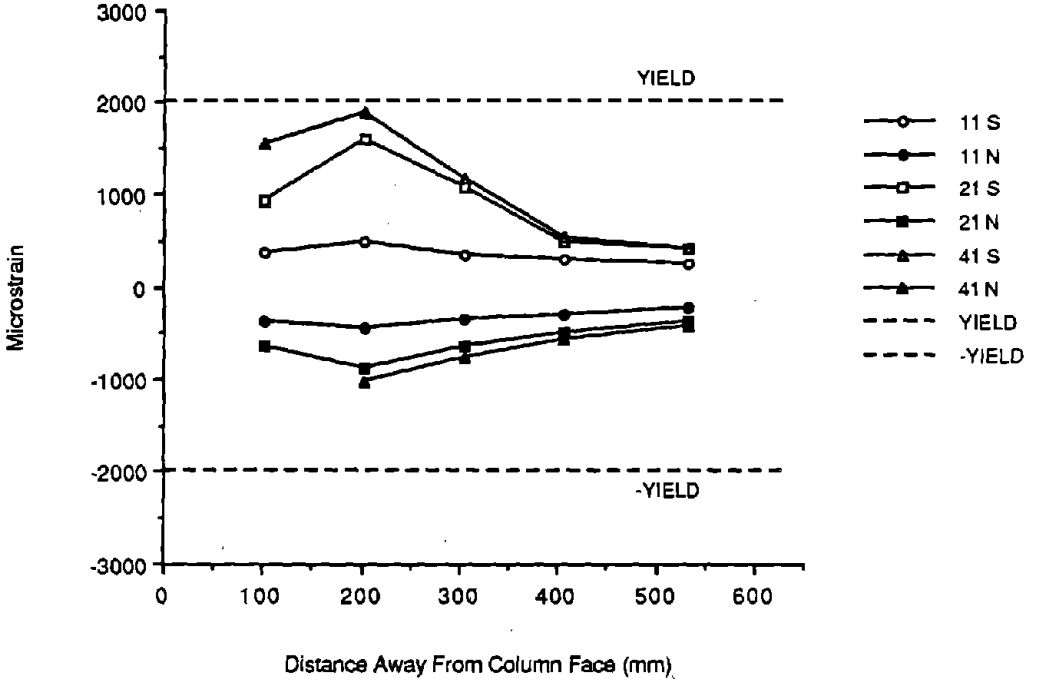

Fig. 3.80 Bottom southeast reinforcing bar strains - B-P-Z2.

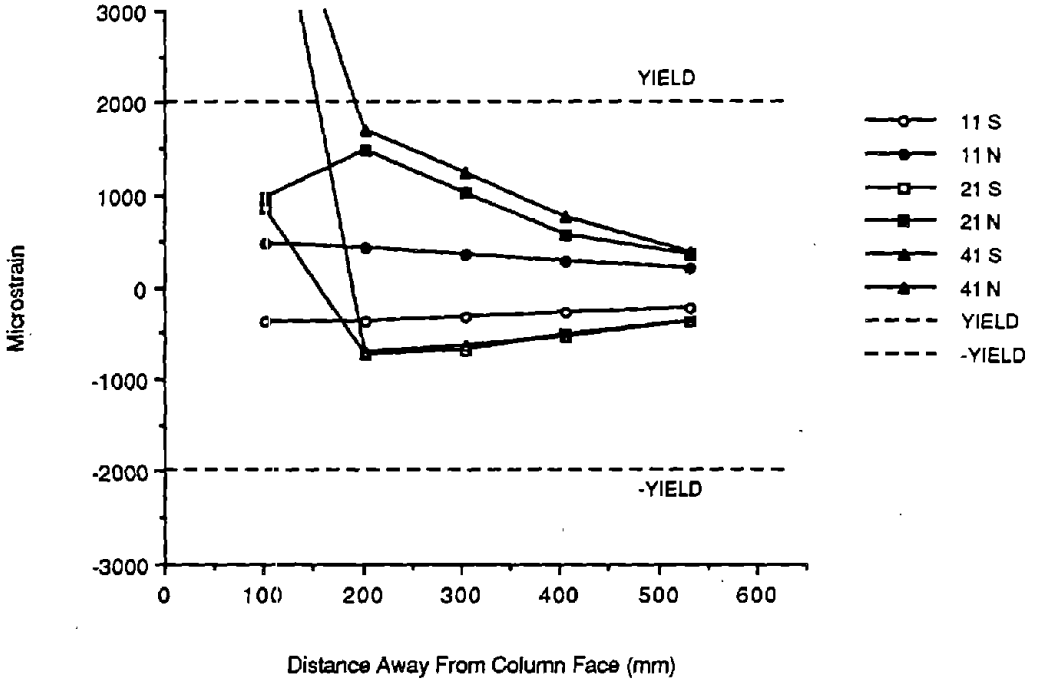

Fig. 3.81 Top southwest reinforcing bar strains - B-P-Z2.

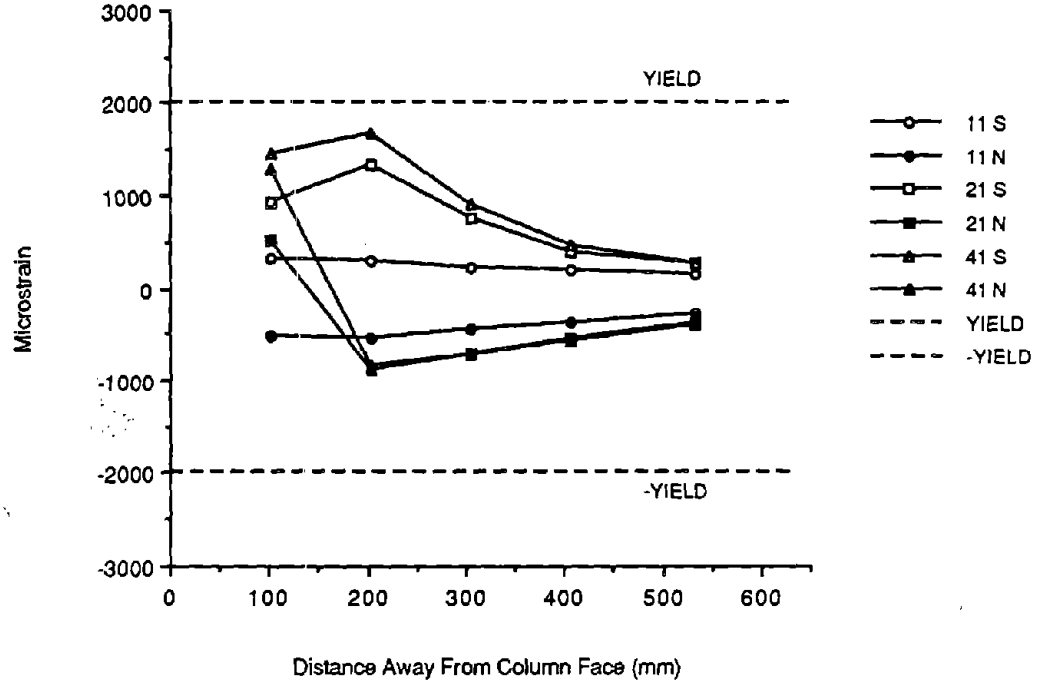

Fig. 3.82 Bottom southwest reinforcing bar strains - B-P-Z2.

4.0 DISCUSSION OF TEST RESULTS

4.1 Displacement Ductility

The ultimate displacement ductilities for all the specimens (Phase I and Phase II) are given in Table 4.1. Also shown in Table 4.1 are the connection stiffnesses and story drifts at failure. Story drift is defined as the ratio of the story displacement to the story height.

Table 4.1 Yield Displacement and Displacement Ductility.

Specimen	f'_c[a]		Exp. Yield		μ_u	Init. Elast. Connection Stiffness[b]		Ult. Story Drift
	MPa	(psi)	mm	(in.)		kN/mm	(k/in)	(%)
A-M-Z2	43.5	6310)	9.12	(0.359)	6[c]	7.7	(44)	4.1
B-M-Z2	41.1	(5960)	9.42	(0.371)	6	6.6	(38)	4.3
A-P-Z2	34.0	(4930)	8.46	(0.333)	4	12.4	(71)	2.6
B-P-Z2	36.4	(5280)	8.38	(0.330)	4	11.0	(63)	2.5
A-M-Z4	30.7	(4450)	6.68	(0.263)	6	21.2	(121)	3.0
B-M-Z4	32.2	(4670)	7.44	(0.293)	6	18.0	(103)	3.4
A-P-Z4	40.6	(5890)	4.06	(0.160)	10	35.7	(204)	3.1
B-P-Z4	44.5	(6450)	4.55	(0.179)	10	37.8	(216)	3.4
C-P-Z4	46.8	(6780)	5.31	(0.209)	12	31.5	(180)	4.8
D-P-Z4	44.9	(6510)	5.41	(0.213)	12	45.2	(258)	4.9
E-P-Z4	29.2	(4230)	5.71	(0.225)	12	42.2	(241)	5.2
F-P-Z4	27.7	(4020)	5.28	(0.218)	12	50.1	(286)	5.0

a These strengths were obtained at the time of the specimen tests. See Table 2.3 for the 28-day strengths.
b These values are the initial elastic stiffness as obtained from the slope of the load-displacement plot for the initial excursion to $+0.75\ \Delta_y$.
c See explanation below.

The ultimate displacement ductility, μ_u, for both precast Zone 2 specimens was 4. The ultimate displacement ductility for specimen A-M-Z2, monolithic Zone 2 specimen A, was reported incorrectly in Ref. 1. As defined in Chapter 2, failure was based on the lateral load applied to the connection. However,

μ_u = 4 as reported in Ref. 1 for specimen A-M-Z2 was based on the load recorded in one of the beams and not on the lateral load applied to the connection. Therefore, based on the lateral load applied to the connection, μ_u for A-M-Z2 was 6 instead of 4. As a result, it would appear that the precast Zone 2 specimens achieved lower ultimate displacement ductilities than did the monolithic Zone 2 specimens. The yield displacements for the Zone 2 specimens, monolithic and precast, were approximately the same. However, the precast Zone 2 specimens were approximately 65% stiffer than the monolithic Zone 2 specimens.

As shown in Table 4.1, all the Zone 4 precast specimens achieved higher ultimate displacement ductilities than did the monolithic Zone 4 specimens. Although the precast specimens achieved higher ultimate displacement ductilities than did the precast specimens in Phase I, it cannot be stated with certainty that this increase is a result of moving the post-tensioning bars closer to the beam center. This is because of the unsymmetric loading of the specimens in Phase I. The precast Zone 4 specimens were also stiffer than the monolithic Zone 4 specimens - approximately 90% stiffer for precast specimens A and B, 95% stiffer for precast specimens C and D, and 135% for precast specimens E and F. It would appear that the precast specimens post-tensioned with prestressing strands were stiffer and achieved slightly higher story drifts at failure than did the specimens post-tensioned with post-tensioning bars. Also, the connection stiffness increased when the post-tensioning bars were moved closer to the beam center.

4.2 Flexural Strength

The measured maximum and calculated ultimate moments are given in Table 4.2. The calculated values were based on an ultimate concrete strain of 0.003 and actual material properties. The calculated ultimate moments for the monolithic specimens had a factor of 1.25 applied to the steel yield stress to account for strain-hardening. No factor for strain hardening was used in calculating the moments for the precast specimens. The experimental values were obtained by multiplying the peak load recorded in the beam load cell and the moment arm to the column face.

The measured maximum moments for the monolithic specimens were achieved at or close to the ultimate displacement ductility of the connections. This was also true for precast specimens A-P-Z2, B-P-Z2, A-P-Z4, and B-P-Z4. However, the measured maximum moments for the precast specimens with the post-tensioning bars/prestressing strands closer to the beam center (C-P-Z4 through F-P-Z4) were achieved earlier in the tests - at $\mu \approx 4$ whereas $\mu_u = 12$.

Table 4.2 Measured and Calculated Ultimate Moments.

Specimen	f'_c [a]		Calculated Ultimate Moment		Measured Maximum Moment[b]		Avg. Exp. Mom / Calc. Ult. Mom
	MPa	(psi)	kN-m	(k-ft)	kN-m	(k-ft)	
A-M-Z2	43.5	(6310)	68	(50)	69 & 80	(51 & 59)	1.10
B-M-Z2	41.1	(5960)	68	(50)	70 & 75	(52 & 55)	1.07
A-P-Z2	34.0	(4930)	46	(34)	52 & 54	(38 & 40)	1.15
B-P-Z2	36.4	(5280)	46	(34)	50 & 54	(37 & 40)	1.13
A-M-Z4	30.7	(4450)	132	(97)	148 & 144	(109 & 106)	1.11
B-M-Z4	32.2	(4670)	132	(97)	148 & 153	(109 & 113)	1.14
A-P-Z4	40.6	(5890)	155	(114)	176 & 186	(130 & 137)	1.16
B-P-Z4	44.5	(6450)	155	(114)	184 & 186	(136 & 137)	1.20
C-P-Z4	46.8	(6780)	145	(107)	169 & 171	(125 & 126)	1.17
D-P-Z4	44.9	(6510)	145	(107)	165 & 169	(122 & 125)	1.15
E-P-Z4	29.2	(4230)	111	(82)	138 & 136	(102 & 100)	1.24
F-P-Z4	27.7	(4020)	111	(82)	146 & 137	(108 & 101)	1.28

a These concrete strengths were obtained at the time of the specimen tests. See Table 2.3 for the 28-day strengths.
b Moments are at the column face. There are two values because the specimens were interior joints.

As seen in the last column of Table 4.2, the precast specimens were as strong or stronger than their monolithic counterparts. When comparing the results of A-P-Z4 and B-P-Z4 with those of C-P-Z4 and D-P-Z4, the reduction in strength caused by moving the post-tensioning bars closer to the beam centroid was approximately 8%. It also appears that the precast specimens post-tensioned with prestressing strands had more "reserve" strength than did the precast specimens post-tensioned with post-tensioning bars - an average of 26% increase over the calculated moment as opposed to 17%.

4.3 Failure Modes

The failure mode for the precast Zone 2 specimens was beam crushing and inability of the connection to sustain additional load. This is unlike the failure mode for the monolithic Zone 2 specimens which failed predominantly in shear in the column joint region. The difference in the failure mode is likely a result of the debonding of the strands in the column joint region which would reduce the joint stress. The beam-column opening for the precast Zone 2 specimens was approximately 5 mm (0.2 in). This opening size

is one-fifth of the opening size for the precast Zone 4 specimens. There is insufficient data to determine if this is a result of the higher initial beam stress imposed on the Zone 2 specimens or if it is the result of the lower loads experienced by these specimens.

The failure modes for all the precast Zone 4 specimens were similar to the failure modes for the precast Zone 2 specimens. The precast beams sustained less cracking than did the monolithic specimens and no visible beam hinging was observed. However, more beam crushing and a wider opening between the beam and column, approximately 50% greater, was observed in the precast specimens which had the post-tensioning bars/prestressing strands closer to the beam centroid.

4.4 Energy Absorbed

A comparison of the energy absorbed by all the specimens to 6 Δ_y, cycle 3 is given in Fig. 4.1. The comparison was made at this stage because this was the approximate point at which the monolithic specimens failed. As shown in the figure, the monolithic Zone 4 specimens absorbed more energy per cycle than the precast Zone 4 specimens. The energy absorbed per cycle by the precast Zone 4 specimens was comparable to the energy absorbed per cycle by the monolithic Zone 2 specimens.

Figure 4.2 shows the comparison of the per cycle energy absorbed for all the precast Zone 4 specimens. As seen in the figure, specimens E-P-Z4 and F-P-Z4 performed the best and specimens A-P-Z4 and B-P-Z4 performed the worst in terms of energy absorption characteristics. The per cycle energy absorbed increased by an average of 45% with a standard deviation of 24% when the post-tensioning bars were moved closer to the beam center. This increase is likely due to the increased crushing of the beam concrete as observed during the test. An increase in the per cycle enery of an average of 30% with a standard deviation of 22% was noted when prestressing strands were used in place of post-tensioning bars. As seen by the large standard deviations, the percent increase in per cycle energy absorbed varied quite a bit. In spite of the improved performance, the per cycle energy absorbed by the precast specimens, E-P-Z4 and F-P-Z4, was only an average of approximately 60% of that absorbed by the monolithic Zone 4 specimens. This is because the hysteresis curves for the all the precast Zone 4 specimens were still severely pinched. This pinching may be a result of debonding of the prestressing strands as observed during the test.

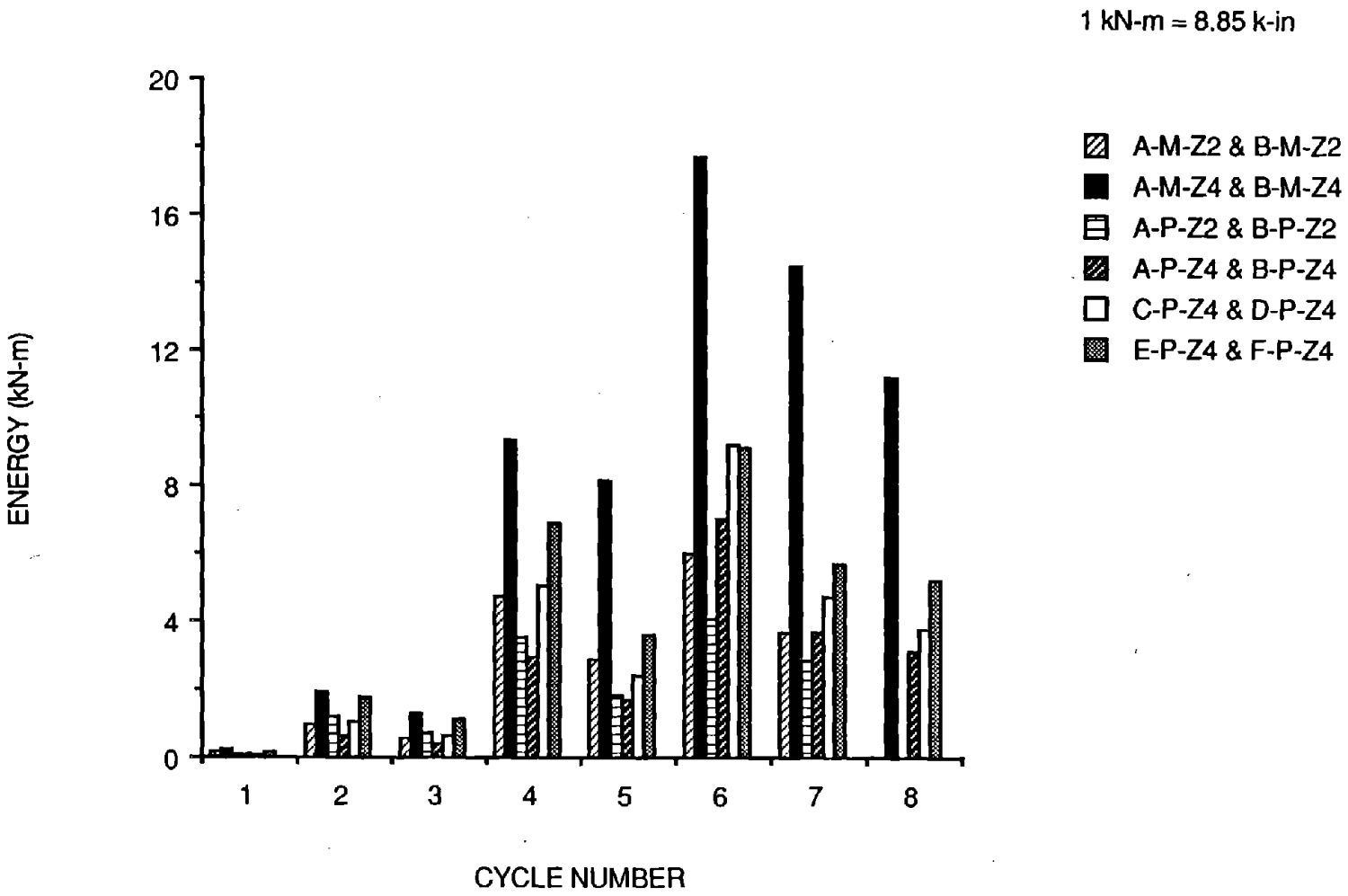

Fig. 4.1 Comparison of cyclic energy absorbed to 6 Δ_y, cycle 3.

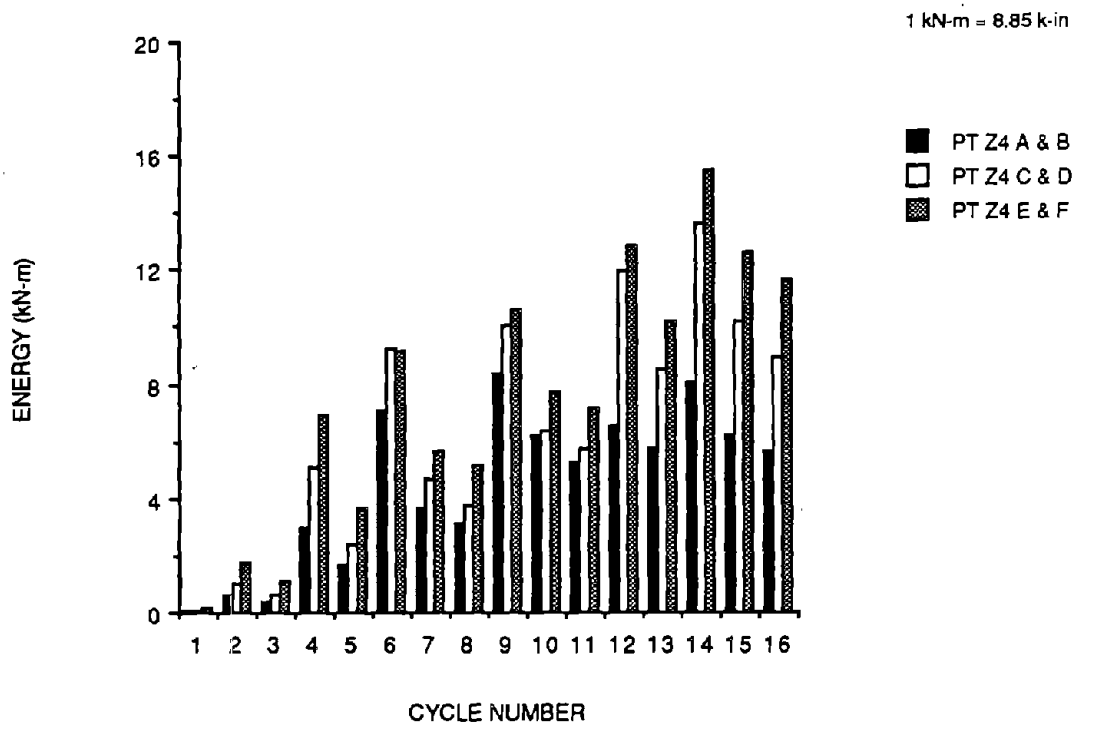

Fig. 4.2 Cyclic energy absorbed by precast Zone 4 specimens.

Fig. 4.3 shows a comparison of the cyclic energy absorbed to failure by the Zone 2 specimens. As shown in Fig. 4.2, the monolithic and precast Zone 2 specimens absorbed similar amounts of energy per cycle until failure occurred. Again, there is insufficient data to determine if the higher level of initial prestress caused this improved behavior.

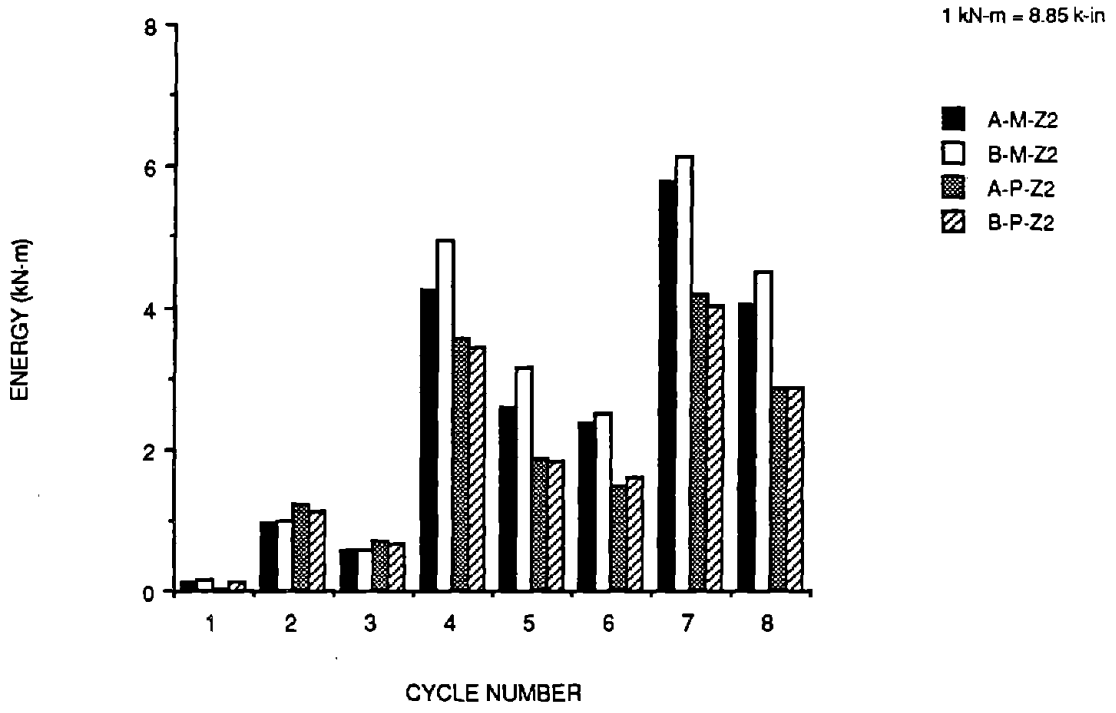

Fig. 4.3 Cyclic energy absorbed by Zone 2 specimens.

The cumulative energy absorbed to failure by all the specimens is shown in Fig. 4.4. Precast specimens C through F performed better than did the monolithic Zone 4 specimens. This was because the precast Zone 4 specimens failed at a higher displacement ductility than did the monolithic Zone 4 specimens. The cumulative energy absorbed to failure by specimens C-P-Z4 and D-P-Z4 was 45% greater than that absorbed by the monolithic Zone 4 specimens. Similarly, the cumulative energy absorbed to failure by specimens E-P-Z4 and F-P-Z4 was 71% greater. The cumulative energy absorbed to failure by specimens A-P-Z4 and B-P-Z4 was, however, 20% less. The cumulative energy absorbed at various stages is given in Table 4.3.

The effect of moving the post-tensioning bars closer to the beam centroid (C-P-Z4 and D-P-Z4 vs. A-P-Z4 and B-P-Z4) on the cumulative energy absorbed was an increase of approximately 80 %. This increase is due largely to the increased crushing of the beam concrete.

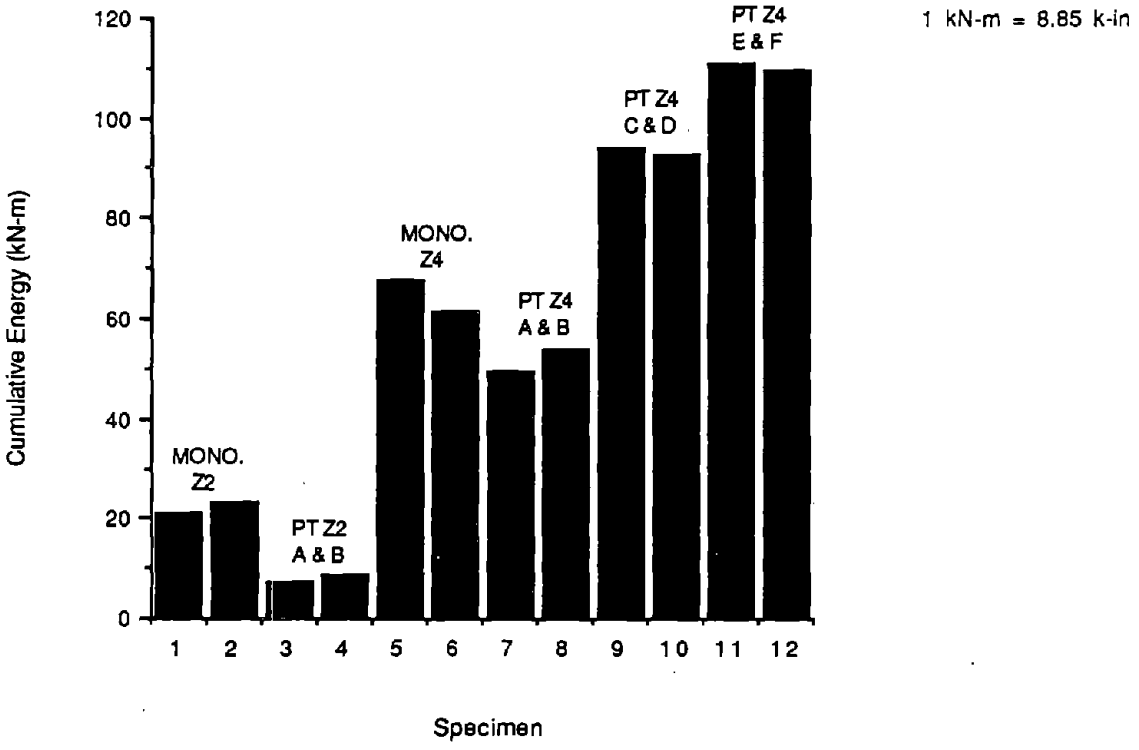

Fig. 4.4 Comparison of the cumulative energy absorbed.

Table 4.3 Cumulative Energy Absorbed.

Specimen	μ_u	Cumulative Energy Absorbed			
		to Failure		to 6 Δ_y, cycle 3	
		kN-m	(k-in)	kN-m	(k-in)
A-M-Z2	6	21.0	(186)	18.6	(165)[a,b]
B-M-Z2	6	23.0	(204)	24.0	(212)[b]
A-P-Z2	4	7.3	(65)	15.9	(141)
B-P-Z2	4	8.8	(78)	15.6	(138)
A-M-Z4	6	67.4	(597)	67.4	(597)
B-M-Z4	6	61.3	(543)	61.3	(543)
A-P-Z4	10	49.5	(438)	18.6	(165)
B-P-Z4	10	53.9	(477)	20.4	(181)
C-P-Z4	12	93.9	(831)	26.8	(237)
D-P-Z4	12	92.9	(822)	27.1	(240)
E-P-Z4	12	110.7	(980)	34.7	(307)
F-P-Z4	12	109.4	(968)	32.4	(287)

a Cumulative energy absorbed through 6 Δ_y, cycle 2.
b For purposes of comparison, the energy absorbed in the third cycle at 4 Δ_y was not included in this summation as the Zone 4 specimens did not undergo this particular cycle.

4.5 Reinforcing Bar Yield

Table 4.4 shows the extent of reinforcing bar and tie yielding for all the specimens. For each specimen, all the beam reinforcing bars and three ties in each beam were instrumented. Each of beam reinforcing bar was instrumented at five locations along the bar.

Table 4.4 Reinforcing Bar Yield Length.

Specimen	Length of Yield		Avg. Length of Set[a]		Extent of Tie Yield	
	mm	(in)	mm	(in)	mm	(in)
A-M-Z2	450	(17.7)	432	(17.0)	76	(3.0)
B-M-Z2	414	(16.3)			0	(0.0)
A-P-Z2	110	(4.3)	111	(4.4)	110	(4.3)
B-P-Z2	112	(4.4)			110	(4.3)
A-M-Z4	523	(20.6)	532	(20.9)	229	(9.0)
B-M-Z4	541	(21.3)			406	(16.0)
A-P-Z4	156	(6.1)	271	(10.7)	178	(7.0)
B-P-Z4	387	(15.3)			42	(1.7)
C-P-Z4	393	(15.5)	365	(14.4)	42	(1.7)
D-P-Z4	337	(13.3)			42	(1.7)
E-P-Z4	95	(3.7)	122	(4.8)	42	(1.7)
F-P-Z4	148	(5.8)			42	(1.7)

a Two identical specimens make a set.

As expected and as shown in Table 4.4, the monolithic specimens exhibited a longer reinforcing bar yield length than did the precast specimens. However, among the precast specimens, the specimens post-tensioned with post-tensioning bars had longer reinforcing bar yield lengths than did those post-tensioned with prestressing strands. It would appear that the strains were more concentrated at the column joint for the precast specimens which were post-tensioned with prestressing strands.

5.0 SUMMARY AND CONCLUSIONS

5.1 Summary

Phase II of the precast concrete beam-column connection experimental test program being conducted at NIST involved the testing of six precast concrete specimens - three sets with each set consisting of two identical specimens. Two sets, C-P-Z4 & D-P-Z4 and E-P-Z4 & F-P-Z4, were designed similarly to the Phase I specimens, A-P-Z4 & B-P-Z4, whose design was based on the 1985 UBC seismic Zone 4 criteria. The other set, A-P-Z2 & B-P-Z2, was designed based on the criteria for the monolithic Zone 2 specimens. Again, the design of the monolithic Zone 2 specimens were based on the 1985 UBC seismic Zone 2 criteria.

The objective of the overall test program was to develop an economical moment-resistant precast concrete beam-to-column connection in seismically active regions. The primary goal in Phase I was to identify a viable precast concrete connection. The emphasis of Phase II was to improve the energy absorption characteristics of the precast concrete connection identified in Phase I.

The two parameters studied in Phase II were type of material used to post-tension the precast specimens and the location of the post-tensioning force. In reference to the first parameter, post-tensioning bars were used for specimens C-P-Z4 & D-P-Z4 while prestressing strands were used for specimens E-P-Z4 & F-P-Z4 and A-P-Z2 & B-P-Z2. With regard to the second parameter, the post-tensioning bars were moved closer to the beam center for specimens C-P-Z4 & D-P-Z4. These specimens were identical to specimens A-P-Z4 & B-P-Z4 except for the location of the post-tensioning bars.

The construction of the precast concrete specimens was similar to the Phase I precast concrete specimens. A 25 mm (1 in) wide construction joint was filled with a fiber reinforced grout. The initial beam prestress was 10.5 MPa (1.5 ksi) for the precast Zone 2 specimens and 7.0 MPa (1.0 ksi) for the precast Zone 4 specimens.

Comparisons were made between the specimens in this phase and also with specimens in Phase I. The comparisons were made based on strength, energy absorption, and ductility of the connection. The following section presents the conclusions drawn based on Phase I and Phase II test results.

5.2 Conclusions

Failure of all the precast concrete specimens in Phase II was similar and was a result of the inability of the connection to sustain additional load. It was characterized by beam crushing and an opening between the beam and column. Other than fine cracks in the column connection region, this region did not suffer additional distress. This failure mode was the same as that experienced by the precast specimens in Phase I with the exception of a 50% increase of the beam-column opening for the Zone 4 specimens. The width of the opening does not appear to be influenced by the type of post-tensioning system (post-tensioning bars or prestressing strands) used to connect the precast elements.

Unlike the monolithic Zone 2 specimens which failed predominantly in shear in the column joint region, the precast Zone 2 specimens did not experience severe joint distress. This was likely due to the debonding of the prestressing strands in the column joint which lessened the joint stress.

The ultimate displacement ductilities for the precast Zone 2 specimens, $\mu_u = 4$, were lower than that obtained for the monolithic Zone 2 specimens, $\mu_u = 6$. As a result, the average story drift at failure was

2.5% for the precast Zone 2 specimens and 4.2% for the monolithic Zone 2 specimens. The precast Zone 2 specimens were approximately 65% stiffer than the monolithic Zone 2 specimens.

Ultimate displacement ductilities for the precast Zone 4 specimens were 12. These values were slightly higher than those achieved by precast specimens A-P-Z4 and B-P-Z4 (Phase I), $\mu_u = 10$. However, due to the unsymmetrical loading of specimens A-P-Z4 and B-P-Z4, this increase in displacement ductility cannot be conclusively attributed to the change made in this test phase, i.e. moving the post-tensioning bars closer to the beam center. The average story drift at failure for specimens C-P-Z4 and D-P-Z4 was 4.9% and was approximately 50% greater than for the monolithic Zone 4 specimens. Similarly, the average story drift at failure for E-P-Z4 and F-P-Z4 was 5.1% and was 60% greater than for the monolithic Zone 4 specimens. In general, the precast specimens post-tensioned with post-tensioning bars were approximately 90% stiffer than the monolithic Zone 4 specimens and the precast specimens post-tensioned with prestressing strands were 135% stiffer than the monolithic Zone 4 specimens.

With reference to the connection strength, the precast specimens, Zone 2 and Zone 4, performed satisfactorily and as well as the monolithic specimens. It appears that the precast specimens post-tensioned with prestressing strands had more "reserve" strength than did the precast specimens post-tensioned with post-tensioning bars. On average, the measured maximum moments for the precast Zone 4 specimens post-tensioned with strands were 26% greater than the calculated values while the average values for precast Zone 4 specimens post-tensioned with bars were 17% greater than the calculated values. In addition, moving the post-tensioning force closer to the beam center does not appear to have a significant adverse effect on the connection strength.

As in Phase I, the per cycle energy absorbed by the precast Zone 4 specimens was much less than the per cycle energy absorbed by the monolithic Zone 4 specimens. However, improved energy absorption characteristics due to the changes made in this test phase were evident. The per cycle energy absorption increased by 45% when the post-tensioning bars were moved closer to the beam center. An increase of 30% was noted when prestressing strands were used instead of post-tensioning bars. However, the per cycle energy absorbed by the specimens E-P-Z4 and F-P-Z4 (the precast specimens which performed best with respect to per cycle energy absorbed) was only 60% of that for the monolithic Zone 4 specimens. The poor performance of the precast Zone 4 specimens with respect to the per cycle energy absorption is a result of the severely pinched hysteresis curves for these specimens. Debonding of the prestressing strands may have caused the pinching of the hysteresis curves. In contrast, the precast Zone 2 specimens performed as well as the monolithic Zone 2 specimens in terms of per cycle energy absorbed until failure occurred.

The cumulative energy absorbed by precast Zone 4 specimens C through F was greater than the cumulative energy absorbed by the monolithic Zone 4 specimens. With reference to the monolithic Zone 4 specimens, the cumulative energy absorbed by precast specimens C and D was 45% greater and for precast specimens E and F the increase was 70%. This is in contrast to precast specimens A and B (Phase I) which had an average cumulative energy absorption than was 20% lower than the monolithic Zone 4 specimens.

Although the per cycle energy absorbed by the precast Zone 2 specimens was similar to the monolithic Zone 2 specimens, the cumulative energy absorbed by the precast specimens was less than that for the monolithic Zone 2 specimens because the precast specimens failed at a lower displacement ductility.

Based on the above findings, the effect of moving the post-tensioning force closer to the beam center improves the energy absorption characteristics of the connection with little effect on the strength of the connection. The use of prestressing strands as opposed to the use of post-tensioning bars seems to improve the energy absorption characteristics of the connection and seems to increase the "reserve" strength of the connection. Although the energy absorption characteristics were improved, the per cycle

energy absorbed is still poor when compared to the monolithic connections. The precast Zone 2 specimens did not perform as well as the monolithic Zone 2 specimens in terms of the ductility and cumulative energy absorption. However, the failure mode of the precast Zone 2 specimens was more desirable than the failure mode of the monolithic Zone 2 specimens.

REFERENCES

1. Cheok, G. S. and Lew, H. S., "Performance of 1/3-Scale Model Precast Concrete Beam-Column Connections Subjected to Cyclic Inelastic Load", NISTIR 4433, National Institute of Standards and Technology, Gaithersburg, MD, October, 1990.

2. Woodward, K. and Rankin, F., "The NBS-Tri-Directional Tst Facility", NBSIR 84-2879, National Bureau of Standards, Gaithersburg, MD, May, 1984.

PB91-222570

NIST-114A
(REV. 3-90)

U.S. DEPARTMENT OF COMMERCE
NATIONAL INSTITUTE OF STANDARDS AND TECHNOLOGY

BIBLIOGRAPHIC DATA SHEET

1. PUBLICATION OR REPORT NUMBER
NISTIR 4589

2. PERFORMING ORGANIZATION REPORT NUMBER

3. PUBLICATION DATE
JUNE 1991

4. TITLE AND SUBTITLE

Performance of 1/3-Scale Model Precast Concrete Beam-Column Connections Subjected to Cyclic Inelastic Loads - Report No. 2

5. AUTHOR(S)

Geraldine S. Cheok
H. S. Lew

6. PERFORMING ORGANIZATION (IF JOINT OR OTHER THAN NIST, SEE INSTRUCTIONS)

U.S. DEPARTMENT OF COMMERCE
NATIONAL INSTITUTE OF STANDARDS AND TECHNOLOGY
GAITHERSBURG, MD 20899

7. CONTRACT/GRANT NUMBER

8. TYPE OF REPORT AND PERIOD COVERED

9. SPONSORING ORGANIZATION NAME AND COMPLETE ADDRESS (STREET, CITY, STATE, ZIP)

NIST CATEGORY # 140

10. SUPPLEMENTARY NOTES

11. ABSTRACT (A 200-WORD OR LESS FACTUAL SUMMARY OF MOST SIGNIFICANT INFORMATION. IF DOCUMENT INCLUDES A SIGNIFICANT BIBLIOGRAPHY OR LITERATURE SURVEY, MENTION IT HERE.)

Results are presented from the experimental test program on precast concrete beam-column connections subjected to inelastic cyclic loads being conducted at the National Institute of Standards and Technology. This report is the second in a series and covers the test results from Phase II of a three phase program. The objective of the test program is to develop an economical moment resistant precast beam-column joint for high seismic zones.

Test specimens are 1/3-scale models of a prototype interior concrete beam-column connection. The 1985 UBC design criteria for seismic Zones 2 and 4 were used. Six specimens were tested. The experimental variables include the location of the post-tensioning force and the type of post-tensioning tendons used. Comparisons of the performance among these specimens are made. Comparisons with the monolithic specimens (Phase I [Ref. 1]) are also presented. These comparisons are made based on the failure mode, energy absorption characteristics, strength and ductility of the connection.

12. KEY WORDS (6 TO 12 ENTRIES; ALPHABETICAL ORDER; CAPITALIZE ONLY PROPER NAMES; AND SEPARATE KEY WORDS BY SEMICOLONS)

beam-column; concrete; connections; cyclic loading; ductility; energy absorption; joints; moment resistance; post-tensioning; precast concrete.

13. AVAILABILITY

[X] UNLIMITED

[ ] FOR OFFICIAL DISTRIBUTION. DO NOT RELEASE TO NATIONAL TECHNICAL INFORMATION SERVICE (NTIS).

[ ] ORDER FROM SUPERINTENDENT OF DOCUMENTS, U.S. GOVERNMENT PRINTING OFFICE, WASHINGTON, DC 20402.

[X] ORDER FROM NATIONAL TECHNICAL INFORMATION SERVICE (NTIS), SPRINGFIELD, VA 22161.

14. NUMBER OF PRINTED PAGES
84

15. PRICE
A05

ELECTRONIC FORM